A one-two punch model for cancer therapy

Liqin Wang

The research described in this thesis was performed at the Division of Molecular Carcinogenesis of the Netherlands Cancer Institute (Amsterdam, The Netherlands) and was financially supported by the Dutch Cancer Society (KWF), Euroean Research Council (ERC), Cancer Genomics Center (CGC) and Oncode institute.

ISBN: 978-94-028-1024-0
Printed by: Ipskamp Printing
Copyright © 2018 Liqin Wang. All rights reserved.

Cover: Idea by Liqin Wang, Design by Thomas van der Vlis

A one-two punch model for cancer therapy

Een "one-two punch" model
voor de behandeling van kanker
(met een samenvatting in het Nederlands)

Proefschrift

ter verkrijging van de graad van doctor aan de Universiteit Utrecht
op gezag van de rector magnificus, prof.dr. H.R.B.M. Kummeling, ingevolge het
besluit van het college voor promoties in het openbaar te verdedigen
op maandag 4 juni 2018 des middags te 2.30 uur

door

Liqin Wang

geboren op 10 augustus 1985
te Hunan, China

Promotor: Prof. dr. R. Bernards

Table of contents

Chapter 1 General introduction 7
Partly adapted from Frontiers of Medicine (2018)

Chapter 2 A functional genetic screen identifies the phosphoinositide 3-kinase pathway as a determinant of resistance to fibroblast growth factor receptor inhibitors in FGFR mutant urothelial cell carcinoma 23
European Urology (2017)

Chapter 3 Reversible and adaptive resistance to BRAF(V600E) inhibition in melanoma 35
Nature (2014)

Chapter 4 An acquired vulnerability of drug resistant melanoma with therapeutic potential 61
Cell (2018)

Chapter 5 High throughput functional genetic and compound screens identify targets for senescence induction in cancer 101
Cell Report (2017)

Chapter 6 General discussion 127

Appendix
Nederlandse samenvatting 134
English summary 136
Curriculum vitae 138
Publication list 139
Acknowledgments 141

Introduction

1

Partly adapted from
Frontier of medicine (2018)

Introduction

The various cancer genome-sequencing projects have yielded profound insights into the mutations that contribute to malignant growth in the various human tissues. An important insight with relevance to therapy from this work is that the major oncogenic "driver" mutations in specific cancers often create a dependency on the signaling pathway that is affected by the mutation. This phenomenon of "oncogene addiction" forms the basis of nearly all targeted cancer therapies today (Weinstein, 2002). The clinically most successful examples include the use of BRAF inhibitors in *BRAF*^{V600E} mutant melanomas, the use of ABL kinase inhibitors in *BCR-ABL* translocated chronic myeloid leukemia, the use of trastuzumab in *HER2* amplified breast cancer, and use of EGFR inhibitors in *EGFR* mutant lung cancer (Sun and Bernards, 2014).

Resistance mechnisms to targeted cancer therapies

The use of targeted drugs in these patients often results in a significant increase progression-free survival, but this improvement does not necessarily translate into a meaningful overall survival, as acquired resistance to these drugs invariably develops. It seems that the cancer cells can have a robust self-defense system to adapt to the selective pressure imposed by the drugs in one-way or the other. Before discussing how to overcome the drug-resistance, I will first discuss a number of mechanisms of resistance to targeted cancer therapies.

Alternation of the driver oncogenes

Most of small molecules kinase inhibitors bind to their target within the ATP-binding pocket. Cancer cells can develop resistance to these inhibitors by mutating a so-called "gatekeeper" residue within the pocket. This amino acid substitution often does not significantly alter the pocket's ATP-binding affinity, but prevents kinase-inhibitor binding (Kobayashi et al., 2005; Yun et al., 2008). For example, the gatekeeper T790M mutation in *EGFR* is found in almost half of the lung cancer patients who develop resistance to not only the first generation of EGFR inhibitors, gefitinib and erlotinib, but also to the second generation of EGFR inhibitors, afatinib, neratinib and dacomitinib (Pao et al., 2005) (Figure 1A). Although the third generation of EGFR inhibitor, osimertinib can overcome the drug-resistance caused by T790M, lung cancer cells can develop another mutation (C797S) to become resistant to this drug (Wang et al., 2016). Another example, The BRAF inhibitor, vemurafenib, can specifically target the BRAF-V600E mutant protein and effectively inhibit MAPK pathway signaling. This drug has shown excellent single-agent activity in 70–80% of *BRAF*^{V600E} mutant melanoma patients, *BRAF*^{V600E} amplification has been reported as a resistance mechanism in vemurafenib treated melanomas (Shi et al., 2012). The amplification can reduce the potency of vemurafenib, because there will be fewer drug molecules per molecule of the mutant-BRAF protein. Therefore, the vemurafenib can no longer fully block the MAPK pathway resulting in the drug-resistance (Figure 1B).

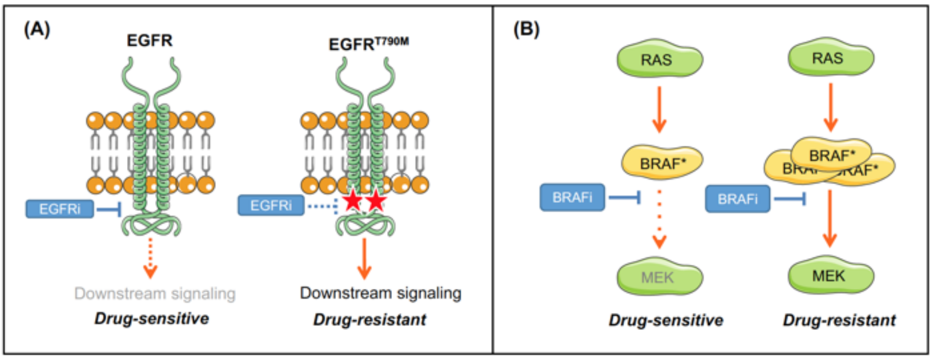

Figure 1: Alternation of the drug targets.
(A) Point-mutations of targeted genes confer drug-resistance. Treatment of EGFR inhibitor (EGFRi) can block the downstream signaling pathways (indicated by dotted arrow line) that control many cellular activities including cell survival and proliferation. Cancer cells can gain point mutation $EGFR^{T790M}$ (indicated by red stars) to disrupt the binding affinity of EGFR inhibitor (EGFRi) to EGFR; therefore, the signaling pathways are no longer inhibited (indicated by solid arrow line). As the consequence, the cancer cells are now resistant to EGFR inhibition (B) Targeted genes can be amplified to become drug-resistance. *BRAF*-mutant melanoma cells are driven by *BRAF* mutations (indicated by yellow BRAF*). BRAF inhibitors (BRAFi) can specifically target the mutated BRAF protein and effectively inhibit MAPK pathway signaling. Melanoma cells can develop resistant to BRAF inhibitors by amplifying their mutated *BRAF* gene to reduce the potency of BRAF inhibition.

RTK upregulation to escape pathway inhibition

Cancer cells can also develop resistance to a targeted therapy by upregulating expression or activating upstream receptors that signal through the same pathways. In this way, despite continued suppression of the initial driver oncoprotein by the small molecule inhibitor, critical parallel signaling persists under the control of the newly up-regulated receptor activity. As discussed previously, BRAF inhibitor can rapidly shrink melanomas by efficiently blocking the MAPK pathway. However, melanoma cells can up-regulate their tyrosine kinase receptors, EGFR and PDGFRB leading to increased MAPK signaling, which BRAF inhibitor then no longer can fully inhibit. This can result in drug-resistance (Sun et al., 2014) (Figure 2A). Responsiveness to targeted therapy can be very context-dependent. Response rates to BRAF inhibitors vary from 80% in melanoma to only 5% in colon cancer, which both harbor the $BRAF^{V600E}$ mutation. This differential response can be attributed to the fact that EGFR is highly expressed in many colon cancers. Therefore, colon cancer cells do not need to up-regulate expression of EGFR; they just need to simply find a way to activate it. A work from our group has shown that BRAF inhibition in these cells causes a rapid feedback activation of EGFR through its substrate phosphatase CDC25C repression, which reactivates PI3K/AKT and MAPK signaling pathways to support the proliferation of these cells in the presence of the BRAF inhibitor (Prahallad et al., 2012) (Figure 2B).

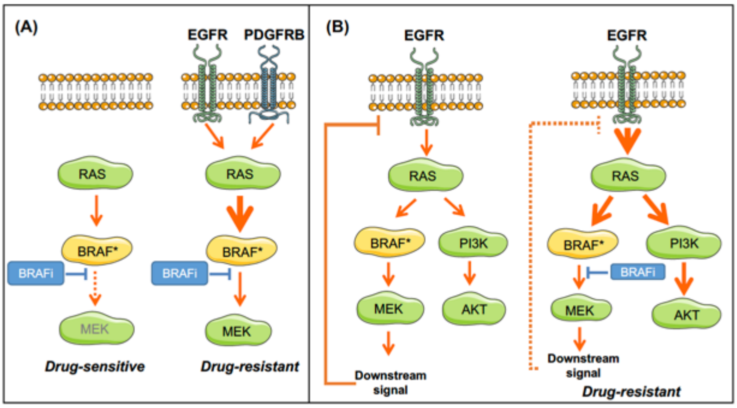

Figure 2: RTKs regulation escapes the pathway inhibition.
(A) Cancer cells can develop drug-resistance through upregulating RTKs. *BRAF*-mutant melanomas are initially sensitive to BRAF inhibitors, which can inhibit the mutated BRAF protein and suppress the downstream pathway signaling. However, melanomas can upregulate their EGFR and PDGFRB to hyperactivate (indicated by bold arrow line) the MAPK signaling pathway to bypass the BRAF inhibition. (B) Cancer cells can use negative feedback mechanisms to activate RTKs. *BRAF*-mutant colon cancer cells intrinsically express EGFR at a high level. The activation of EGFR is suppressed by a negative feedback mechanism through RAS-RAF-MEK pathway. In the presence of BRAF inhibitor, the feedback mechanism is suppressed. This leads to hyperactivation (indicated by bold arrow lines) of EGFR and the downstream BRAF-MEK and PI3K-AKT signaling, which results in not only bypassing the BRAF inhibition, but also enhancing the PI3K-AKT pathway signaling.

Upstream or downstream mutations reactivate the inhibited signaling pathway

BRAF-mutant melanoma cells can also become resistant to BRAF inhibitor or a combination of BRAF and MEK inhibitors by acquiring activation mutations in either upstream or downstream pathway genes, such as *NRAS, KRAS, MEK1, MEK2* (Emery et al., 2009; Long et al., 2014a; Sanchez-Laorden et al., 2014). Interestingly, the *NRAS* mutant melanoma cells treated with the MEK inhibitor can develop an additional *BRAF* mutation to become insensitive to the drug. These mutations enhance MAPK signaling, therefore the drugs can no longer fully inhibit the pathway, and the remaining signal can sufficiently maintain cell proliferation.

Cetuximab and panitumumab, two monoclonal antibodies targeting EGFR, have been used for the treatment of colorectal cancer, leading to inhibition of its downstream signaling pathways. However, the patients with *KRAS* mutations do not benefit from anti-EGFR antibodies (Benvenuti et al., 2007; Lievre et al., 2006). Clinical data also indicate that not only *KRAS* mutations, but also mutations in components of downstream signaling cascades such as *BRAF* and *PIK3CA* could be critical to identify colon cancer patients who are unlikely to respond to anti-EGFR antibodies (Bardelli and Siena, 2010; Sartore-Bianchi et al., 2009).

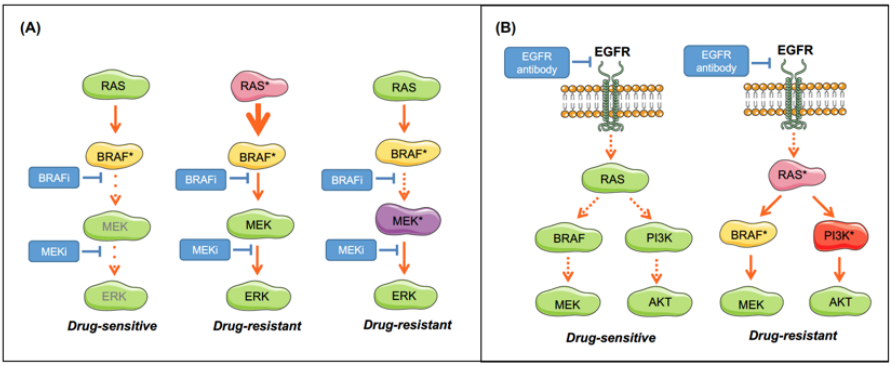

Figure 3: Upstream or downstream mutations reactivate the inhibited signaling pathway.
(A) RAF-MEK-ERK signaling in *BRAF* mutant melanomas can be inhibited (indicated by dotted arrow lines) using a BRAF inhibitor (BRAFi) only or combining with a MEK inhibitor (MEKi), which leads to a good initial drug response. However, these melanomas can develop acquired drug-resistance though gaining *RAS* mutations (indicated by pink RAS*) and *MEK* mutations (indicated by purple MEK*). The *RAS* mutations can enhance the RAS-RAF-MEK-ERK signaling (indicated by bold arrow line) to bypass the drug inhibition. The *MEK* mutations can ignore the BRAF and MEK inhibition and result in drug-resistance. (B) EGFR-driven cancer cells can develop resistance to monoclonal EGFR antibody. These antibodies can bind and block the EGFR that inhibits the downstream signaling. Cancer cells can acquire mutations in *RAS, BRAF* or *PI3K* (indicated by different colors and superscripted with *) to bypass the upstream inhibition.

Heterogeneity and tumor microenvironment

The ultimate challenge in overcoming drug-resistance is the heterogeneity within the tumors. Tumors are highly heterogeneous, formed by different cancer cell clones embedded with variant genetic mutations. This also causes diversity in drug-resistance mechanisms (Dexter and Leith, 1986). Back in1859, Charles Darwin formulated the theory of “natural selection”, which has striking similarities to what we see from tumor heterogeneity and clonal evolution. As a result of selective pressures exerted by drug treatment, there would eventually be the selection of the clones or tumor lesions that do not respond to the drugs. Moreover, it is commonly thought that the high mutational rate of cancer cells leads to diversification of the population, after which one clone ultimately gains an advantageous mutation and is able to outgrow the other clones, which take over the tumor mass and contribute to therapy resistance. As selective pressures change, this process is repeated, enabling tumors to adapt to their environment (Lipinski et al., 2016) (Figure 4). Besides the heterogeneity of cancer cells, many studies have implicated an important role for the microenvironment of tumors, such as stromal cells and inflammatory cells. Stromal cells in the tumors can secrete factors including hepatocyte growth factor (HGF), which can induce drug-resistance. This has been reported in EGFR inhibitor resistance in lung cancer and BRAF inhibitor resistance in melanoma (Mueller et al., 2012; Straussman et al., 2012). In addition, immune cells within the tumor microenvironment can secrete immunosuppressive cytokines that potentially induce resistance to chemotherapy and immunotherapy.

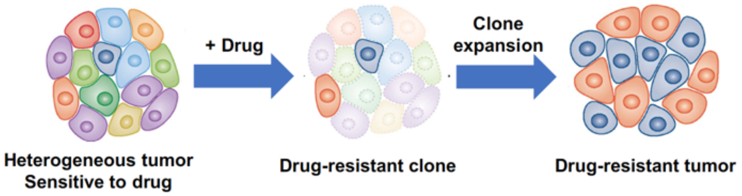

Figure 4: Heterogeneity leading to the drug-resistance.
The selective resistance of specific clonal variants can be enriched in response to the drug treatment. Tumors are often heterogeneous, formed by different cancer cell clones embedded with variant genetic mutations. In the case of a good responsiveness from the drug treatment, the drug can kill all the drug-sensitive cells, but not the drug-resistant clones. These drug-resistant clones can survive and expand to take over the tumor mass during the drug treatment.

Avoiding resistance to targeted cancer drugs

The clinical use of targeted cancer therapeutics has been modeled primarily on the decades-long experience with chemotherapies. Two strategies have emerged from the use of chemotherapies. First, drugs need to be given at maximum tolerated dose to be effective. Second, chemotherapies need to be combined to avoid resistance development. The combinations of chemotherapies that are given for each cancer type have been determined mostly through empirical "trial and error" methods. The major underlying rationale used to identify effective chemotherapy combinations is that drugs that act through different mechanisms are less likely to yield cross-resistance to other drugs. With the advent of targeted therapies and with the development of detailed insights how signaling pathways are connected, it has become possible to develop more rational combinations of targeted therapies. Examples of this include the "vertical targeting" of the BRAF and MEK kinases in *BRAF*-mutant melanoma. This approach was based on the insight that resistance to BRAF inhibitors is frequently caused by re-activation of MAPK signaling pathway (Holderfield et al., 2014). This suggested that a more powerful blockade of this pathway with two drugs would lead to more effective pathway suppression. Indeed, the combination of BRAF and MEK inhibition is effective in the clinic in slowing the progression of *BRAF*-mutant melanomas (Flaherty et al., 2012; Flaherty et al., 2010; Long et al., 2014b).

The question of which drug combination is the most effective to treat a given cancer is sometimes less straightforward. For instance, the oncogene addiction model would predict that all *BRAF*-mutant cancers would respond to BRAF inhibitors. However, in the case of *BRAF*-mutant colon cancer, this turned out to be incorrect in that hardly any patients responded to BRAF inhibitors (Kopetz et al., 2015). In situations where the best drug combination cannot be predicted, functional genetic screens can serve as a powerful platform to investigate in an unbiased way which combinations of pathway inhibitions are particularly effective in killing the cancer cells. This is referred to as "synthetic lethality" genetic screens. Synthetic lethality refers to a situation in which the inactivation of two genes individually is not lethal to a cell, but the combined inactivation of the two genes is lethal (Brunen and Bernards, 2017) (Figure 5). Synthetic lethality genetic screens have been used to identify kinases whose suppression synergizes with BRAF inhibition in *BRAF*-mutant colon cancer. The combination of BRAF and EGFR inhibition identified in this genetic screen has already proven successful in clinical studies (Prahallad et al., 2012; van Geel et al., 2017). Chapter 2 describes a similar study in *FGFR*-mutant bladder and lung cancer. The growth of these cancer cells is driven by the constitutively activated FGF receptors, but they only have a moderate response to the pan-FGFR inhibitors. To study the drug-resistance mechanism and potential synthetic lethal partners of an FGFR inhibitor, we performed a FGFR inhibitor synthetic lethality screen in an *FGFR*-mutant bladder cancer model using a small hairpin RNA (shRNA) library targeting kinases. From this screen, we discovered that silencing several components of the PI3K pathway: AKT3, PIK3CA, and PIK3R1 can enhance the responsiveness to the FGFR inhibitor. In addition, we also found that PI3K can be reactivated in the cells through a feedback signaling by HER2/3 and EGFR during FGFR inhibition. This suggests that targeting common downstream signaling molecules of the FGFR and ERBB family members, such as PI3K may block an adaptive pathway and convert the responses from cytostatic to cytotoxic (Wang et al., 2017b). And indeed, we found that combining an FGFR inhibitor with a PI3K inhibitor can synergistically kill multiple FGFR-mutant bladder and lung cancer models (Wang et al., 2017b).

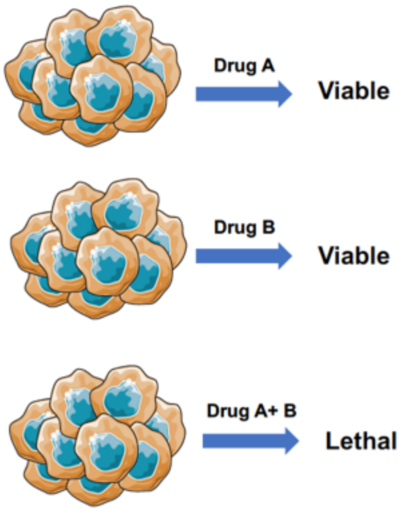

Figure 5: Schematic outline of the concept of synthetic lethality.
Synthetic lethality refers to a genetic principle in which the combination of two genetic perturbations is lethal, whereas each individually is not. In the example shown here, only the combination of drug A and drug B is lethal to the cell, making the combination of A and B synthetic lethal.

Taking advantage of drug-resistance

The proverb "if you can't beat them, join them" means that if your adversaries are stronger than you, it is better to join their side. In terms of cancer therapy resistance that translates into: if cancer drug-resistance development is unavoidable, should we not focus on taking advantage of drug-resistance rather than fighting it? It was already recognized over 50 years ago that drug-resistance of cancer cells can come at a fitness cost that in turn can cause sensitivity to other drugs, a situation referred to as "collateral sensitivity" (Hutchison, 1963). This phenomenon is widespread in biology, as also bacteria that develop resistance to antibiotics can acquire collateral sensitivity to other antibiotics (Imamovic and Sommer, 2013). A case in point is what happens when *BRAF*-mutant melanomas develop resistance to BRAF inhibitors. Clinical data shows that melanoma patients that have developed resistance to BRAF inhibitors and whose therapy is discontinued show an initial stabilization or even a decline of the tumor rather than a disease flare-up. This phenomenon is referred to as the "drug holiday effect" (McMahon, 2015; Seghers et al., 2012; Treiber et al., 2017). That a drug-resistant tumor is stabilized by drug withdrawal suggests that drug-resistant cells are at a disadvantage in the absence of the drug. Indeed, in melanoma, drug withdrawal after acquisition of resistance to BRAF inhibitors has been shown to cause hallmarks of oncogene-induced senescence due to hyperactivation of MAPK pathway signaling and points towards an acquired vulnerability of drug-resistant cells that was not present in the parental drug-sensitive cells (Sun et al., 2014) (Chapter 3). This model implies that in melanoma, intermittent dosing may be more effective than continuous dosing, as the intermittent dosing alternates between providing an advantage to the drug sensitive and the drug-resistant cells (Figure 6A). Indeed, in animal models of *BRAF*-mutant melanoma, an intermittent dosage with BRAF inhibitor resulted in longer disease control than continuous dosing (Das Thakur et al., 2013). Based on this concept, number of clinical trials have been conducted to study whether intermittent dosing leads to more durable response than continuous dosing in *BRAF*-mutant melanoma patients with either a BRAF inhibitor LGX818 (NCT01894672, NCT02263898) or combination of BRAF inhibitor dabrafenib and MEK inhibitor trametinib (NCT02196181) (Luke et al., 2017).

In chapter 4 we show an improved version of an intermittent dosing approach to the treatment of drug resistant cancer by using a second drug that selectively targets the acquired vulnerability of the drug resistant cells (Figure 6B). In this model, the drug-resistant cells are actively killed by the second drug rather than being only at a disadvantage, as is the case in the intermittent dosing scenario. The alternating drug model should, at least in theory, therefore be more effective than the intermittent dosing. But which are the vulnerabilities of drug resistant cells? Our study shows that once the *BRAF* or *NRAS*-mutant melanoma cells become resistant to the MAPK inhibition, they harbor higher reactive oxygen species (ROS) levels compared to their parental cells, which may potentially be explored as a selective vulnerability of the drug-resistant cells. Indeed, our study shows that these resistant cells are highly vulnerable not only to classic ROS inducers, but also HDAC inhibitors. Upon treatment, there is a massive ROS induction that cells are no longer able to tolerate and induce an apoptotic cell death. This strategy elevates ROS level and turns the drug-resistant cells from a cytostatic response into a cytotoxic response, which presents as a novel therapeutic strategy that can be potentially applied as an alternating dosing schedule treatment between two drugs. By administrating the first drug to push the cancer cells into a "trap" to develop a vulnerability, and then follow by killing them with the second drug, which targets the vulnerability. By using this strategy, we may also avoid drug-toxicities as the drugs are given sequentially rather than simultaneously.

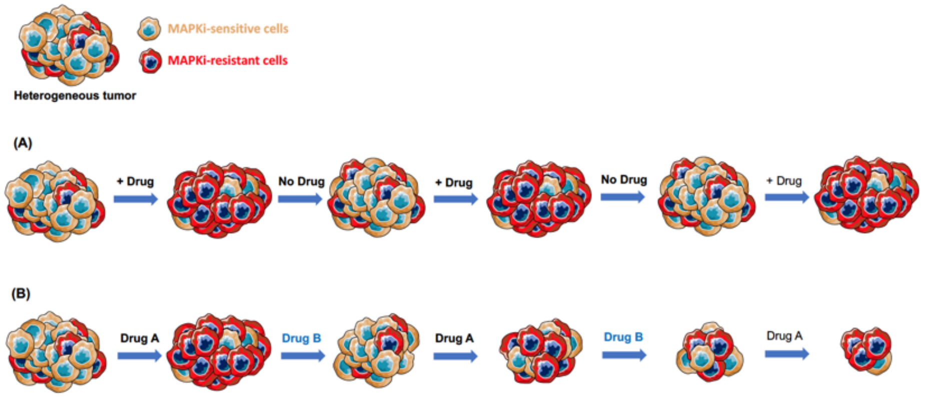

Figure 6: Alternative drug administration schedules.
(A) Intermittent dosing uses regular "drug holidays" in which the patient is not exposed to the drug. Cancer cells that have developed resistance to a cancer drug may be at a selective disadvantage in the absence of drug, leading to a decline in the fraction of drug resistant cells in this drug holiday. This should result in increased response when the drug is given again, as the fraction of drug sensitive cells should have increased during the drug holiday. (B) Alternating dosing can be applied if a vulnerability of drug-resistant cells has been identified. After the first treatment with a given cancer drug, the drug-resistant cells can be selectively eliminated with a second drug, after which the population should be sensitive to the first drug again.

A one-two punch model for cancer therapy

Yet, the cases of intermittent dosing and MAPKi-HDACi alternating dosage are limited to the setting of MAPK inhibition in melanomas. Can the model of sequential or alternating drug treatment be generalized to apply to all forms of cancer? In Chapter 5, we demonstrate a more broadly applicable therapeutic concept: the "one-two punch" model for the treatment of cancer. In this study we show that functional genetic or compound screens can be used to identify potent senescence inducers. We firstly use these senescence inducers as the first punch to drive cancer cells into senescence. Such senescent cells display a stable proliferation arrest but remain viable. Importantly, their cellular state is quite distinct from that of proliferating cells (Munoz-Espin and Serrano, 2014). For instance, senescent cells are distinct in terms of gene expression, chromatin structure and metabolism (Fridman and Tainsky, 2008; Jiang et al., 2013; Narita et al., 2003; Wiley and Campisi, 2016). This suggests that they might be sensitive to drugs that specifically target this acquired state and therefore do not kill their proliferating counterparts. As the second punch, we use a senolytic agent to efficiently kill these drug-induced senescent cancer cells (Figure 7). For example, ABT263, a specific inhibitor of anti-apoptotic proteins has been shown to selectively kill senescent cells *in vivo* (Chang et al., 2016; Zhu et al., 2016). Indeed, ABT263 can be applied to eradicate senescent cells induced by the drugs we identified from our functional genetic and compound screens (Wang et al., 2017a) (Chapter 5). If first punch can drive tumors into a senescent state, why is there a need to give the second punch? Although the cell arrest character of senescent cancer cells has been considered as a favorable outcome to control tumor growth in the clinic, these non-dividing senescent cancer cells are alive and produce a complex mixture of cytokines, chemokines, growth factors, proteases and metabolites (collectively called the Senescence-Associated Secretory Phenotype, SASP), which represents a potentially double-edged sword with respect to tumor control (Coppe et al., 2010; Coppe et al., 2008). On the one hand, the SASP can inhibit the growth of cancer by triggering an immunological response against the tumor through recruitment of phagocytic cells and lymphocytes from the adaptive immune system (Eggert et al., 2016). On the other hand, the SASP can also be potentially deleterious. When senescent cells remain present in a tumor, they can contribute to a chronic inflammatory response and stimulate the infiltration of leukocytes, which produce reactive toxic moieties that can cause DNA damage, which can result in acceleration of age-associated conditions (Baker et al., 2016; Kang et al., 2011) and cancer metastases (Angelini et al., 2013). Besides, senescent cells also contribute to the side effects of certain anti-cancer therapies. A recent study showed that elimination of chemotherapy-induced senescent cells reduced several side effects of treatment, including heart toxicity, bone marrow suppression, loss of strength and physical activity and cancer recurrence and metastasis (Demaria et al., 2017). These characters of senescent cells underscore the potential need to apply a senolytic drug as the second punch to eliminate the senescent cancer cells that arose during the first therapy. This potential strategy may not only control the tumor growth, but also reduce the side effects of the pro-senescence therapy.

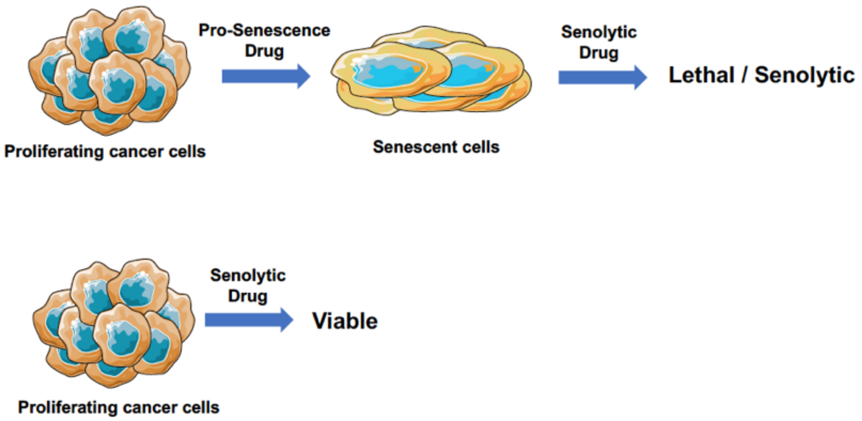

Figure 7: A one-two punch model for cancer therapy.
Pro-senescence drugs can be used to induce a stable proliferation arrest associated with the onset of senescence in cancer cells. A subsequent therapy with agents that kill senescent cells (senolytic drugs) can then be applied to selectively eradicate the senescent cancer cells. Note that the proliferating cancer cells are not sensitive to the senolytic agents, which makes a sequential treatment schedule necessary.

An important advantage of such a one-two punch therapy model is that drugs are not given in combination but sequentially, which allows for more drugs to be combined as sequential or alternating treatments avoid toxicity of simultaneous drug administration. As such, the "one-two" punch therapeutic concept provides an opportunity to design sequential or alternating anti-cancer treatment strategies, which can be broadly apply to multiple cancer types and thereby provides opportunities to improve not only the use of existing anti-cancer drugs, but also develop of novel senescence-inducing and senolytic drugs.

References

Angelini, P.D., Zacarias Fluck, M.F., Pedersen, K., Parra-Palau, J.L., Guiu, M., Bernado Morales, C., Vicario, R., Luque-Garcia, A., Navalpotro, N.P., Giralt, J., et al. (2013). Constitutive HER2 signaling promotes breast cancer metastasis through cellular senescence. Cancer Res 73, 450-458.

Baker, D.J., Childs, B.G., Durik, M., Wijers, M.E., Sieben, C.J., Zhong, J., Saltness, R.A., Jeganathan, K.B., Verzosa, G.C., Pezeshki, A., et al. (2016). Naturally occurring p16(Ink4a)-positive cells shorten healthy lifespan. Nature 530, 184-189.

Bardelli, A., and Siena, S. (2010). Molecular mechanisms of resistance to cetuximab and panitumumab in colorectal cancer. J Clin Oncol 28, 1254-1261.

Benvenuti, S., Sartore-Bianchi, A., Di Nicolantonio, F., Zanon, C., Moroni, M., Veronese, S., Siena, S., and Bardelli, A. (2007). Oncogenic activation of the RAS/RAF signaling pathway impairs the response of metastatic colorectal cancers to anti-epidermal growth factor receptor antibody therapies. Cancer Res 67, 2643-2648.

Brunen, D., and Bernards, R. (2017). Drug therapy: Exploiting synthetic lethality to improve cancer therapy. Nat Rev Clin Oncol 14, 331-332.

Chang, J., Wang, Y., Shao, L., Laberge, R.M., Demaria, M., Campisi, J., Janakiraman, K., Sharpless, N.E., Ding, S., Feng, W., et al. (2016). Clearance of senescent cells by ABT263 rejuvenates aged hematopoietic stem cells in mice. Nat Med 22, 78-83.

Chapman, P.B., Hauschild, A., Robert, C., Haanen, J.B., Ascierto, P., Larkin, J., Dummer, R., Garbe, C., Testori, A., Maio, M., et al. (2011). Improved survival with vemurafenib in melanoma with BRAF V600E mutation. N Engl J Med 364, 2507-2516.

Coppe, J.P., Desprez, P.Y., Krtolica, A., and Campisi, J. (2010). The senescence-associated secretory phenotype: the dark side of tumor suppression. Annu Rev Pathol 5, 99-118.

Coppe, J.P., Patil, C.K., Rodier, F., Sun, Y., Munoz, D.P., Goldstein, J., Nelson, P.S., Desprez, P.Y., and Campisi, J. (2008). Senescence-associated secretory phenotypes reveal cell-nonautonomous functions of oncogenic RAS and the p53 tumor suppressor. PLoS Biol 6, 2853-2868.

Das Thakur, M., Salangsang, F., Landman, A.S., Sellers, W.R., Pryer, N.K., Levesque, M.P., Dummer, R., McMahon, M., and Stuart, D.D. (2013). Modelling vemurafenib resistance in melanoma reveals a strategy to forestall drug resistance. Nature 494, 251-255.

Demaria, M., O'Leary, M.N., Chang, J., Shao, L., Liu, S., Alimirah, F., Koenig, K., Le, C., Mitin, N., Deal, A.M., et al. (2017). Cellular Senescence Promotes Adverse Effects of Chemotherapy and Cancer Relapse. Cancer Discov 7, 165-176.

Dexter, D.L., and Leith, J.T. (1986). Tumor heterogeneity and drug resistance. J Clin Oncol 4, 244-257.

Eggert, T., Wolter, K., Ji, J., Ma, C., Yevsa, T., Klotz, S., Medina-Echeverz, J., Longerich, T., Forgues, M., Reisinger, F., et al. (2016). Distinct Functions of Senescence-Associated Immune Responses in Liver Tumor Surveillance and Tumor Progression. Cancer Cell 30, 533-547.

Emery, C.M., Vijayendran, K.G., Zipser, M.C., Sawyer, A.M., Niu, L., Kim, J.J., Hatton, C., Chopra, R., Oberholzer, P.A., Karpova, M.B., et al. (2009). MEK1 mutations confer resistance to MEK and B-RAF inhibition. Proc Natl Acad Sci U S A 106, 20411-20416.

Flaherty, K.T., Infante, J.R., Daud, A., Gonzalez, R., Kefford, R.F., Sosman, J., Hamid, O., Schuchter, L., Cebon, J., Ibrahim, N., et al. (2012). Combined BRAF and MEK inhibition in melanoma with BRAF V600 mutations. N Engl J Med 367, 1694-1703.

Flaherty, K.T., Puzanov, I., Kim, K.B., Ribas, A., McArthur, G.A., Sosman, J.A., O'Dwyer, P.J., Lee, R.J., Grippo, J.F., Nolop, K., et al. (2010). Inhibition of mutated, activated BRAF in metastatic melanoma. N Engl J Med 363, 809-819.

Fridman, A.L., and Tainsky, M.A. (2008). Critical pathways in cellular senescence and immortalization revealed by gene expression profiling. Oncogene 27, 5975-5987.

Holderfield, M., Deuker, M.M., McCormick, F., and McMahon, M. (2014). Targeting RAF kinases for cancer therapy: BRAF-mutated melanoma and beyond. Nat Rev Cancer 14, 455-467.

Hutchison, D.J. (1963). Cross Resistance and Collateral Sensitivity Studies in Cancer Chemotherapy. Adv Cancer Res 7, 235-250.

Imamovic, L., and Sommer, M.O. (2013). Use of collateral sensitivity networks to design drug cycling protocols that avoid resistance development. Sci Transl Med 5, 204ra132.

Jiang, P., Du, W., Mancuso, A., Wellen, K.E., and Yang, X. (2013). Reciprocal regulation of p53 and malic enzymes modulates metabolism and senescence. Nature 493, 689-693.

Kang, T.W., Yevsa, T., Woller, N., Hoenicke, L., Wuestefeld, T., Dauch, D., Hohmeyer, A., Gereke, M., Rudalska, R., Potapova, A., et al. (2011). Senescence surveillance of pre-malignant hepatocytes limits liver cancer development. Nature 479, 547-551.

Kobayashi, S., Boggon, T.J., Dayaram, T., Janne, P.A., Kocher, O., Meyerson, M., Johnson, B.E., Eck, M.J., Tenen, D.G., and Halmos, B. (2005). EGFR mutation and resistance of non-small-cell lung cancer to gefitinib. N Engl J Med 352, 786-792.

Kopetz, S., Desai, J., Chan, E., Hecht, J.R., O'Dwyer, P.J., Maru, D., Morris, V., Janku, F., Dasari, A., Chung, W., et al. (2015). Phase II Pilot Study of Vemurafenib in Patients With Metastatic BRAF-Mutated Colorectal Cancer. J Clin Oncol 33, 4032-4038.

Lievre, A., Bachet, J.B., Le Corre, D., Boige, V., Landi, B., Emile, J.F., Cote, J.F., Tomasic, G., Penna, C., Ducreux, M., et al. (2006). KRAS mutation status is predictive of response to cetuximab therapy in colorectal cancer. Cancer Res 66, 3992-3995.

Lipinski, K.A., Barber, L.J., Davies, M.N., Ashenden, M., Sottoriva, A., and Gerlinger, M. (2016). Cancer Evolution and the Limits of Predictability in Precision Cancer Medicine. Trends Cancer 2, 49-63.

Long, G.V., Fung, C., Menzies, A.M., Pupo, G.M., Carlino, M.S., Hyman, J., Shahheydari, H., Tembe, V., Thompson, J.F., Saw, R.P., et al. (2014a). Increased MAPK reactivation in early resistance to dabrafenib/trametinib combination therapy of BRAF-mutant metastatic melanoma. Nat Commun 5, 5694.

Long, G.V., Stroyakovskiy, D., Gogas, H., Levchenko, E., de Braud, F., Larkin, J., Garbe, C., Jouary, T., Hauschild, A., Grob, J.J., et al. (2014b). Combined BRAF and MEK inhibition versus BRAF inhibition alone in melanoma. N Engl J Med 371, 1877-1888.

Luke, J.J., Flaherty, K.T., Ribas, A., and Long, G.V. (2017). Targeted agents and immunotherapies: optimizing outcomes in melanoma. Nat Rev Clin Oncol 14, 463-482.

McMahon, M. (2015). Intermittent dosing in melanoma. Clin Adv Hematol Oncol 13, 348-350.

Mueller, K.L., Madden, J.M., Zoratti, G.L., Kuperwasser, C., List, K., and Boerner, J.L. (2012). Fibroblast-secreted hepatocyte growth factor mediates epidermal growth factor receptor tyrosine kinase inhibitor resistance in triple-negative breast cancers through paracrine activation of Met. Breast Cancer Res 14, R104.

Munoz-Espin, D., and Serrano, M. (2014). Cellular senescence: from physiology to pathology. Nat Rev Mol Cell Biol 15, 482-496.

Narita, M., Nunez, S., Heard, E., Narita, M., Lin, A.W., Hearn, S.A., Spector, D.L., Hannon, G.J., and Lowe, S.W. (2003). Rb-mediated heterochromatin formation and silencing of E2F target genes during cellular senescence. Cell 113, 703-716.

Pao, W., Miller, V.A., Politi, K.A., Riely, G.J., Somwar, R., Zakowski, M.F., Kris, M.G., and Varmus, H. (2005). Acquired resistance of lung adenocarcinomas to gefitinib or erlotinib is associated with a second mutation in the EGFR kinase domain. PLoS Med 2, e73.

Prahallad, A., Sun, C., Huang, S., Di Nicolantonio, F., Salazar, R., Zecchin, D., Beijersbergen, R.L., Bardelli, A., and Bernards, R. (2012). Unresponsiveness of colon cancer to BRAF(V600E) inhibition through feedback activation of EGFR. Nature 483, 100-103.

Sanchez-Laorden, B., Viros, A., Girotti, M.R., Pedersen, M., Saturno, G., Zambon, A., Niculescu-Duvaz, D., Turajlic, S., Hayes, A., Gore, M., et al. (2014). BRAF inhibitors induce metastasis in RAS mutant or inhibitor-resistant melanoma cells by reactivating MEK and ERK signaling. Sci Signal 7, ra30.

Sartore-Bianchi, A., Martini, M., Molinari, F., Veronese, S., Nichelatti, M., Artale, S., Di Nicolantonio, F., Saletti, P., De Dosso, S., Mazzucchelli, L., et al. (2009). PIK3CA mutations in colorectal cancer are associated with clinical resistance to EGFR-targeted monoclonal antibodies. Cancer Res 69, 1851-1857.

Seghers, A.C., Wilgenhof, S., Lebbe, C., and Neyns, B. (2012). Successful rechallenge in two patients with BRAF-V600-mutant melanoma who experienced previous progression during treatment with a selective BRAF inhibitor. Melanoma Res 22, 466-472.

Shi, H., Moriceau, G., Kong, X., Lee, M.K., Lee, H., Koya, R.C., Ng, C., Chodon, T., Scolyer, R.A., Dahlman, K.B., et al. (2012). Melanoma whole-exome sequencing identifies (V600E) B-RAF amplification-mediated acquired B-RAF inhibitor resistance. Nat Commun 3, 724.

Straussman, R., Morikawa, T., Shee, K., Barzily-Rokni, M., Qian, Z.R., Du, J., Davis, A., Mongare, M.M., Gould, J., Frederick, D.T., et al. (2012). Tumour micro-environment elicits innate resistance to RAF inhibitors through HGF secretion. Nature 487, 500-504.

Sun, C., and Bernards, R. (2014). Feedback and redundancy in receptor tyrosine kinase signaling: relevance to cancer therapies. Trends Biochem Sci 39, 465-474.

Sun, C., Wang, L., Huang, S., Heynen, G.J., Prahallad, A., Robert, C., Haanen, J., Blank, C., Wesseling, J., Willems, S.M., et al. (2014). Reversible and adaptive resistance to BRAF(V600E) inhibition in melanoma. Nature 508, 118-122.

Treiber, N., Huber, M.A., Schneider, L.A., Scharffetter-Kochanek, K., Schultz, E., and Debus, D. (2017). Intermittent vemurafenib therapy in malignant melanoma. J Dtsch Dermatol Ges 15, 451-454.

van Geel, R., Tabernero, J., Elez, E., Bendell, J.C., Spreafico, A., Schuler, M., Yoshino, T., Delord, J.P., Yamada, Y., Lolkema, M.P., et al. (2017). A Phase Ib Dose-Escalation Study of Encorafenib and Cetuximab with or without Alpelisib in Metastatic BRAF-Mutant Colorectal Cancer. Cancer Discov 7, 610-619.

Wang, L., Leite de Oliveira, R., Wang, C., Fernandes Neto, J.M., Mainardi, S., Evers, B., Lieftink, C., Morris, B., Jochems, F., Willemsen, L., et al. (2017a). High-Throughput Functional Genetic and Compound Screens Identify Targets for Senescence Induction in Cancer. Cell Rep 21, 773-783.

Wang, L., Sustic, T., Leite de Oliveira, R., Lieftink, C., Halonen, P., van de Ven, M., Beijersbergen, R.L., van den Heuvel, M.M., Bernards, R., and van der Heijden, M.S. (2017b). A Functional Genetic Screen Identifies the Phosphoinositide 3-kinase Pathway as a Determinant of Resistance to Fibroblast Growth Factor Receptor Inhibitors in FGFR Mutant Urothelial Cell Carcinoma. Eur Urol 71, 858-862.

Wang, S., Tsui, S.T., Liu, C., Song, Y., and Liu, D. (2016). EGFR C797S mutation mediates resistance to third-generation inhibitors in T790M-positive non-small cell lung cancer. J Hematol Oncol 9, 59.

Weinstein, I.B. (2002). Cancer. Addiction to oncogenes--the Achilles heal of cancer. Science 297, 63-64.

Wiley, C.D., and Campisi, J. (2016). From Ancient Pathways to Aging Cells-Connecting Metabolism and Cellular Senescence. Cell Metab 23, 1013-1021.

Yun, C.H., Mengwasser, K.E., Toms, A.V., Woo, M.S., Greulich, H., Wong, K.K., Meyerson, M., and Eck, M.J. (2008). The T790M mutation in EGFR kinase causes drug resistance by increasing the affinity for ATP. Proc Natl Acad Sci U S A 105, 2070-2075.

Zhu, Y., Tchkonia, T., Fuhrmann-Stroissnigg, H., Dai, H.M., Ling, Y.Y., Stout, M.B., Pirtskhalava, T., Giorgadze, N., Johnson, K.O., Giles, C.B., et al. (2016). Identification of a novel senolytic agent, navitoclax, targeting the Bcl-2 family of anti-apoptotic factors. Aging Cell 15, 428-435.

A functional genetic screen identifies the PI3K pathway as a determinant of resistance to FGFR inhibitors in FGFR mutant urothelial cell carcinoma

2

Liqin Wang[1*], Tonci Sustic[1*], Rodrigo Leite de Oliveira[1*], Cor Lieftink[1], Pasi Halonen[1], Marieke van de Ven[2], Roderick L. Beijersbergen[1], Michel M. van den Heuvel[3], René Bernards[1#] and Michiel S. van der Heijden[1,3#]
* Co-first author
# Correspondence

1 Division of Molecular Carcinogenesis, Cancer Genomics Netherlands. The Netherlands Cancer Institute, Plesmanlaan 121, 1066 CX Amsterdam, The Netherlands.
2 Mouse Clinic Intervention unit. The Netherlands Cancer Institute, Plesmanlaan 121, 1066 CX Amsterdam, The Netherlands.
3 Division of Medical Oncology, Antoni van Leeuwenhoek Hospital, Plesmanlaan 121, 1066 CX Amsterdam, The Netherlands.

European Urology (2017)

Abstract

Activating mutations and translocations of the *FGFR3* gene are commonly seen in urothelial cell carcinoma (UCC) of the bladder and urinary tract. Several FGFR inhibitors are currently in clinical development and response rates appear promising for advanced UCC. A common problem with targeted therapeutics is intrinsic or acquired resistance of the cancer cells. To find potential drug targets that can act synergistically with FGFR inhibition, we performed a synthetic lethality screen for the FGFR inhibitor AZD4547 using an shRNA library targeting the human kinome in the UCC cell line RT112 (*FGFR3-TACC3* translocation). We identified multiple members of the PI3K pathway and found that inhibition of PIK3CA acts synergistically with FGFRi. The PI3K inhibitor BKM120 acted synergistically with inhibition of FGFR in multiple UCC and lung cancer cell lines having *FGFR* mutations. Consistently, we observed an elevated PI3K-AKT pathway activity resulting from EGFR or ERBB3 reactivation caused by FGFR inhibition as the underlying molecular mechanism of the synergy. Our data show that feedback pathways activated by FGFR inhibition converge on the PI3K pathway. These findings provide a strong rationale to test FGFR inhibitors in combination with PI3K inhibitors in cancers harboring genetic activation of *FGFR* genes.

Molecular pathways activated in urothelial cell carcinoma (UCC) could provide targets for new treatments. Fibroblast Growth Factor Receptors (FGFRs) are activated in a subset of UCC, most commonly by *FGFR3* mutation (hotspot mutation or translocation) or overexpression of *FGFR1*[1]. Clinical trials with FGFR inhibitors (FGFRi), such as AZD4547 and BGJ398, are currently ongoing in UCC. Initial results with BGJ398 showed encouraging response rates[2], though information on durability of these responses is currently lacking. Akin to other molecularly targeted therapies, resistance is likely to be a major concern. Resistance to FGFR inhibition was observed in vitro (Fig. 1a; Methods: see supplement): the *FGFR-TACC3* translocated cell line RT112 responded initially, but cells quickly adapted to AZD4547, an inhibitor of FGFR1, 2 and 3 (weaker activity against FGFR4). As resistance to targeted therapies often develops through feedback activation of additional signaling pathways, it is likely that FGFRi has to be combined with agents targeting additional molecular pathways. One such example is synergy between FGFRi with inhibitors of EGFR3. Feedback mechanisms that render cells insensitive to kinase inhibition often occur through activation of other kinases. Therefore we set out to screen an shRNA library targeting all 518 human kinases and 17 additional kinase-related genes to find genes whose inhibition enhances the sensitivity to FGFRi AZD4547 in *FGFR3* mutant UCC (Fig 1b). RT112 cells were infected with a lentiviral library containing some 5000 shRNAs and cultured in the absence or presence of AZD4547 for 14 days. Cells were then harvested, DNA was isolated and the relative abundance of shRNA vectors was measured by deep-sequencing. The readcounts were normalized and analyzed with DESeq2 to identify shRNAs and their corresponding target genes that show significant depletion in the presence and not in the absence of AZD4547 (supplemental table 1, 2). We observed multiple components of the PI3K signaling pathway including the catalytic component PIK3CA, the regulatory subunit PIK3R1 and the downstream target AKT3 (Fig1c). In addition, with the same criteria, we found EGFR for which synergy with FGFR inhibition has been described[3]. Because of the presence of several components of the PI3K pathway, we decided to focus our validation on the central node, the catalytic subunit of PI3K, PIK3CA. Three different shRNAs targeting *PIK3CA* were significantly depleted in the drug-treated group compared to the control. This suggested that suppression of *PIK3CA* synergizes with FGFRi in *FGFR3* mutant bladder cancer. To validate this finding, we infected RT112 cells with each of these 3 shRNAs targeting *PIK3CA* and treated with or without AZD4547 for 2 weeks. All three shRNAs against *PIK3CA* induce efficient knockdown of PIK3CA protein expression as determined by western blot analysis (Fig 1d). Parental RT112 cells did not significantly respond to FGFR inhibition or *PIK3CA* suppression alone, but knockdown of *PIK3CA* strongly enhanced the response to the FGFRi AZD4547 (Fig 1e).

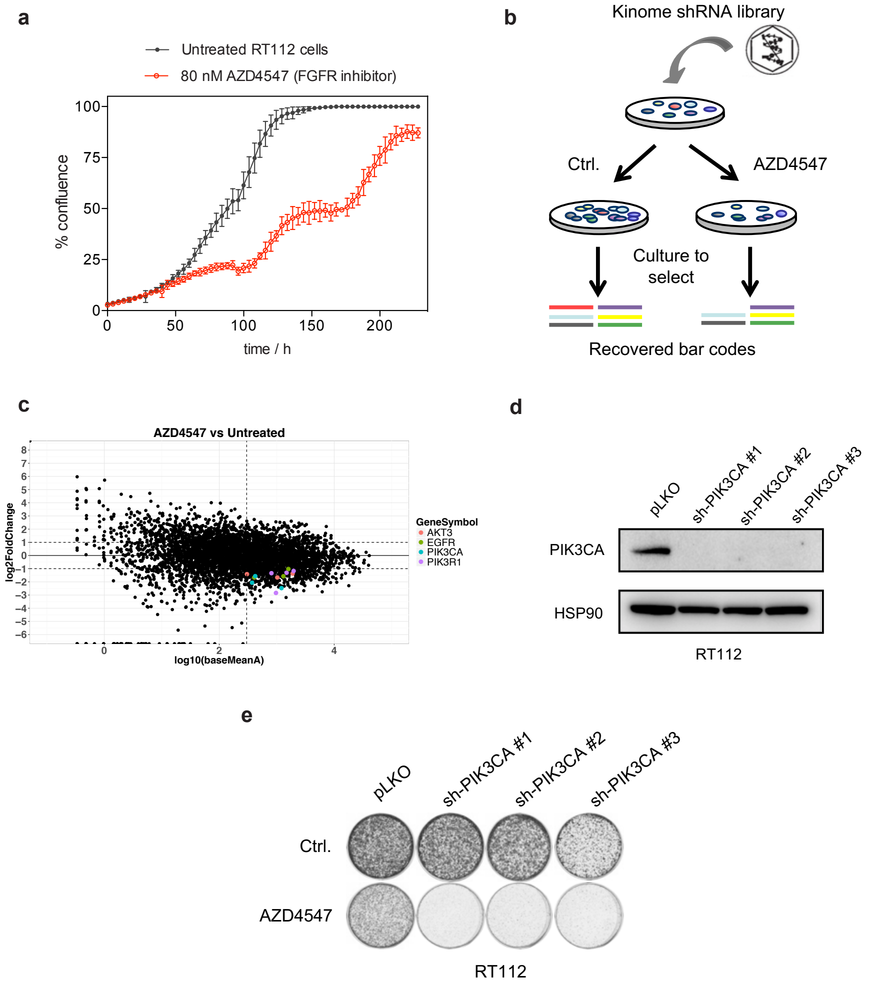

Fig 1: PIK3CA suppression enhances sensitivity to FGFR inhibition in UCC.

(a) RT112 cells were treated with AZD4547 (80 nM) and viability was followed using an incucyte assay. Error bars represent 4 biological replicates. (b) Outline of synthetic lethality shRNA screen for enhancers of AZD4547 sensitivity. Human kinome shRNA library polyclonal virus was produced to infect RT112 cells, which were then left untreated (Ctrl.) for 10 days or treated with 30 nM AZD4547 for 14 days. After selection, shRNA inserts from both arms were recovered by PCR and their abundance was quantified by deep sequencing. (c) Representation of the relative abundance of the shRNA barcode sequences from the shRNA screen. The y-axis shows log2 of the fold change of shRNA abundance of the treated and untreated samples. The x-axis indicates the log 10 of the average read count of each shRNA in the untreated sample. shPIK3CA, shPIK3R1, shAKT3 and shEGFR identified as the top hit according to the presence of at least 3 independent shRNAs in 3 biological screen replicates. (d) The level of knockdown of *PIK3CA* by 3 different shRNAs was measured by PIK3CA protein levels by western blot. HSP90 protein expression is used for normalization. (e) The functional phenotypes of independent shPIK3CA vectors are indicated by colony formation assay in 50 nM AZD4547. The cells were fixed, stained and photographed after 10 days.

We next investigated whether pharmaceutical inhibition of the PI3K pathway was also synergistic with FGFR inhibition using BKM120 a pan-PI3K inhibitor with modest anti-tumor activity in cancer patients as a single agent. We found that both RT112 (*FGFR3-TACC3* translocation[4]) and JMSU1 (*FGFR1* amplification[5]) were not significantly inhibited by BKM120 or AZD4547 monotherapy. However, synergy was observed with the combination, tested by long-term in vitro colony formation assays (Fig 2a,b), incucyte proliferation assay (Supplementary Fig 1. a, b) and synergy assays (Supplementary Fig 1. c). Moreover, biochemical analysis indicated that the combination resulted in the induction of cleaved poly (ADP-ribose) polymerase (c-PARP), a hallmark of apoptosis (Fig 2c, d). To expand our results to another cancer type with FGFR alterations, we tested this drug combination in two independent *FGFR1* amplified lung cancer cell line models: H520 (squamous cell carcinoma) and DMS114 (small cell carcinoma)[6]. As observed in the UCC lines, these two lung cancer cell models showed apoptosis in response to the drug combination, but not to either drug alone (Supplementary Fig 1. d-g). Of note, similar results were recently obtained for ponatinib (a FGFR inhibitor) in combination with mTOR inhibition in NSCLC cells[7].

To address the molecular mechanism underlying the synergy between PI3K and FGFR inhibition, we further analyzed signaling pathways in AZD4547-treated RT112 cells using Receptor Tyrosine Kinase (RTK) phosphorylation blots (Fig 2e). We found that FGFR inhibition induced a feedback mechanism to activate ERBB3 and to a lesser extent EGFR. As a consequence, PI3K-AKT signaling was activated, thereby presumably blunting the effects of FGFRi (Fig 2f). Feedback activation of RTKs (EGFR3 and ligand-associated ERBB2/ERBB3[8]) has been reported before. Our findings provide a strong rationale that feedback signaling converges on the PI3K pathway, but not on the BRAF-MEK-ERK pathway (Fig 2f), and resistance could be counteracted by PI3K inhibitors, in order to enhance the FGFRi sensitivity.

To test the combination treatment in vivo, we engrafted RT112 bladder cancer cells into immunodeficient NMRI-nu mice. When tumors reached approximately 100 mm^3, mice were randomized into different cohorts and treated with vehicle, AZD4547, BKM120 or the drug combination. As shown in Fig 2g, treatment with the single drugs AZD4547 or BKM120 resulted in limited tumor growth inhibition. However, treatment with the combination of AZD4547 and BKM20 resulted in persistent suppression of tumor growth throughout the duration of the experiment. Immunohistochemistry staining of the tumors at the end of the experiment (supplementary Fig 1. i) shows the combination suppressed tumor proliferation (Ki67) and inducted apoptosis (cleaved caspase 3).

We also found that in two FGFR3-activated cell lines, MGHU3 and SW780, synergy was not observed (Supplementary Fig 1. h j). MGHU3 cells carry an activating mutation in the *AKT1* (E17K) gene, causing pathway activation downstream of PIK3CA[9]. Indeed, these cells were highly sensitive to mTOR inhibition (AZD8055). This finding suggests that comprehensive genetic profiling remains relevant before initiating combination tre-

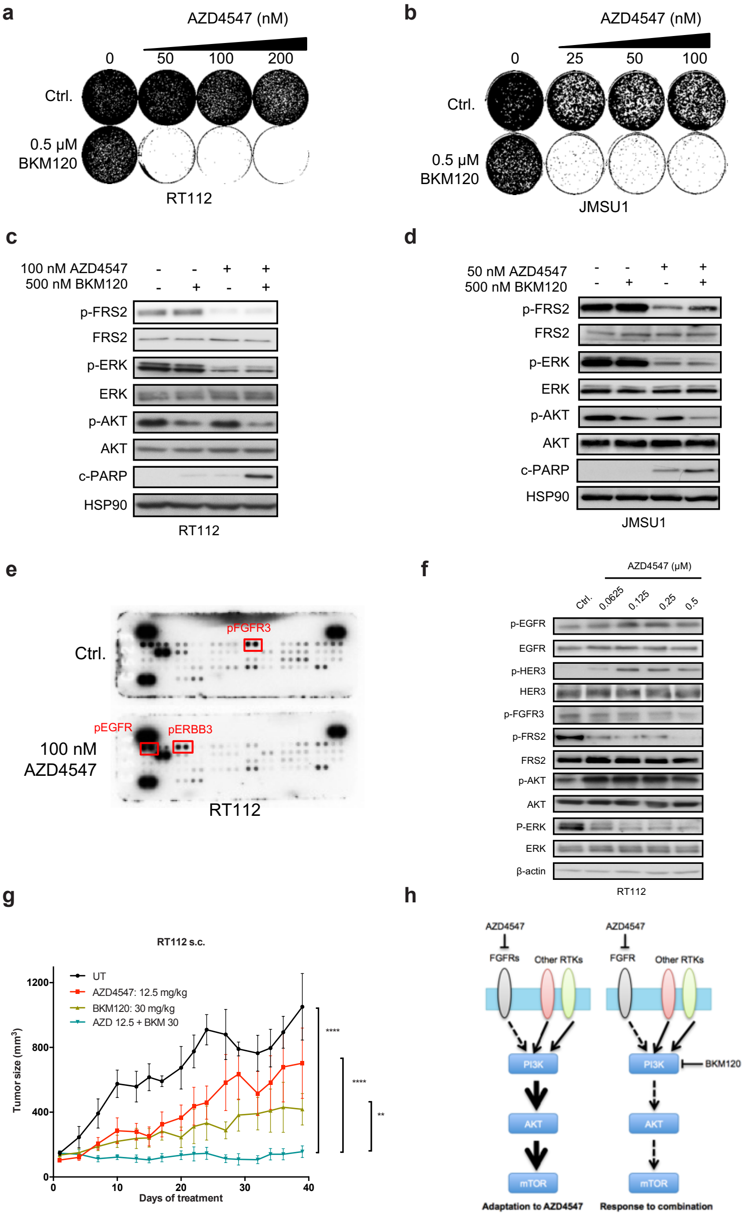

Fig 2: Functional and biochemical interaction between FGFR and PI3K inhibition in UCC.
(a,b) Synergistic response of RT112(a) and JMSU1(b) to combinations of FGFR (AZD4547) and PI3K (BKM120) inhibitors. RT112 and JMSU1 cells were cultured in increasing concentration of FGFRi AZD4547 alone, PI3Ki BKM120 (0.5 µM) alone, or their combination. The cells were fixed, stained and photographed after 14 days. (c,d) Biochemical analysis of combination of FGFR and PI3K inhibitors. RT112 and JMSU1 cells were harvested after 24 hours of drug treatment. Phosphorylated-AKT (p-AKT), total AKT (AKT), cleaved-PARP (c-PARP), phosphorylated-FRS2 (p-FRS2), total FRS2 (FRS2), phosphorylated-ERK (p-ERK) and total ERK (ERK) were measured. HSP90 served as a loading control. (e) RTK blot analysis of FGFRi (100nM, 7 days) treated RT112. AZD4547 induced feedback activation of

EGFR and ERBB3. (f) Biochemical analysis indicated the reactivation of EGFR and ERBB3 in association with elevated PI3K-AKT signaling, but not MAPK signaling after treating RT112 cells for 1 week with 50 mM AZD4547. Phosphorylated-EGFR (p-EGFR), Total EGFR (EGFR), phosphorylated-ERBB3 (p-ERBB3), total HER3 (HER3), phosphorylated-FGFR3 (p-FGFR3), phosphorylated-AKT (p-AKT), total AKT (AKT), phosphorylated-FRS2 (p-FRS2), total FRS2 (FRS2), phosphorylated-ERK (p-ERK) and total ERK (ERK) were measured. β-actin served as a loading control. (g) FGFRi (AZD4547) in combination with PI3Ki (BKM120) significantly suppresses tumor growth in RT112 xenograft model. (**** $p<0.0001$, ** $p<0.01$ ANOVA)(h) FGFR altered tumors initially respond to FGFR inhibition. However, the tumor cells are able to up-regulate other RTKs that result in enhanced signaling through the PI3K-AKT pathway, leading to drug resistance. Combining FGFR inhibition with a PI3K inhibitor eliminates the PI3K-AKT activity and synergistically kills cancer cells.

atment, in order to establish the best possible treatment. SW780 cells carry a translocation, *FGFR3-BAIAP2L1*[4]. This translocation has not been found in other cancers and the mechanism of FGFR activation is unknown, though cells appear to be dependent on FGFR signaling[10]. Other resistance pathways could therefore be active in this cell line.

In conclusion, our data show that resistance pathways to FGFR inhibition often converge on the PI3K pathway. In addition to upstream RTK activation, FGFR-activated tumors can have co-occurrence of mutations in the *PIK3CA* gene. These activating mutations would not be targeted by addition of upstream RTK inhibitors. Our data provide a strong rationale to treat FGFR3-altered UCC with a combination of FGFR and PI3K inhibitors (Fig 2h). These results may apply to other cancer types as well, for example squamous NSCLC.

References

1.Cancer Genome Atlas Research N. Comprehensive molecular characterization of urothelial bladder carcinoma. Nature 2014;507:315-22.

2.Herrera-Abreu MT, Pearson A, Campbell J, et al. Parallel RNA interference screens identify EGFR activation as an escape mechanism in FGFR3-mutant cancer. Cancer Discov 2013;3:1058-71.

3.Prahallad A, Sun C, Huang S, et al. Unresponsiveness of colon cancer to BRAF(V600E) inhibition through feedback activation of EGFR. Nature 2012;483:100-3.

4.Williams SV, Hurst CD, Knowles MA. Oncogenic FGFR3 gene fusions in bladder cancer. Hum Mol Genet 2013;22:795-803.

5.Pearson A, Smyth E, Babina IS, et al. High-Level Clonal FGFR Amplification and Response to FGFR Inhibition in a Translational Clinical Trial. Cancer Discov 2016;6:838-51.

6.Weiss J, Sos ML, Seidel D, et al. Frequent and focal FGFR1 amplification associates with therapeutically tractable FGFR1 dependency in squamous cell lung cancer. Sci Transl Med 2010;2:62ra93.

7.Wang J, Mikse O, Liao RG, et al. Ligand-associated ERBB2/3 activation confers acquired resistance to FGFR inhibition in FGFR3-dependent cancer cells. Oncogene 2015;34:2167-77.
8.Bernard-Pierrot I, Brams A, Dunois-Larde C, et al. Oncogenic properties of the mutated forms of fibroblast growth factor receptor 3b. Carcinogenesis 2006;27:740-7.

9.Wu YM, Su F, Kalyana-Sundaram S, et al. Identification of targetable FGFR gene fusions in diverse cancers. Cancer Discov 2013;3:636-47.

10.Davies BR, Guan N, Logie A, et al. Tumors with AKT1E17K Mutations Are Rational Targets for Single Agent or Combination Therapy with AKT Inhibitors. Mol Cancer Ther 2015;14:2441-51.

Materials and methods

Synthetic lethality screen

A kinome shRNA library targeting the complete 518 human kinases and 17 kinase related genes with 5 shRNA's on average per gene were constructed from The RNAi Consortium (TRC) human genome-wide shRNA collection. The kinome library was used to generate a single pool of lentiviral shRNAs to infect RT112 cells. After infection and selection for lentiviral integration, cells were treated with or without 30 nM AZD4547 for 10 days. Next-generation sequencing was used to determine the relative abundance of each shRNA in the different populations. The read count data was analyzed using DESeq2. The analysis was restricted to those shRNAs with a read count >300 in the untreated sample, a log2 fold change treated/untreated of less than -1 and a adjusted p-value of <0.1. For hit selection, we selected those genes that were represented with 3 or more different shRNAs in the hit list as defined above. This resulted in a final hit list of 18 genes. The detailed screen procedure is described in Prahallad et al[3].

Long-term colony formation assay and IncuCyte cell proliferation assays

Cells were seeded into 6-well plates (20,000-50,000 cells per well) and cultured both in the absence and presence of drugs as indicated for 10-15 days. At the end of the assay, cells were fixed with 4% of formaldehyde (#1.04002, Millipore) diluted in PBS, stained with 2% of crystal violet (#HT90132 Sigma-Aldrich) diluted in water and photographed. For IncuCyte proliferation assays, cells were seeded in 96-well plate (2000 cells per well) and cultured in absence or presence of drugs as indicated. Cell confluence was measured and quantified by the IncuCyte imaging system (Essen Bioscience).

Protein lysate preparation and immunoblotting

Cells were seeded in DMEM-based medium containing 10% fetal bovine serum (FBS) in the absence or presence of drug for indicated time. The drugs were refreshed every 3 days. Afterwards, the cells were washed with PBS and lysed with RIPA buffer supplemented with protease inhibitors (cOmplete, Roche) and phosphatase inhibitor cocktails II and III (Sigma). All lysates were freshly prepared and processed with Novex NuPAGE Gel Electrophoresis Systems (Invitrogen). Antibodies against HSP90 (sc-33755), p-FGFR3 (SC-33041), p-ERK (SC-16982), ERK and β-actin (SC-47778) were from Santa Cruz Biotechnology; cleaved-PARP (#5625), p-AKT (#4046), AKT (#4691), p-HER3 (#4791), HER3 (#12708), PIK3CA (#4254), p-MEK (#9154), ERK (#9102) and MEK (#4694) were from Cell Signaling; p-EGFR (ab5644) and p-FRS2 (ab193363) were from Abcam; FRS2 (11503-1-AP) was from Proteintech.

RTK blot assay

Cells were cultured in the absence or presence of drugs for 1 week, every 3 days refreshed. Phosphorylation of RTKs was measured using Human Phospho-Receptor Tyrosine Kinase

Array Kit (ARY001B, R&D system) according to the manufacturer's instructions.

Synergy assay

To assess whether combined effect of the FGFR and PI3K inhibitor treatment is additive or synergistic, RT112 and H520 cells were plated in 384-well plates and treated with a series of drug concentrations. After 5 days cell viability was measured by Cell Titre Blue assay. Synergy score was determined by subtracting the Loewe additivity matrix scores (calculated from the single drug treatments) from the experimental values of the FGFR and PI3K inhibitor combinations. A positive score indicates that the reduction in cell viability induced by the combination of the two compounds surpasses the effect that can be obtained by increasing concentrations of either two compounds alone.

Mouse xenografts and in vivo drug study

All animal procedures were approved by the Ethical commission of the Netherlands Cancer Institute. One million RT112 bladder cancer cells were injected subcutaneously into 7-week-old immunodeficient NMRI-nu mice (6 mice per group). Tumor volume was monitored three times a week, based on caliper measurements calculated with the formula: tumor volume = ½(length × width2). When tumors reached a volume of approximately 100 mm3, mice were randomized and treated daily by oral gavage with AZD4547 12.5 mg/kg, BKM120 30 mg/kg, combination of both drugs, or vehicle solution.

Online Content

Any additional Methods, tables, display items and Source Data are available in the online version of the paper.

https://www.sciencedirect.com/science/article/pii/S0302283817300374?via%3Dihub

Supplemental Figures

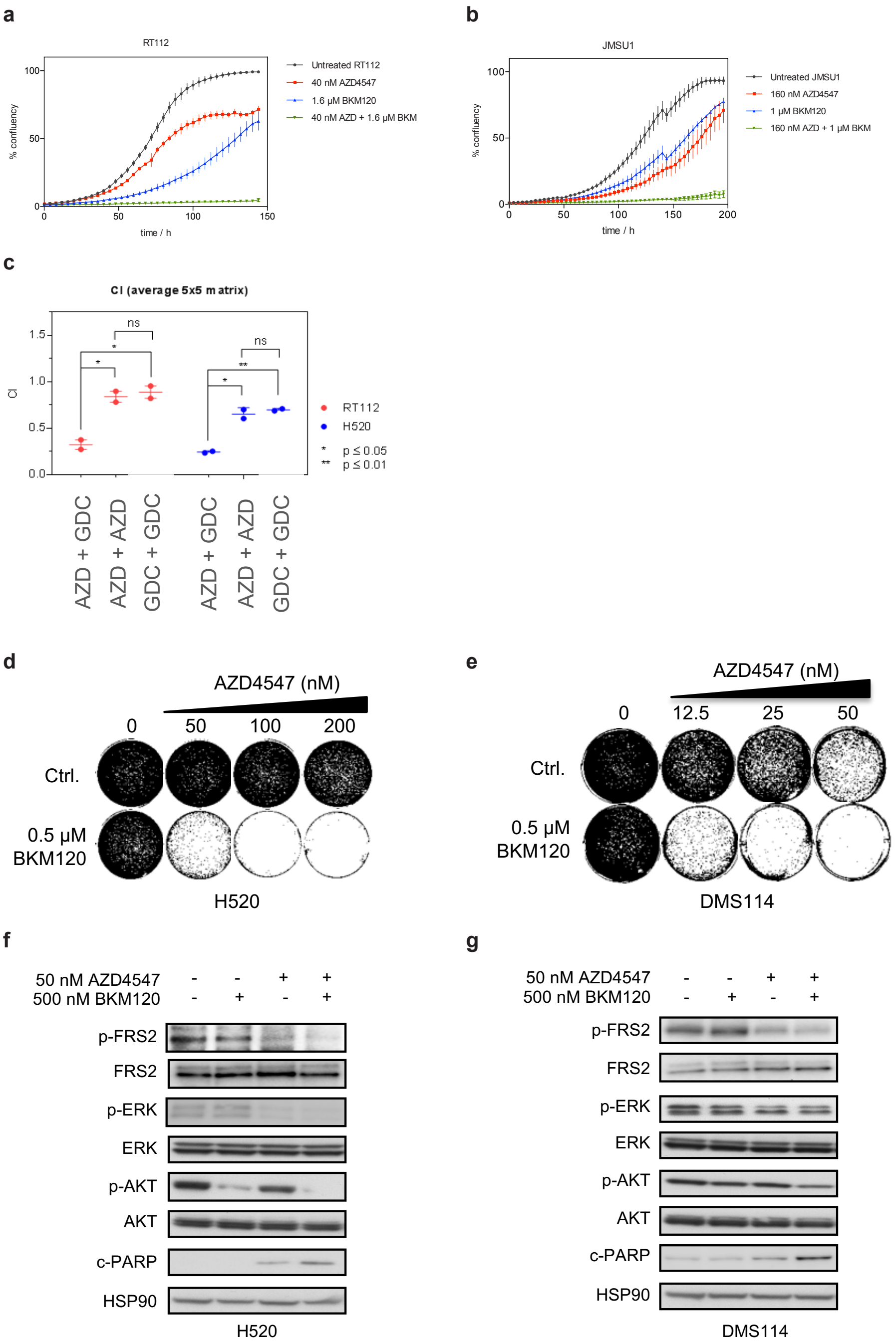

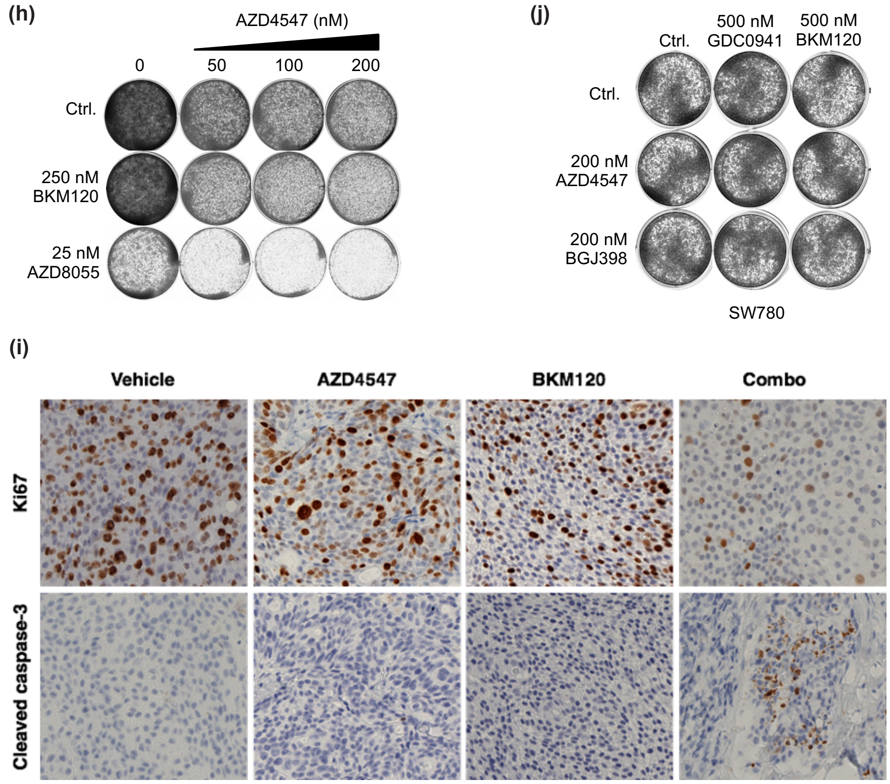

Fig Supplementary 1: Functional and biochemical interaction between FGFR and PI3K inhibition in FGFR-activated cancer models.

(a,b) Incucyte assay of RT112 and JMSU1, the cells were treated with AZD4547 and BKM120 at the indicated drug concentrations. (c) Synergy assay of RT112 and H520, the cells were treated with AZD4547 and GDC0941 at a range of concentrations. Cell titer blue was used as the read-out. (d,e) Synergistic response of H520(d) and DMS114 (e) to the combination of FGFR and PI3K inhibitors. H520 and DMS114 cells were cultured in increasing concentration of FGFRi AZD4547 alone, PI3Ki BKM120 (0,5 µM) alone, or their combination. The cells were fixed, stained and photographed after 14 days. (f,g) Biochemical analysis of the combination of FGFR and PI3K inhibitors. H520 and DMS114 cells lysis were harvested 24 hours after drug treatment. Phosphorylated-AKT (p-AKT), total AKT (AKT), cleaved-PARP (c-PARP) phosphorylated-FRS2 (p-FRS2), total FRS2 (FRS2) were measured. HSP90 served as a loading control. (h) Non-synergistic response of MGHU3 to the combination of FGFR and PI3K inhibitors. MGHU3 cells were cultured in increasing concentrations of FGFRi AZD4547 alone, PI3Ki BKM120 (0,25 µM) alone, or their combination. Targeting downstream molecule mTOR by AZD8055 sensitized MGHU3 cells to FGFR inhibition. The cells were fixed, stained and photographed after 14 days. (j) Non-synergistic response of SW780 to the combination of FGFR and PI3K inhibitors. Cells were cultured in indicated concentrations of FGFRi AZD4547 or BGJ398 alone, PI3Ki BKM120 or GDC0941 alone, or their combination. (i) Fixed tissues were dehydrated and embedded in paraffin. Sections of 2–4 µm were prepared and immunostained with Ki67 and cleaved caspase 3.

Reversible and adaptive resistance to BRAF(V600E) inhibition in melanoma

3

Chong Sun[1*], Liqin Wang[1*], Sidong Huang[1,2*], Guus J. J. E. Heynen[1], Anirudh Prahallad[1], Caroline Robert[3], John Haanen[4], Christian Blank[4], Jelle Wesseling[5], Stefan M.Willems[1,6], Davide Zecchin[7,8], Sebastijan Hobor[8], Prashanth K. Bajpe[1], Cor Lieftink[1], Christina Mateus[3], Stephan Vagner[3], Wipawadee Grernrum[1], Ingrid Hofland[5], Andreas Schlicker[1], Lodewyk F. A. Wessels[1], Roderick L. Beijersbergen[1], Alberto Bardelli[7,8,9], Federica Di Nicolantonio[7,8], Alexander M. M. Eggermont[3] & Rene Bernards[1#]

* Co-first author

# Correspondence

1 Division of Molecular Carcinogenesis, Cancer Systems Biology Centre and Cancer Genomics Centre Netherlands, The Netherlands Cancer Institute, Plesmanlaan 121, 1066 CX Amsterdam, The Netherlands.

2 Department of Biochemistry, The Rosalind and Morris Goodman Cancer Centre, McGill University, Montreal, Quebec H3G 1Y6, Canada.

3 Institut Gustave Roussy, 114 Rue Edouard Vaillant, 94800 Villejuif, France.

4 Division of Medical Oncology, Cancer Systems Biology Centre and Cancer Genomics Centre Netherlands, The Netherlands Cancer Institute, Plesmanlaan 121, 1066CXAmsterdam, The Netherlands.

5 Division of Pathology, Cancer Systems Biology Centre and Cancer Genomics Centre Netherlands, The Netherlands Cancer Institute, Plesmanlaan 121, 1066 CX Amsterdam, The Netherlands.

6 Department of Pathology, University Medical Centre Utrecht, Heidelberglaan 100, 3584 CX, Utrecht, The Netherlands.

7 University of Torino, Department of Oncology, Str prov 142 Km 3.95, 10060 Candiolo, Torino, Italy.

8 Candiolo Cancer Institute – FPO, IRCCS, Str prov 142 Km 3.95, 10060 Candiolo, Torino, Italy. 9FIRC Institute of Molecular Oncology (IFOM), 20139 Milano, Italy.

Nature (2014)

Abstract

Treatment of *BRAF(V600E)* mutant melanoma by small molecule drugs that target the BRAF or MEK kinases can be effective, but resistance develops almost invariably[1,2]. In contrast, colon cancers that harbour the same *BRAF(V600E)* mutation are intrinsically resistant to BRAF inhibitors, due to feedback activation of the Epidermal Growth Factor Receptor (EGFR)[3,4]. We show here that 5 out of 12 (40%) melanoma tumour specimen analysed acquired EGFR expression after the development of resistance to BRAF or MEK inhibitor drugs. Expression of EGFR is a disadvantage for melanoma cells in the absence of drug selection pressure, but becomes beneficial for proliferation in the presence of BRAF or MEK inhibitors. Using a chromatin regulator-focused shRNA library, we find that suppression of sex determining region Y-box 10 (SOX10) in melanoma causes upregulation of EGFR and confers resistance to BRAF and MEK inhibitors. SOX10 loss was also observed in the tumour of a melanoma patient that had acquired drug resistance and was associated with increased EGFR expression. In a heterogeneous population of melanoma cells having different levels of SOX10 suppression, cells with low SOX10 and consequently high EGFR expression are rapidly enriched in the presence of drug, but this is reversed when the drug treatment is discontinued. Our findings provide a rationale for why some melanoma patients that become resistant to BRAF or MEK inhibitors may regain sensitivity to these drugs after a drug holiday. Our data also suggest that melanomas that become EGFR-positive upon drug resistance are candidates for re-treatment after a drug holiday.

Activating mutations in the *BRAF* oncogene are found in over half of the patients with advanced melanoma[5,6]. Inhibition of the oncogenic BRAF protein with the small molecule inhibitor PLX4032 (vemurafenib) or its downstream effector MEK with GSK1120212 (trametinib) have shown impressive initial responses in patients with *BRAF* mutant melanoma[1,2]. However, single-agent therapies for advanced cancers are rarely curative, due to the rapid development of resistance. To date, several drug resistance mechanisms have been identified in melanomas treated with vemurafenib, including increased expression of the gene encoding the COT kinase, mutation of downstream *MEK1* (also known as *MAP2K1*) kinase, *NRAS* mutations and amplification or alternative splicing of the *BRAF* gene[7–11]. Moreover, increased expression of receptor tyrosine kinases (RTKs) has been observed as a mechanism of BRAF inhibitor resistance[11–13].

It has been shown recently that intrinsic resistance of *BRAF* mutant colon cancers to vemurafenib is the result of feedback activation of EGFR when BRAF is inhibited[3,4]. To investigate whether *BRAF(V600E)* mutant melanoma patients frequently develop resistance to BRAF or MEK inhibitors through acquired expression of EGFR in their tumours, we obtained biopsies from *BRAF(V600E)* mutant melanomas from 16 patients treated with either the MEK inhibitor trametinib (n=1) or the BRAF inhibitors dabrafenib (n=3) or vemurafenib (n=12). Tumour biopsies collected both before treatment initiation and after the development of drug resistance were stained for EGFR expression. We found that 6 out of 16 post-treatment biopsies gained notable EGFR expression as judged byimmunohistochemistry (Fig. 1a, b and Supplementary Table 1).

Melanomas are derived from the neural crest and in general do not express EGFR[14]. Hence, acquired EGFR expression during drug selection may represent a stress response that is not favoured in the absence of drug treatment. Indeed, the proliferation rate of A375 *BRAF(V600E)* melanoma cells engineered to express EGFR decreased as the concentration of EGFR ligand increased (Fig. 1c). Moreover, A375 cells that express EGFR also proliferate slowly compared to parental control cells in nude mouse xenografts, but are resistant to trametinib (Fig. 1d). To investigate the cause of this slow-growth phenotype, we performed western blotting for a number of cell-cycle-associated proteins on parental A375 cells and EGFR-expressing derivatives. EGFR expression resulted in hypophosphorylated pRB protein, induction of the CDK inhibitors CDKN1A (p21cip1) and CDKN1B (p27kip1) and acidic β-galactosidase (Fig. 1e, f), markers that have been associated with oncogene-induced senescence[15,16]. These markers were also induced upon expression of oncogenic versions of *BRAF* or *MEK*, but much less when activated mutants of *AKT1* or *PIK3CA* were expressed in A375 cells (Extended Data Fig. 1). We conclude that EGFR expression is disadvantageous for *BRAF(V600E)* melanoma cells in the absence of BRAF or MEK inhibitor drugs, but it confers a selective advantage in the presence of these drugs.

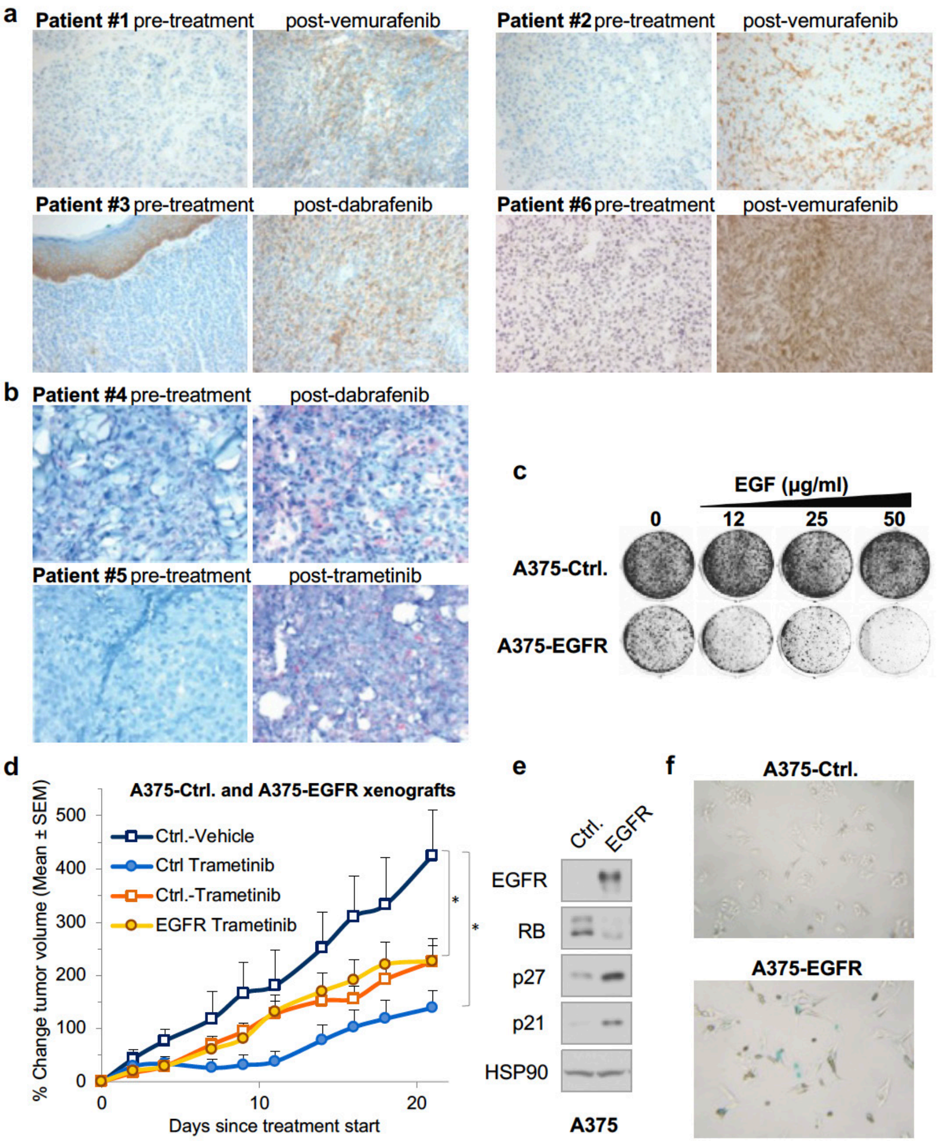
a
Patient #1 pre-treatment
post-vemurafenib
Patient #2 pre-treatment
post-vemurafenib
Patient #3 pre-treatment
post-dabrafenib
Patient #6 pre-treatment
post-vemurafenib
b
Patient #4 pre-treatment
post-dabrafenib
Patient #5 pre-treatment
post-trametinib
c
EGF (μg/ml)
0
12
25
50
A375-Ctrl.
A375-EGFR
d
A375-Ctrl. and A375-EGFR xenografts
% Change tumor volume (Mean ± SEM)
Ctrl.-Vehicle
Ctrl Trametinib
Ctrl.-Trametinib
EGFR Trametinib
0
100
200
300
400
500
0
10
20
Days since treatment start
*
*
e
Ctrl.
EGFR
EGFR
RB
p27
p21
HSP90
A375
f
A375-Ctrl.
A375-EGFR

Figure 1: Acquired EGFR expression in BRAF(V600E) mutant melanoma after vemurafenib resistance. (a,b) Immunohistochemical (IHC) analysis (a, ultraViewDABstain, brown; b, ultraView Red stain, red) showing increased EGFR expression in formalin-fixed paraffin embedded (FFPE) (Patient number 1–5) and frozen (Patient number 6) melanoma tissue sections from *BRAF(V600E)* mutant melanoma patients who developed resistance to vemurafenib, dabrafenib or trametinib as indicated. For each patient, the first biopsy is from the pre-treatment tumour; the second biopsy was performed after the tumour had progressed under treatment. For patient number 4, the first biopsy was performed when the patient was in partial response, but rapidly developed secondary resistance. Then 4.5months later, the second biopsy was taken. (c) EGFR expression confers a growth disadvantage to *BRAF(V600E)* mutant melanoma cells and EGFR ligand potentiates the growth deficiency in vitro. A375 *BRAF(V600E)* melanoma cells transduced with control lentiviral vectors (Ctrl, pLX304-GFP) or vectors expressing EGFR (EGFR, pLX304-EGFR) were seeded at the same density and cultured

in the presence of EGF at indicated concentration for 2 weeks. The cells were fixed, stained and photographed. (d) EGFR expression confers a growth disadvantage to *BRAF(V600E)* mutant melanoma, but induces trametinib resistance *in vivo*. CD1 nude mice were inoculated with *BRAF(V600E)* mutant melanoma A375 cells transduced with control retroviral vectors or vectors expressing *EGFR*. Once tumours were established, animals were treated with vehicle or trametinib. Relative tumour volume is shown. Error bars represent s.e.m. (n=5). *P=0.05, single-sided Wilcoxon–Mann–Whitney test. (e) Western blot analysis of RB protein, CDK inhibitors CDKN1A (p21cip1) and CDKN1B p27kip1) in EGFR expressing A375 cells. HSP90 served as a loading control. (f) EGFR expression induces senescence. Senescence was detected by staining of β-galactosidase activity. All experiments shown, except the ones that involve clinical samples and animals, were performed independently at least 3 times.

Acquired EGFR expression may be the result of an adaptive response of the cancer cell population during drug selection. To ask in an unbiased way which factors might modulate EGFR expression in melanoma cells, we compiled a ‘chromatin regulator’ library of shRNAs targeting 661 genes, including the lysine acetyltransferases (KATs), lysine methyltransferases (KMTs), lysine deacetylases (KDACs), lysine demethylases (KDMs), chromatin remodelling complexes and proteins that harbour chromatin binding/associated domains (Supplementary Table 2). A375 melanoma cells, which express very low levels of EGFR, were infected with the chromatin regulator library and selected with vemurafenib for 3 weeks. Then the vemurafenib-resistant cells were collected and strongly EGFR-positive cells (EGFR^{hi}) were isolated from the drug-resistant population by fluorescence-activated cell sorting (FACS) using an anti-EGFR antibody (Fig. 2a). Treatment of cells with either the chromatin regulator library or vemurafenib alone did not increase the fraction of EGFR^{hi} cells. In contrast, a significant fraction of EGFR^{hi} cells could be retrieved when cells were infected with the chromatin regulator library and were selected for vemurafenib resistance (Fig. 2b). We conclude that EGFR^{hi} melanoma cells do notmerely appear as a consequence of silencing of certain chromatin regulators, but that these cells only emerge when the population is placed under drug-selection pressure. This indicates that silencing of the gene(s) that induce EGFR expression is not favoured in the absence of vemurafenib.

To identify which gene(s) in the chromatin regulator library when suppressed can induce EGFR expression, we isolated genomic DNA from the EGFR^{hi} cells and non-drug-treated control cells and determined the abundance of the shRNA vectors in each cell population by deep sequencing, as described previously[3]. shRNAs that confer resistance to vemurafenib through upregulation of EGFR should be enriched in the EGFR^{hi} fraction. shRNA screens are notorious for yielding false positive results. Therefore, in principle only those genes that are represented by multiple shRNAs should be followed up in a genetic screen[17]. However, in this screen we did not identify any genes for which more than one shRNA was enriched (Supplementary Table 3). We therefore focused on the top 10 most strongly enriched genes for follow-up experiments. We tested several additional shRNA vectors for each of these 10 genes for their ability to increase EGFR expression, as this was a selectioncriterion in the genetic screen (ExtendedData Fig. 2a, b). Only suppressionof the SRY(sex determining region Y)-box 10 (*SOX10*) gene induced prominent EGFR expression when multiple SOX10 shRNAs (shSOX10) were used in four melanoma cell line models (Fig. 2c, d and Extended Data Figs 2c, 4c and 5c). *SOX10* knockdown (*SOX10*^{KD}) induced a slow-growth phenotype and also displayed the hallmarks of oncogene-induced senescence in three melanoma models (Fig. 2e and Extended Data Figs 2e, f, g, 4b, e, f and 5b, e, f).

Next we confirmed that *SOX10*^{KD} indeed induced vemurafenib resistance in melanoma. We infected A375 cells with shSOX10 and cultured cells in the presence of vemurafenib. *SOX10*^{KD} slowed down proliferation of A375 cells in the absence of drug, but in the presence of vemurafenib *SOX10*^{KD} conferred drug resistance in both short-termand longterm assays (Fig. 2e and Extended Data Fig. 2d, e). Moreover, under vemurafenib selective

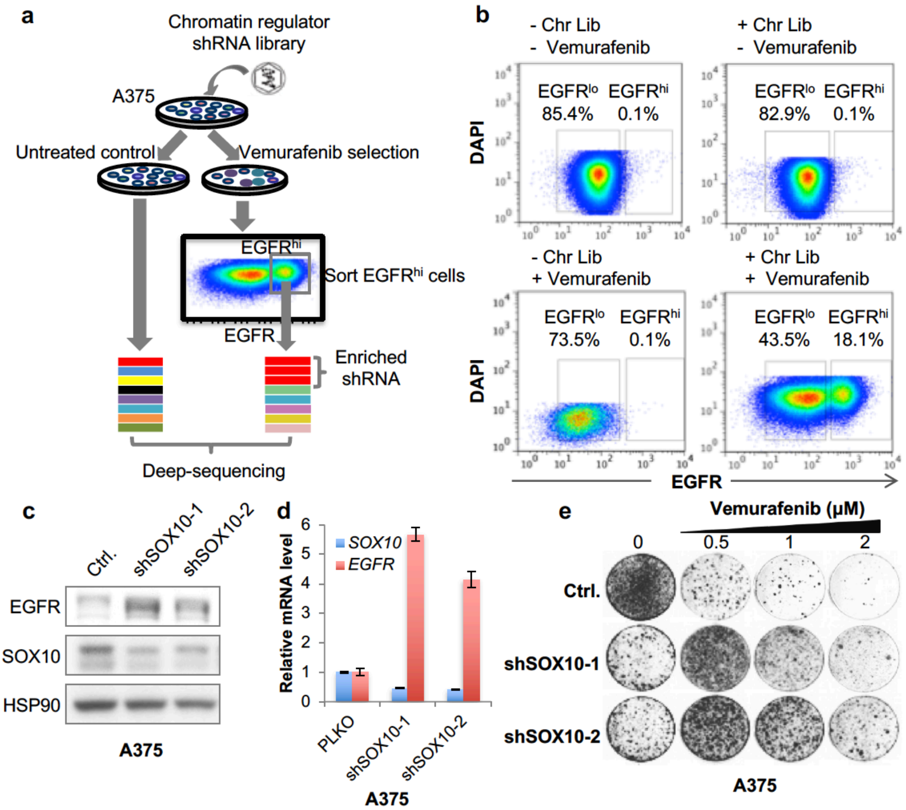

Figure 2: FACS-assisted shRNA genetic screen identifies SOX10 as a determinant of vemurafenib resistance and EGFR expression.
(a) Schematic outline of the of the FACS-assisted shRNA screen. Human 'chromatin regulator' shRNA library polyclonal virus was generated to infect A375 cells, which were then left untreated (control) or treated with 0.5 mM vemurafenib. After 12 days, the untreated cells were collected. The cells that survived from 21 days of vemurafenib treatment were FACS sorted for EGFR expression.

Subsequently, shRNA inserts from both samples were recovered by PCR and identified by massive parallel sequencing. (b) EGFR^{hi} cells result from the combination of infection with chromatin regulator library and vemurafenib selection. A375 cells infected with 'chromatin regulator' library (Chr Lib) were cultured in the presence of 0.5 mM vemurafenib for 21 days (right lower panel). Cells were harvested with 2mM EDTA, stained with anti-EGFR antibody and analysed for EGFRhi cells by flow cytometry. A375 cells cultured with or without vemurafenib, and A375 cells infected by the 'chromatin regulator' library without vemurafenib treatment served as controls. (c,d) Suppression of SOX10 induces EGFR expression. (c) Western blot analysis of EGFR and SOX10 levels in cells targeted by two independent shSOX10 vectors, HSP90 served as a loading control. (d) The level of EGFR induction was determined by quantitative PCR with reverse transcription (qRT–PCR) analysis of the relative mRNA level of *EGFR*. pLKO.1 empty vector served as a control vector (Ctrl). Error bars represent s.d. of measurement replicates (n=3). (e) Two independent shRNAs targeting *SOX10* confer a proliferation disadvantage in the absence of drug, but induce vemurafenib resistance. A375 cells expressing shRNAs (as shown in Fig. 2c) targeting *SOX10* were seeded at the same density in 6-well plates and cultured in the absence (for 2 weeks) or presence of vemurafenib (for 4 weeks) at the indicated concentrations. The cells were fixed, stained and photographed. All experiments shown except shRNA screen were performed independently at least 3 times.

pressure, cells having a higher degree of *SOX10^{KD}* were selected, which consequently also expressed higher levels of EGFR, consistent with the notion that increased EGFR levels drive drug resistance (ExtendedData Fig. 2h). Vemurafenib resistance through *SOX10* suppression was also seen in additional melanoma cell lines (Extended Data Figs 4a and 5a). A low concentration of vemurafenib actually increased the proliferation rate of *SOX10^{KD}* cells, consistentwith the model that hyperactive BRAF–MEK signalling induces senescence markers, a process which is inhibited by vemurafenib (Extended Data Fig. 4a, g).

To study how *SOX10* suppression induces EGFR expression, we performed transcriptome sequencing (RNA-seq) of both parental A375 and A375 *SOX10^{KD}* cells (Supplementary Table 4). Gene set enrichment analysis of the SOX10-upregulated genes revealed an enrichment of genes with SMAD2/3 (downstream mediators of TGF-β signalling) and JUN binding sites in their promoters (Supplementary Table 5). Consistent with this, *SOX10* suppression induced TGF-β receptor 2 (TGFBR2) expression as well as a number of bona fide TGF-β target genes, including JUN, in three melanoma cell models (Fig. 3a, b and Extended Data Figs 4d and 5d). Levels of active JUN (phosphorylated JUN, p-JUN) were also increased by *SOX10^{KD}* (Fig. 3a). That treatment of melanoma cells with recombinant TGF-β causes resistance to vemurafenib further supports a role for TGF-β signalling in vemurafenib resistance (Fig. 3c and ref. 18). TGF-β1 treatment caused not only induction of EGFR expression, but also induction of PDGFRB (Fig. 3d, e) and also resulted in induction of senescence-associated β-galactosidase (Fig. 3f). Consistently, SOX10 suppression also induced PDGFRB expression (Extended Data Figs 3c, 4c and 5c). Moreover, suppression of TGFBR2 inhibited EGFR and PDGFRB induction in *SOX10^{KD}* cells (Figs 3g, h), whereas ectopic expression of TGFBR2 induced p-JUN, EGFR and PDGFRB expression (Fig. 3i). JUN is a regulator of EGFR expression and TGF-β regulates PDGFRB. Moreover, SMADs and JUN cooperate in activation of EGFR expression[22,23]. SOX10 is known to regulate the melanocyte transcription factor MITF[24]. Indeed, A375 cells with shSOX10 also had reduced MITF expression, but MITF suppression alone did not change EGFR or PDGFRB expression and did not cause vemurafenib resistance (Extended Data Fig. 7c–e). Our data provide support for a model in which activation of TGF-β signalling by SOX10 loss leads to increased EGFR and PDGFRB expression and vemurafenib resistance.

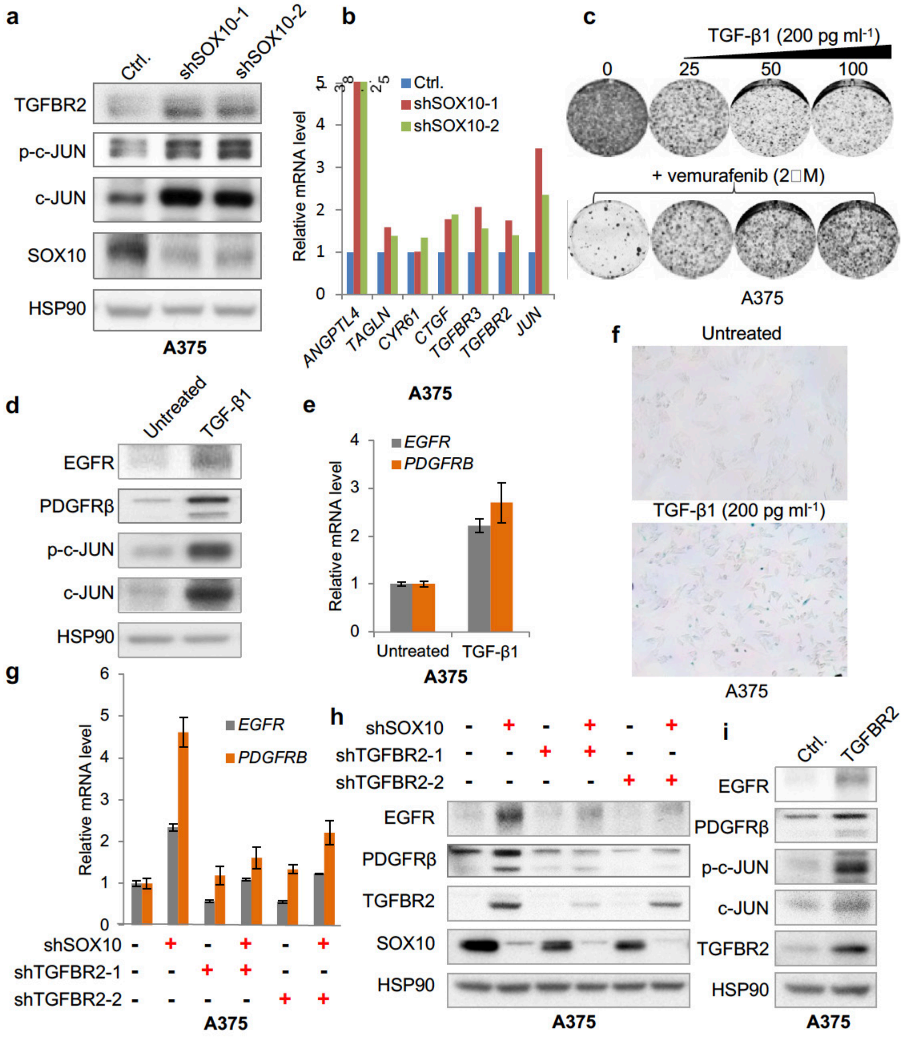

Figure 3: Activation of TGF-β signalling leads to increased EGFR and PDGFRB expression.
(a) Suppression of SOX10 activates TGFBR and JUN signalling. Two independent shRNAs targeting *SOX10* were individually introduced into A375 cells by lentiviral transduction. The levels of TGFBR2, p-JUN and JUN were determined by western blot analysis. HSP90 served as a loading control. (b) SOX10 loss leads to upregulation of TGF-β receptors and its bona fide target genes. Relative mRNA level of *ANGPTL4, TAGLN, CYR61, CTGF, TGFBR3, TGFBR2* and *JUN* were determined by transcriptome sequencing. pLKO.1 empty vector served as a control vector (Ctrl). (c) TGF-β activation confers a growth disadvantage but vemurafenib resistance. A375 cells were seeded at the same density in

6-well plates and cultured in the absence or presence of recombinant TGF-β or vemurafenib at the indicated concentrations. The cells were fixed, stained and photographed. (d,e) Recombinant TGF-β1 treatment activates JUN and upregulates EGFR and PDGFRb expression. A375 cells were cultured in the absence or presence of 200 pg ml-1 recombinant TGF-β1 for 7 days before harvested for western blot or qRT–PCR analysis. Error bars represent s.d. of measurement replicates (n=3). (f) Recombinant TGF-β1 treatment induces senescence. A375 cells were cultured in the presence of 200 pg/ml recombinant TGF-β for 14 days. Senescence was detected by staining of β-galactosidase activity. (g,h) SOX10 loss induced EGFR and PDGFRb upregulation is TGFBR2-dependent. A375 cells were infected with lentiviral shRNA vectors as indicated. Relativem RNA levels of *EGFR* and *PDGFRB* were determined by qRT–PCR analysis; *EGFR, PDGFRb, TGFBR2 and SOX10* levels were determined by western blot analysis. Error bars represent s.d. of replicate measurements (n=3). (i) *TGFBR2* overexpression is sufficient to upregulate EGFR and PDGFRB. TGFBR2 was introduced to A375 cells by lentiviral transduction (TGFBR2, pLX304- TGFBR2). pLX304-GFP served as a control vector (Ctrl). The levels of EGFR, PDGFRb, TGFBR2, p-JUNand JUN were determined by western blot analysis. All experiments shown except RNA-seq were performed independently at least 3 times.

Treatment of A375-*SOX10*^{KD} cells with a combination of both vemurafenib and the EGFR inhibitor gefitinib did not lead to proliferation arrest, indicating that EGFR was not the sole driver of drug resistance in *SOX10*^{KD} cells (Extended Data Fig. 3a). Indeed, an unbiased survey of RTKs revealed that *SOX10*^{KD} activated not only EGFR, but also PDGFRB and ERBB3 (Extended Data Fig. 3b, c). A similar pattern of RTK activation was observed following TGF-β1 treatment, highlighting the similarity between *SOX10* suppression and acquired TGF-β signalling (Extended Data Fig. 3b, d). Many RTKs share two major downstream signalling pathways (RAS–MEK–ERK and PI3K– AKT). Consistent with this, we found that combined inhibition of these two downstream pathways using BRAF and PI3K inhibitors could restore growth inhibition in *SOX10*^{KD} cells (Extended Data Fig. 3a).

Our data are consistent with a model in which cells with low SOX10 and high EGFR and PDGFRB expression are positively selected in the presence of drug, but that such cells are counter-selected in the absence of drug. To test thismodel directly, we infected A375 cells with shSOX10 and subjected this heterogeneous population of *SOX10*^{KD} cells to vemurafenib selection for one week. At this point, we collected part of this population and determined EGFR expression by FACS analysis. Under vemurafenib selection, an increased level of EGFR and a markedly decreased level of SOX10 were observed. When these cells were subsequently cultured for one more week in the absence of vemurafenib, the EGFR^{hi}SOX10^{lo} population was depleted (Fig. 4a and Extended Data Fig. 6a). These data indicate that acquired EGFR expression is only advantageous to melanoma cells in the presence of drug selection, but is counter-selected in the absence of drug.

Consistent with a role for SOX10 in regulation of EGFR expression in melanoma, we found an inverse correlation between *SOX10* and *EGFR* expression in a panel of 34 melanoma cell lines[25] (Fig. 4b) and a similar inverse relationship between SOX10 and PDGFRB (Extended Data Fig. 6b). The most extreme cell line in this panel, LOXIMVI, completely lacked *SOX10* expression and had the highest *EGFR* expression. When we expressed *SOX10* in this cell line, EGFR and PDGFRB were reduced and TGFBR2 and TGFBR3 as well as JUN and p-JUN levels were also downregulated, consistent with the notion that SOX10 regulates these RTKs through an effect on TGF-β signalling (Extended Data Fig. 6c, d). Consistently, expression of *SOX10* in LOXIMVI cells increased their sensitivity to vemurafenib (Extended Data Fig. 6e).

To ask directly whether SOX10 is involved in EGFR-associated drug resistance in *BRAF(V600E)* melanoma patients, we isolated RNA from the six patients studied above who had gained EGFR expression after acquisition of trametinib, dabrafenib or vemurafenib resistance (Supplementary Table 1). We performed RNA-seq analysis to determine changes in transcriptome upon drug resistance. In two patients, the levels of *SOX10* mRNA were reduced (Fig. 4c and Extended Data Fig. 6f). *EGFR* and *PDGFRB* mRNA were greatly increased in patient 5, whereas no evidence was found in this patient of alternative BRAF splicing[7] or *BRAF* overexpression (Extended Data Fig. 7a, b). Patient 3 had strong induction of EGFR protein post-resistance (Fig. 1a), but at first glance, EGFR mRNA levels appeared only minimally induced. However, scrutiny of the RNA-seq data revealed that the apparent lack of induction of *EGFR* in this tumour sample pair is caused by the abnormally high *EGFR* transcript abundance in the pre-treatment sample and not the lack of *EGFR* expression in the post-treatment sample (Extended Data Fig. 6g). This is most probably owing to the contamination of this sample with the strongly EGFR-positive skin material (see Fig. 1a). These tumours also manifested increased TGF-β signalling (Fig. 4c and Extended Data Fig. 6h). Two further pairs of tumour samples showed induction of *EGFR* and *PDGFRB* without notable loss of *SOX10* after drug resistance emerged. These tumours displayed induction of TGF-β receptor expression and induction of a number of bona fide TGF-β targets, indicating that these tumours somehow had acquired TGF-β signalling (and subsequent induction of *EGFR* and *PDGFRB* expression) in a SOX10-independent fashion (Fig. 4c).

Clinical evidence indicates that melanoma patients that have developed vemurafenib resistance can regain sensitivity to the drug after a drug holiday, suggesting a reversible and adaptive transcriptional response to the drug[26]. That drug resistance is reversed in the absence of drug indicates that this adaptive response is not favoured in the absence of drug. Our data provide a molecular underpinning for the concept that drug resistance may arise at a fitness cost in the absence of drug (Fig. 4d). Melanoma patients whose tumours acquire EGFR expression as a result of drug resistance development may be candidates to be re-treated with drug after a drug holiday.

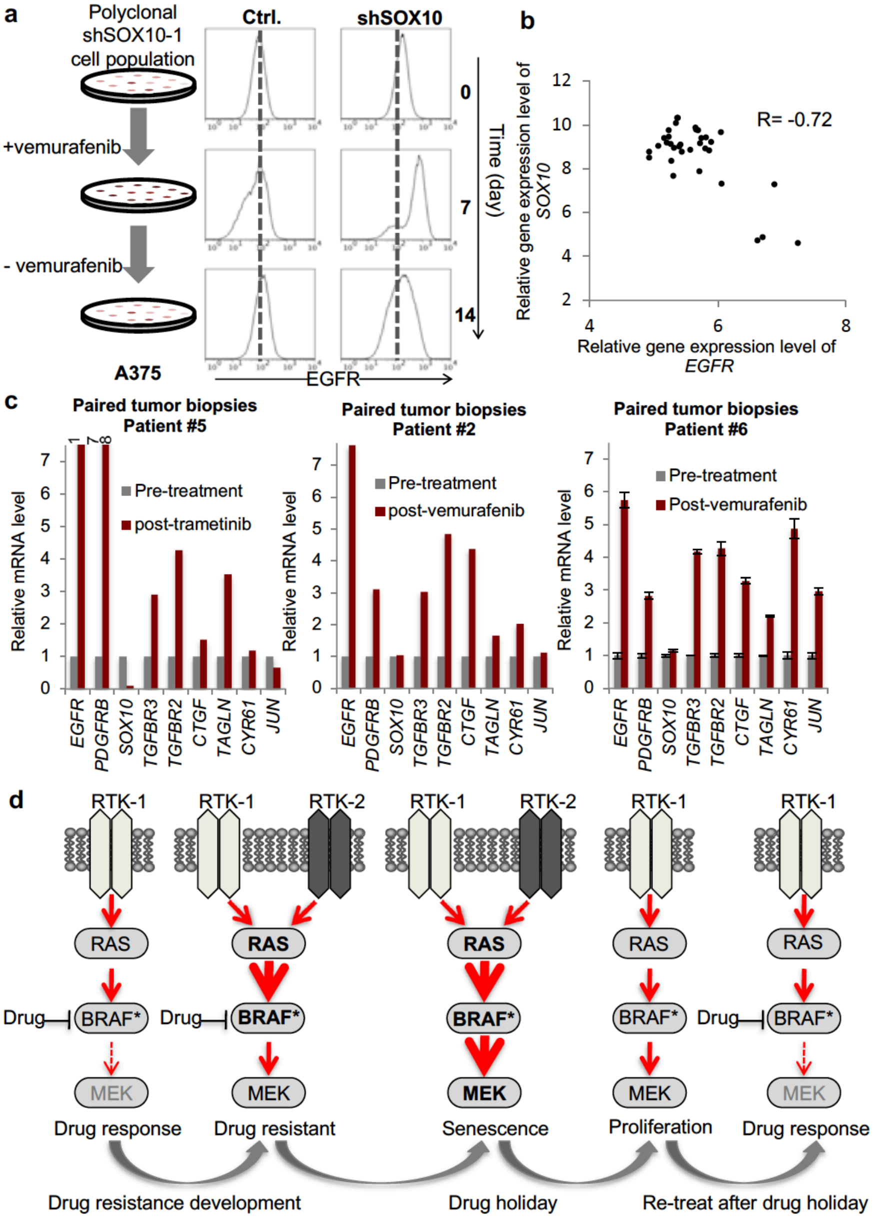

Figure 4: Inverse relationship between SOX10 and receptor tyrosine kinase expression in melanoma. (a) Intermittent drug dosing alters relative proportions of EGFRhi and EGFRlo cell populations. A375 cells were infected with shSOX10-1 to generate a polyclonal cell population of SOX10KD cells. The infected cells were seeded in 6-well plates, samples collected and stained with antibody against EGFR for flow cytometry analysis at day 0, day 7 and day 14 (0.5 mM vemurafenib treatment started on day 0 and stopped on day 7). pLKO.1 (Ctrl) vector served as a control. (b) Inverse correlation between SOX10 and EGFR in a panel of human BRAF mutant melanoma cell lines. Relative gene expression levels of SOX10 and EGFR were acquired from the Cancer Cell Line Encyclopedia (CCLE). R stands for Pearson product-moment correlation coefficient. (c) Differential gene expression of *SOX10, EGFR,*

PDGFRB, TGF-β receptors and TGF-β target genes in pre- and posttreatment patient tumour biopsies. Total RNA was isolated from FFPE specimens derived from tumour biopsies of patient 5, 2 and 6 both before and after development of drug resistance. After reverse transcription, gene expression levels were determined by transcriptome sequencing (patient 5 and patient 2) qRT–PCR analysis (patient 6). Error bars represent s.d. of measurement replicates (n=3). (d) Model for senescence induction after development of vemurafenib resistance. Upregulation of RTKs leads to enhanced signalling through the RAS–BRAF–MEK pathway. Consequently, vemurafenib is no longer able to fully silence the signalling to MEK and drug resistance is seen. When the drug is removed, supra-physiological levels of BRAF–MEK signalling induced a state of oncogene-induced senescence, which subsequently leads to negative selection of the RTKs and restores drug responsiveness. All experiments shown, except the ones that involve clinical samples, were performed independently at least 3 times.

References

1. Chapman, P. B. et al. Improved survival with vemurafenib in melanoma with BRAF V600E mutation. N. Engl. J. Med. 364, 2507–2516 (2011).

2. Flaherty, K. T. et al. Improved survival with MEK inhibition in BRAF-mutated melanoma. N. Engl. J. Med. 367, 107–114 (2012).

3. Prahallad, A. et al. Unresponsiveness of colon cancer to BRAF(V600E) inhibition through feedback activation of EGFR. Nature 483, 100–103 (2012).

4. Corcoran, R. B. et al.EGFR-mediated re-activation ofMAPKsignaling contributes to insensitivity ofBRAFmutant colorectal cancers toRAF inhibitionwith vemurafenib. Cancer Discov. 2, 227–235 (2012).

5. Davies, H. et al. Mutations of the BRAF gene in human cancer. Nature 417, 949–954 (2002).

6. Flaherty, K. T., Hodi, F. S.&Fisher, D. E. Fromgenes to drugs: targeted strategies for melanoma. Nature Rev. Cancer 12, 349–361 (2012).

7. Poulikakos, P. I. et al. RAF inhibitor resistance is mediated by dimerization of aberrantly spliced BRAF(V600E). Nature 480, 387–390 (2011).

8. Johannessen, C. M. et al. COT drives resistance to RAF inhibition through MAP kinase pathway reactivation. Nature 468, 968–972 (2010).

9. Wagle, N. et al. Dissecting therapeutic resistance to RAF inhibition inmelanoma by tumour genomic profiling. J. Clin. Oncol. 29, 3085–3096 (2011).

10. Shi, H. et al. Melanoma whole-exome sequencing identifies (V600E)B-RAF amplification-mediated acquired B-RAF inhibitor resistance. Nature Commun. 3, 724 (2012).

11. Nazarian, R. et al. Melanomas acquire resistance to B-RAF(V600E) inhibition by RTK or N-RAS upregulation. Nature 468, 973–977 (2010).

12. Girotti, M. R. et al. Inhibiting EGF receptor or SRC family kinase signaling overcomes BRAF inhibitor resistance in melanoma. Cancer Discov 3, 158–167 (2013).

13. Villanueva, J. et al. Acquired resistance to BRAF inhibitors mediated by a RAF kinase switch in melanoma can be overcome by cotargeting MEK and IGF-1R/ PI3K. Cancer Cell 18, 683–695 (2010).

14. Real, F. X. et al. Expression of epidermal growth factor receptor in human cultured cells and tissues: relationship to cell lineage and stage of differentiation. Cancer Res. 46, 4726–4731 (1986).

15. Serrano, M., Lin, A. W., McCurrach, M. E., Beach, D. & Lowe, S. W. Oncogenic ras provokes premature cell senescence associated with accumulation of p53 and p16INK4a. Cell 88, 593–602 (1997).

16. Michaloglou, C. et al. BRAFE600-associated senescence-like cell cycle arrest of human naevi. Nature 436, 720–724 (2005).

17. Brummelkamp, T. R. & Bernards, R. New tools for functional mammalian cancer genetics. Nature Rev. Cancer 3, 781–789 (2003).

18. Huang, S. et al. MED12 controls the response to multiple cancer drugs through regulation

of TGF-β receptor signaling. Cell 151, 937–950 (2012).
19. Johnson, A. C. et al. Activator protein-1 mediates induced but not basal epidermal growth factor receptor gene expression. Mol. Med. 6, 17–27 (2000).
20. Zenz, R. et al. c-Jun regulates eyelid closure and skin tumor development through EGFR signaling. Dev. Cell 4, 879–889 (2003).
21. Steller, E. J. et al. PDGFRB promotes liver metastasis formation of mesenchymallike colorectal tumor cells. Neoplasia 15, 204–217 (2013).
22. Zhang, Y., Feng, X.-H.&Derynck, R.Smad3andSmad4cooperate with c-Jun/c-Fos to mediate TGF-β-induced transcription. Nature 394, 909–913 (1998).
23. Mialon, A. et al. DNA topoisomerase I is a cofactor for c-Jun in the regulation of epidermal growth factor receptor expression and cancer cell proliferation. Mol. Cell. Biol. 25, 5040–5051 (2005).
24. Bondurand, N. et al. Interaction among SOX10, PAX3 and MITF, three genes altered in Waardenburg syndrome. Hum. Mol. Genet. 9, 1907–1917 (2000).
25. Garnett, M. J. et al. Systematic identification of genomicmarkers of drug sensitivity in cancer cells. Nature 483, 570–575 (2012).
26. Seghers, A. C., Wilgenhof, S., Lebbe, C. & Neyns, B. Successful rechallenge in two patients with BRAF-V600-mutant melanoma who experienced previous progression during treatment with a selective BRAF inhibitor. Melanoma Res. 22, 466–472 (2012).
27. Yang, X. et al. A public genome-scale lentiviral expression library of humanORFs. Nature Methods 8, 659–661 (2011).
28. Cronin, J. C. et al. Frequentmutations in the MITF pathway inmelanoma. Pigment Cell Melanoma Res 22, 435–444 (2009).
29. Huang, S. et al. ZNF423 is critically required for retinoic acid-induced differentiation and is a marker of neuroblastoma outcome. Cancer Cell 15, 328–340 (2009).

Materials and methods

Pooled shRNA Screen

A 'chromatin regulator' shRNA library targeting 661 genes was constructed from the TRC human genome-wide shRNA collection (TRC-Hs1.0). Lentiviral shRNA vectors generated from the pooled library were used to infect A375 cells. Cells stably expressing shRNA were selected by vemurafenib and then FACS sorted for EGFR expression. Massive parallel sequencing was used to determine the enriched shRNA in the selected cell population.

Melanoma patient tumour samples

Permission was granted by the NKI and IGR ethical committee to take biopsies fromBRAF(V600E) mutant patients before and after vemurafenib, dabrafenib or trametinib treatment. All patients consented to participate in the study. BRAF(V600E) mutation status was determined by Departments of Pathology at NKI and IGR.

Cell lines

The A375 melanoma cell line was obtained from ATCC. SK-MEL-28 andCOLO679were gifts fromD. Peeper (Amsterdam, The Netherlands).WM266- 4 cell line was provided by R. Marais (Manchester, UK) A375 andWM266-4 cells were cultured inDMEMmedium supplemented with 8% FBS, 1% penicillin/streptomycin and 2mM L-glutamine. COLO679 cell was cultured in RPMI medium supplemented with 8% FBS, 1% penicillin/streptomycin and 2mM L-glutamine.

Compounds, antibodies and reagents

Trametinib (#S2673), vemurafenib (# S1267), gefitinib (#S1025) and GDC0941 (#S1065) were purchased from Selleck Chemicals. TGF-b1 was purchased from R&D (#240-B-010). Antibodies againstHSP90 (H-114), p21 (C-19),TGFBR2 (C-16), p-c-JUN(KM-1) and c-JUN (N) were from Santa Cruz Biotechnology; anti-EGFR for FACS application (GR01L)was fromMillipore; anti-EGFR for western blot analysis (610017),RB (554136) and p27 (610242) antibodies and RTK arrays were from BD Biosciences; Antibodies against TGFBR3(#2519), p-RB (#9307), p-MEK(#9154), MEK (#4694) and PDGFRB(#4564, #3166) were from Cell Signaling; antibody against SOX10 (ab155279)was from Abcam. CellTiter-BlueCellViability Assaywas from Promega.

Plasmids

Individual shRNA vectors usedwere collected from theTRClibrary (Supplementary Table 6). The following plasmids were purchased from Addgene to generate pLX304-EGFP, pLX301-SOX10, pLX304-EGFR, pLX301-EGFRand pLX304-TGFBR2 constructs by Gateway cloning8,27,28. Plasmid 24749: pDONR221-hSOX10; Plasmid 25890: pLX304; Plasmid 25895: pLX301; Plasmid 25899: pDONR221_EGFP; Plasmid 23935: pDONR223-EGFR;

Plasmid 23623: pDONR223-TGFBR2.

FACS-assisted shRNA screen with a customized library

Lentiviral vectors (pLKO.1) encoding shRNAs that target chromatin regulator genes are listed in Supplementary Table 2. The chromatin regulator library contains six plasmids pools. Lentiviral supernatants of the plasmids were produced as described at (http://www.broadinstitute.org/ rnai/public/resources/protocols). A375 cells were infected independently by the six virus pools (multiplicity of infection,1) and selected with puromycin (2 mg/ml) for cells containing integrated shRNA.Cellswere then pooled and seeded at 350,000 cells per 15cm dish in the absence or presence of 0.5 mMvemurafenib (8 dishes for each condition) for 21 days.Themediumwas refreshed every 3 days. The cells without vemurafenib treatment were collected at day 12. At day 21, the cells treated with vemurafenib were collected using 2mM EDTA (#E4884, Sigma-Aldrich). Then, the cells were stainedwithmouse anti-human EGFR antibody primarily (#GR01L, Clone 528, Millipore), followed by secondary staining with Alexa Fluor 647 conjugated goat anti-mouse IgG antibody (#A-21236, Invitrogen), after which the cells were washed and suspended in DMEM medium containing 2% FBS. BD FACSAria III (BD Bioscience) was used to sort out EGFRhi cells. The FACS data was analysed by FlowJo programme version 7.6.3 (Tree Star). The genomicDNAwas isolated from non-drugtreated control cells and drug-treatedEGFRhi cells usingDNeasyBlood andTissueKit (#69506 Qiagen). shRNA inserts were recovered from 500 ng genomic DNA following by the experimental steps of PCR amplification (PCR1 and PCR2) as described3. PCR product purification was performed using High Pure PCR Product Purification Kit according to the manufacturer's instructions (#11732676001, Roche). Purified PCR products were subjected to deep sequencing to identify the shRNA inserts.

Staining of b-galactosidase activity

For Fig. 1f, Extended Data Fig. 2f and Extended Data Fig. 4e, the staining method is as follows. Cells were washed with PBS and fixed with 0.5% glutaraldehyde solution (in PBS pH7.4) for 15 min at room temperature. Then the cells were washed with PBS for 5 min and with 0.925mM MgCl2 solution (in PBS pH 6.0) twice for 5 min at room temperature. X-gal staining solution (freshly prepared) was added to the cells and the incubation was performed at 37 uC for 8 h to overnight. Cells were washed again 3 times with PBS for 5 min at room temperature before the pictures were taken. For Fig. 3f and ExtendedData Fig. 5e, Senescence Cells Histochemical StainingKit (CS0030-1KT) fromSigmawas applied according to themanufacturer's instructions. Long-term cell proliferation assays. Cells were seeded into 6-well plates (33104 cells per well) and cultured both in the absence and presence of drugs as indicated. For full details, see ref. 29.

Protein lysate preparation and immunoblots

Cells were seeded in medium containing 8% fetal bovine serum (FBS) for 24 h, and then washed with PBS and lysed with RIPA buffer supplemented with protease inhibitor (cOmplete, Roche) and Phosphatase Inhibitor Cocktails II and III (Sigma). All lysates were freshly prepared and processed with Novex NuPAGE Gel Electrophoresis Systems (Invitrogen).

Mouse xenografts

Retroviral vector–transducedA375 cells (53106 cells permouse) were injected subcutaneously into the right posterior flanks of 7-week-old immunodeficient CD1 nude female mice (6 mice per group; Charles River Laboratories, Calco, Italy). Tumour formation wasmonitored twice a week, and tumour volume based on calliper measurements was calculated by the modified ellipsoidal formula (tumour volume51/2(length3width2)).When tumours reached a volume of approximately 0.3 cm3, mice were randomized into treatment arms and treated for a 21-day period. Trametinib was formulated in 0.5% hydroxypropylmethylcellulose (Sigma) and 0.2% Tween-80 in distilled water pH8.0, and it was dosed at 0.15mg per kg daily by oral gavage. All animal procedures were approved by the Ethical Commission of the University of Turin and by the Italian Ministry of Health and they were performed in accordance with institutional guidelines.

Immunohistochemistry

For EGFR staining, FFPE samples, immunohistochemistry was performed on a BenchMark Ultra autostainer (VentanaMedical Systems, Inc.) Briefly, paraffin sections were cut at 4 mm, heated at 75 uC for 28min and deparaffinized in the instrument with EZ prep solution (VentanaMedical Systems). Heat-induced antigen retrieval was carried out using Cell Conditioning 1 (CC1, Ventana Medical Systems). EGFR was detected by incubating sections with antibody clone 5B7 (5278457001; Roche (Ventana)) for 16 min. Specific reactions were detected using UltraView Universal Alkaline Phosphatase Red Detection or DAB Kit (Ventana Medical Systems), and slides were counterstainedwith haematoxylin. EGFR staining, fresh-frozen samples. Fresh-frozen sections (4-mm thick) were mounted on 3-aminopropylethoxysilane (Sigma) and glutaraldehyde coated slides. After 10 min fixation with ethanol, slides were incubated with anti-EGFR using clone 31G7 (1:50; Life technologies, Zymed) using standard procedures, followed by incubation with the PowerVision Poly-HRP anti-mouse IgG (ImmunoLogic). Sections were counterstained with haematoxylin.

RNA isolation, qRT–PCR and RNA sequencing FFPE samples

Method of total RNA isolation from FFPE samples is as described previously[18]. cDNA was obtained by reverse transcription using High-CapacitycDNA Reverse Transcription kit (Applied Biosystems, AB) according to the manufacturer's instructions. EGFR expression assay (Hs01076078_m1), SOX10 expression assay (Hs00366918_m1), PDGFRB expression assay (Hs01019589_m1), TGFBR3 expression assay (Hs01114253_m1), TGFBR2 expression assay (Hs00234253_m1), CTGF expression assay (Hs01026927_g1), TAGLN expression assay (Hs01038777_g1), CYR61 expression assay (Hs00998500_g1), JUN expression assay

(Hs01103582_s1) and ACTBexpression assay (Hs01060665_g1)were used to detect the gene expression on theAB 7500 Fast Real-time PCRsystem following the manufacturer's instructions. Cell line samples. RNA isolation from cell lines harvested with TRIzol reagent (Invitrogen) according to the manufacturer's instruction. cDNA synthesis was performed with Maxima Universal First Strand cDNA Synthesis Kit (#K1661, Thermo scientific) according to manufacturer's instruction. The primers were used for qRT–PCR are described in Supplementary Table 7. For RNA sequencing, the library was prepared using TruSeq RNA sample prep kit according to the manufacturer's protocol (Illumina). RNA sequencing data are available at http://www.ncbi.nlm.nih.gov under accession number GSE50535.

Online Content

Any additional Methods, tables, display items and Source Data are available in the online version of the paper.

https://www.nature.com/articles/nature13121#supplementary-information

Acknowledgements

We thank the NKI Core Facilities for Genomics and Molecular Pathology & Biobanking for tumour tissue and support in DNA sequencing. We thank S. Roy for collecting clinical data and N. Kamsu Kom for tissue preparation. This work was supported by grants fromthe European Research Council (ERC), theDutch Cancer Society (KWF), the EU COLTHERES project and grants by the Netherlands Organization for Scientific Research (NWO) to Cancer Genomics Netherlands (CGC.NL). Additional support was provided by Fondazione Piemontese per la Ricerca sul Cancro—ONLUS grant 'Farmacogenomica—5 per mille 2009 MIUR' (F.D.N.); AIRC MFAG 11349 (F.D.N.); AIRC IG grant n. 12812 (A.B.); and Canadian Institutes of Health Research (CIHR) grant MOP-130540 (S.Hu).

Supplemental Figures

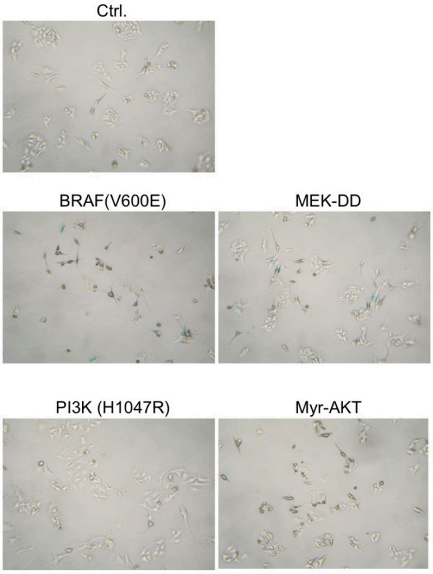

Extended Data Figure 1 | Ectopic expression of oncogenic version of EGFR effectors induces senescence at different levels. Oncogenic BRAF(V600E), MEK (MED-DD), PIK3CA(H1047R), or AKT (Myr-AKT) were introduced to A375 cells by retroviral transduction. pBabe empty vector served as a control vector (Ctrl). Senescence was detected by staining of β-galactosidase activity. All experiments shown were performed independently at least three times.

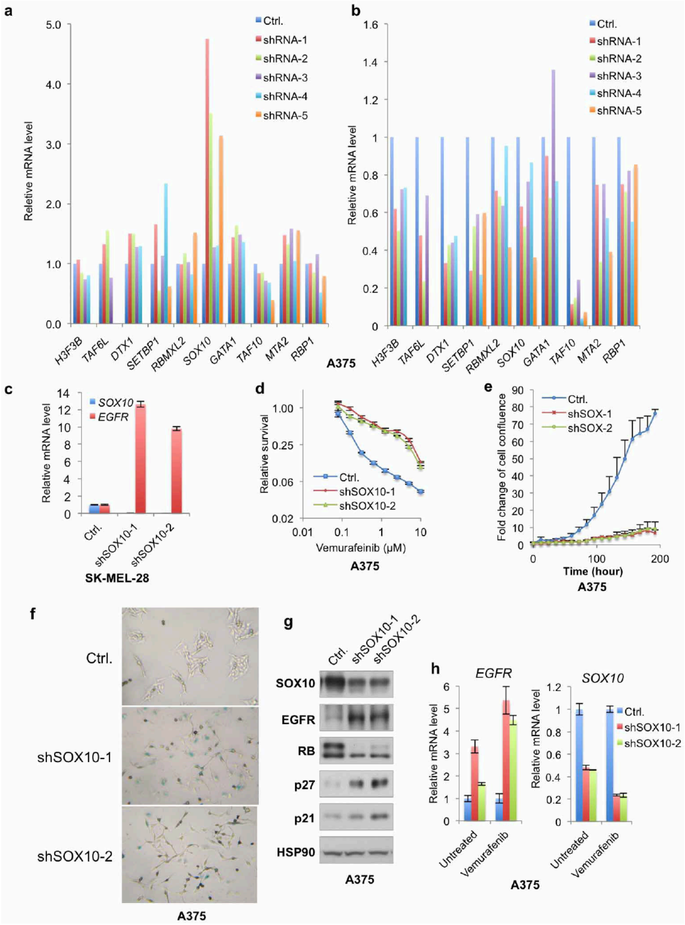

Extended Data Figure 2 | Effects of *SOX10* suppression in melanoma. **a,** Suppression of *SOX10* strongly induces *EGFR* expression. Multiple independent shRNA vectors (5 vectors per gene) targeting the top 10 gene candidates were individually introduced to A375 cells by lentiviral transduction. The level of *EGFR* induction was determined by qRT–PCR analysis of the relative mRNA level of EGFR. pLKO.1 empty vector served as a control vector (Ctrl). **b,** Knockdown efficiency of the shRNA vectors targeting the top 10 gene candidates from the genetic screen. Multiple independent shRNA vectors targeting the top 10 candidate genes were individually introduced to A375 cells by lentiviral transduction. The knockdown efficiency of the shRNA vectors was determined by qRT–PCR analysis of the mRNA levels of the corresponding genes. Means of duplicate measurements are shown. **c,** *SOX10* suppression leads to *EGFR* upregulation in a second *BRAF(V600E)* mutant melanoma cell line SK-MEL-28. Error bars represent s.d. of measurement replicates ($n = 3$). **d,** Two independent shRNAs targeting *SOX10* confer vemurafenib resistance. A375 cells expressing shRNAs against *SOX10* were seeded at the same density in 96-well plates and treated with vemurafenib at the indicated concentrations for 6 days. Cell viability was determined by CellTiter-Blue assay according to the manufacturer's instruction. Relative survival is presented as the ratio of cell viability in the presence of vemurafenib to that in the absence of drug treatment. Error bars represent the s.d. of triplicate independent experiments. **e,** *SOX10* suppression is a disadvantage for melanoma cell proliferation. shRNAs targeting *SOX10* were introduced into A375 cells by lentiviral transduction. pLKO.1 empty vector served as a control vector (Ctrl). After puromycin selection, cells were seeded in 384-well and cell confluence was measured by IncuCyte imaging system. Error bars represent s.d. of triplicate independent experiments. **f,** *SOX10* suppression induces senescence. Senescence was detected by staining of β-galactosidase activity. **g,** Western blot analysis of RB protein, CDK inhibitors CDKN1A (p21$^{\mathrm{cip1}}$) and CDKN1B (p27$^{\mathrm{kip1}}$) in SOX10 knockdown A375 cells. HSP90 served as a loading control. **h,** Vemurafenib treatment selects for cells that have higher level of EGFR and lower level of *SOX10*. A375 cells expressing shRNAs targeting SOX10 as described above were cultured in the absence or presence of 1 μM vemurafenib for 10 days before the sample collection for qRT–PCR analysis. Error bars represent s.d. of measurement replicates ($n = 3$). All experiments shown, except panels **a** and **b**, were performed independently at least three times.

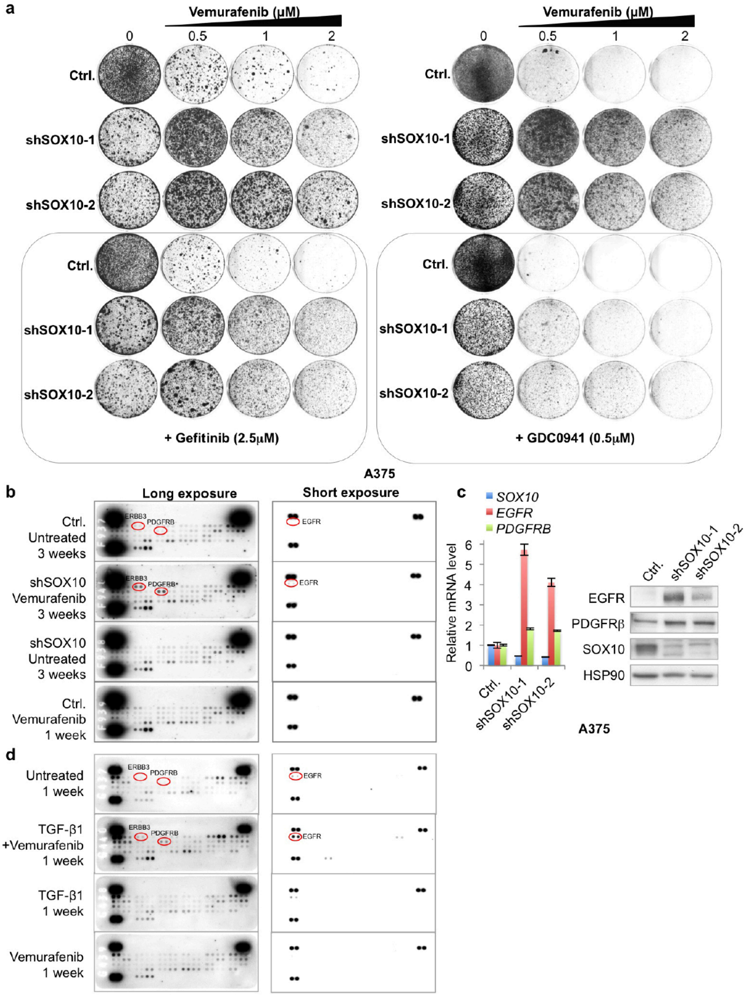

Extended Data Figure 3 | SOX10 knockdown and TGF-β activation induce multiple RTKs. **a**, EGFR inhibition (gefinitib) is not sufficient to restore vemurafenib sensitivity of *SOX10* knockdown cells. Targeting PI3K, a common downstream effector of RTKs, with a selective inhibitor (GDC0941) sensitizes *SOX10* knockdown cells to vemurafenib. shRNAs targeting *SOX10* were introduced into A375 cells by lentiviral transduction. pLKO.1 empty vector served as a control vector (Ctrl). Cells were seeded in 6-well plates at the same density in the presence or absence of drug(s) at the indicated concentration. Cells were cultured for 2 weeks in the absence of vemurafenib or 4 weeks in the presence of vemurafenib before fixing and staining. Figure 2e is shown again as a reference. **b**, Increased RTKs activation in *SOX10* knockdown cells by long-term vemurafenib treatment. A375 cells infected by shSOX10-1 vector or the PLKO.1 empty vector (Ctrl) were cultured in the absence or presence of 1 μM vemurafenib for the indicated number of days and processed with Human Phospho-Receptor Tyrosine Kinase Array Kit (R&D) according to the manufacturer's instructions. **c**, SOX10 knockdown upregulates both EGFR and PDGFRβ. Quantification of protein and mRNA were accomplished by western blot and qRT–PCR analysis. Error bars represent s.d. of measurement replicates ($n = 3$). **d**, Increased RTKs activation in A375 cells by long-term treatment with recombinant TGF-β (200 pg ml^{-1}) and vemurafenib (1 μM). A375 cells were cultured in the presence of vemurafenib (1 μM), recombinant TGF-β (200 pg ml^{-1}) or their combination for indicated number of days and processed with Human Phospho-Receptor Tyrosine Kinase Array Kit (R&D) according to the manufacturer's instructions. All experiments shown except RTK array analysis were performed independently at least twice.

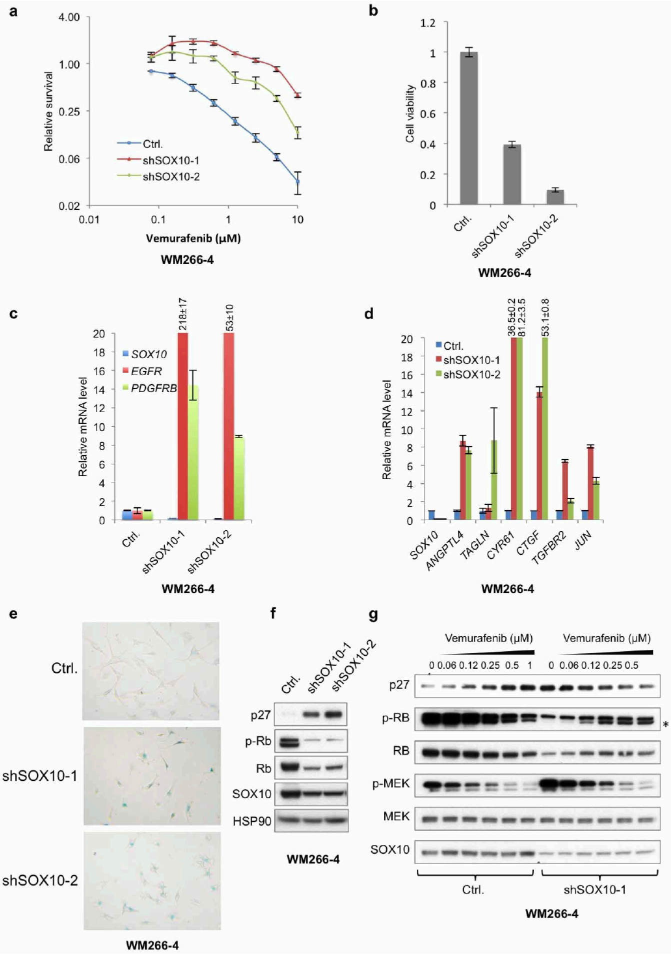

Extended Data Figure 4 | SOX10 loss activates TGF-β signalling and induces senescence in WM266-4 cells. **a**, SOX10 loss confers vemurafenib resistance in BRAF(V600D) melanoma cell line WM266-4. Cells expressing empty vector PLKO.1 (Ctrl) or shRNAs targeting *SOX10* transduced by lentivirus were treated with increasing concentrations of vemurafenib for 6 days. Cell viability was determined by CellTiter-Blue assay according to the manufacturer's instructions. Relative survival is represented as the ratio of cell viability in the presence of vemurafenib to that in the absence of drug treatment. Error bars represent s.d. of triplicate independent experiments. **b**, SOX10 downregulation leads to growth deficit in WM266-4 cells. Cells expressing the control vector pLKO.1 (Ctrl) or shRNAs against *SOX10* were seeded at the same density in 96-well plates and cultured for 6 days. Cell viability was determined by CellTiter-Blue assay. Error bars represent s.d. of triplicate independent experiments. **c**, *SOX10* suppression results in *EGFR* and *PDGFRB* upregulation in WM266-4 cells. Error bars represent s.d. of measurement replicates ($n = 3$). **d**, *SOX10* loss upregulates TGF-β receptor and its bona fide target genes. Relative mRNA level of *EGFR, PDGFRB, SOX10, ANGPTL4, TAGLN, CYR61, CTGF, TGFBR2* and *JUN* were determined by qRT–PCR analysis. pLKO.1 empty vector served as a control vector (Ctrl). Error bars represent s.d. of measurement replicates ($n = 3$). **e**, *SOX10* suppression induces senescence in WM266-4 cells. Senescence was detected by staining of β-galactosidase activity. **f**, Western blot analysis of RB protein, p-RB (S780), and CDK inhibitor CDKN1B ($p27^{kip1}$) in *SOX10* knockdown cells. HSP90 served as a loading control. **g**, Vemurafenib treatment compromises oncogene induced senescence in SOX10 knockdown cells. WM266-4 cells expressing pLKO.1 (Ctrl) or shSOX10-1 were seeded at the same density in 6-well plates and cultured in the absence or presence of vemurafenib at indicated concentration for 72 h before the sample collection for western blot analysis. All experiments shown were performed independently at least three times.

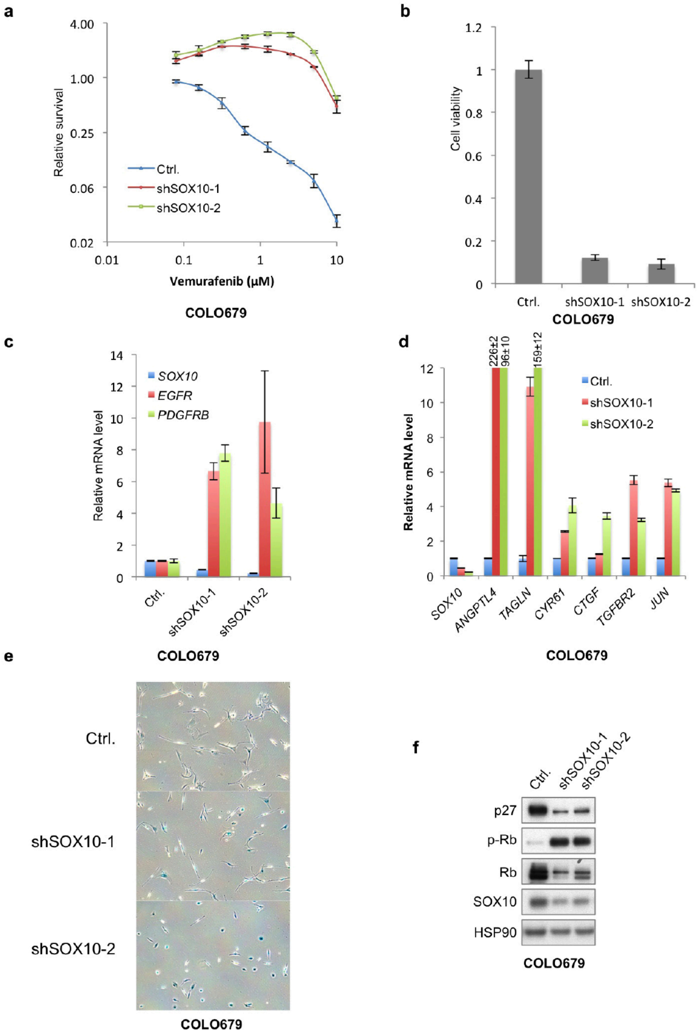

Extended Data Figure 5 | SOX10 loss activates TGF-β signalling and induces senescence in COLO679 cells. **a**, SOX10 loss confers vemurafenib resistance in BRAF(V600E) melanoma cell line COLO679. Cells expressing empty vector pLKO.1 (Ctrl.) or shRNAs targeting *SOX10* transduced by lentivirus were treated with increasing concentrations of vemurafenib for 6 days. Cell viability was determined using CellTiter-Blue according to the instruction of manufacturer. Relative survival is represented as the ratio of cell viability in the presence of vemurafenib to that in the absence of drug treatment. Error bars represent s.d. of triplicate independent experiments. **b**, SOX10 downregulation leads to growth deficit in COLO679 cells. Cells expressing the control vector pLKO.1 (Ctrl) or shRNAs targeting *SOX10* were seeded at the same density in 96-well plates and cultured for 6 days. Cell viability was determined using CellTiter-Blue assay. Error bars represent s.d. of triplicate independent experiments. **c**, *SOX10* suppression results in *EGFR* and *PDGFRB* upregulation in COLO679 cells. Error bars represent s.d. of measurement replicates ($n = 3$). **d**, *SOX10* loss upregulates TGF-β receptor and its bona fide target genes in COLO679 cells. Relative mRNA level of *EGFR*, *PDGFRB*, *SOX10*, *ANGPTL4*, *TAGLN*, *CYR61*, *CTGF*, *TGFBR2* and *JUN* were determined by qRT–PCR analysis. pLKO.1 empty vector served as a control vector (Ctrl). Error bars represent s.d. of measurement replicates ($n = 3$). **e**, *SOX10* suppression induces senescence in COLO679 cells. Senescence was detected by staining of β-galactosidase activity. **f**, Western blot analysis of RB protein, p-RB (S780) and CDK inhibitor CDKN1B (p27$^{\mathrm{kip1}}$) in SOX10 knockdown cells. HSP90 served as a loading control. All experiments shown were performed independently at least three times.

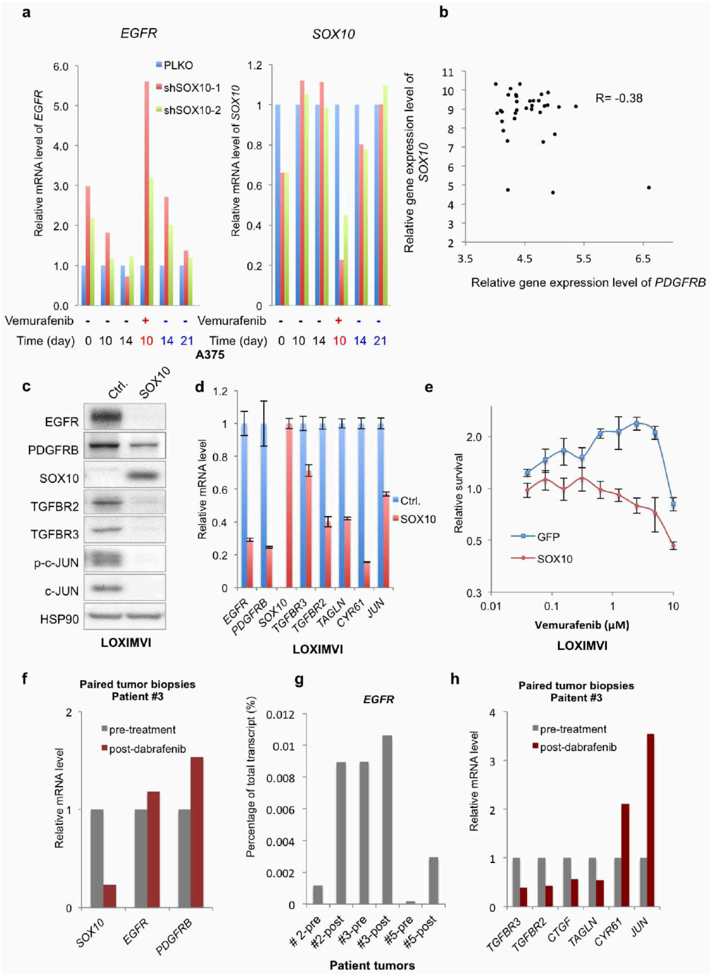

Extended Data Figure 6 | *EGFR* and *SOX10* expression are inversely correlated in melanoma. **a**, A375 cells infected by two independent non-overlapping sh*SOX10* vectors or the pLKO.1 empty vector (Ctrl) were cultured in the absence or presence of 1 µM vemurafenib for the indicated number of days. The last two samples (labelled in blue) were first treated with 1 µM vemurafenib for 10 days and subsequently cultured in the absence of vemurafenib for the indicated number of days. Means of duplicate measurements are shown. **b**, Inverse correlation between *SOX10* and *PDGFRB* in panel of human *BRAF* mutant melanoma cell lines. Relative gene expression levels of *SOX10* and *PDGFRB* were acquired from Cancer Cell Line Encyclopedia (CCLE). *R* stands for Pearson product-moment correlation coefficient. **c, d**, Ectopic expression of SOX10 suppresses TGF-β signalling and downregulates EGFR and PDGFRB in LOXIMVI cell line. SOX10 was introduced to LOXIMVI cells by lentiviral transduction (SOX10, pLX301-SOX10). pLX301-GFP served as a control vector (Ctrl). Protein levels were determined by western blot analysis and mRNA levels were determined by qRT–PCR analysis. Error bars represent s.d. of measurement replicates ($n = 3$). **e**, Ectopic expression of SOX10 sensitizes LOXIMVI cell to vemurafenib. Cells expressing GFP or SOX10 transduced by lentivirus were treated with increasing concentrations of vemurafenib for 6 days. Cell viability was determined using CellTiter-Blue assay. Relative survival is represented as the ratio of cell viability in the presence of vemurafenib to that in the absence of drug treatment. Error bars represent s.d. of triplicate independent experiments. **f**, *SOX10*, *EGFR* and *PDGFRB* expression levels in tumour biopsies from patient 3. **g**, *EGFR* expression levels in patient tumour samples (patient 2, 3 and 5), represented as percentage of *EGFR* transcript reads of the total number of transcript reads obtained through RNA-seq analysis. **h**, Gene expression level of TGF-β receptors and target genes in tumour biopsies from patient 3. **f–h**, Total RNA was isolated from FFPE specimens derived from tumour biopsies of patient as indicated both before and after development of drug resistance (Fig. 1a, b). After reverse transcription, gene expression levels were determined by transcriptome sequencing. All experiments shown except the ones that involve clinical samples were performed independently at least twice.

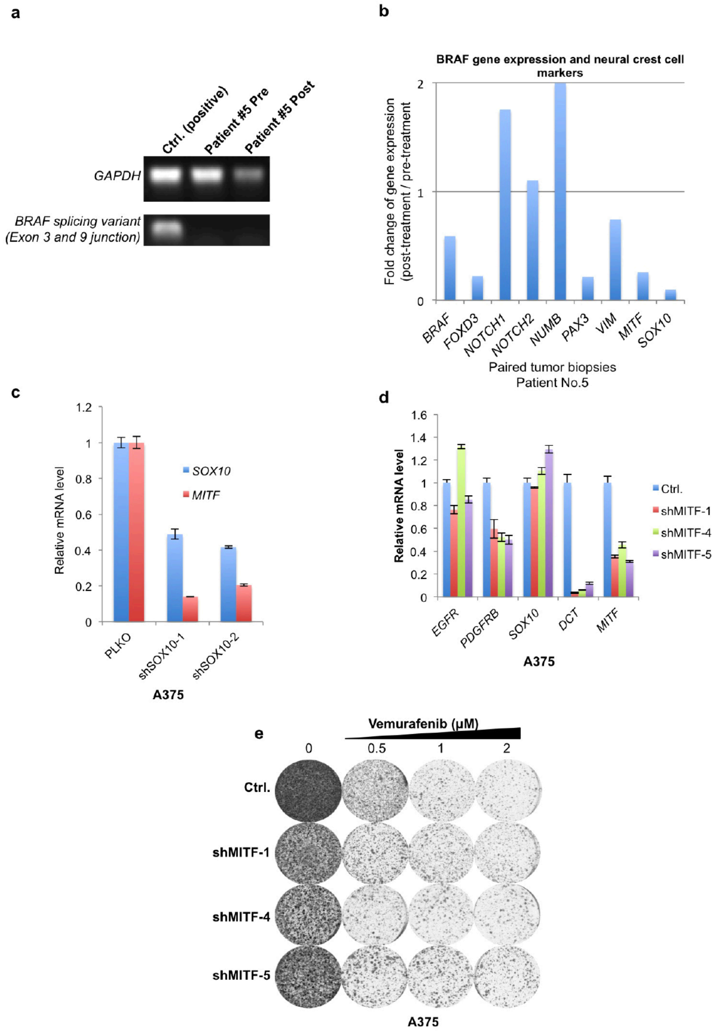

Extended Data Figure 7 | Role of BRAF and MITF in *SOX10*-induced drug resistance. **a**, PCR analysis of a *BRAF* splicing variant in cDNA from patient 5. PCR primers flanking the junction of exon 3 and exon 9 was used to detect the 61 kDa BRAF variant identified by ref. 7. cDNA derived from C4 clone of SKMEL-239 cells served as a positive control. **b**, Differential gene expression of *BRAF* and neural cell markers in patient biopsies. Total RNA was isolated from FFPE specimens derived from tumour biopsies of patient 5 before and after development of drug resistance (Fig. 1b). After reverse transcription, gene expression levels were determined by transcriptome sequencing. **c**, *SOX10* suppression leads to *MITF* downregulation. The mRNA levels of *MITF* and *SOX10* were determined by qRT–PCR analysis. pLKO.1 empty vector served as a control vector (Ctrl). Error bars represent s.d. of measurement replicates ($n = 3$). **d**, Suppression of *MITF* does not induce *EGFR* or *PDGFRB*. shRNAs targeting *MITF* were introduced to A375 cells by lentiviral transduction. Relative mRNA level of *SOX10, MITF, EGFR, PDGFRB* and *DCT* were determined by qRT–PCR analysis. Error bars represent s.d. of measurement replicates ($n = 3$). **e**, *MITF* knockdown does not affect vemurafenib sensitivity. shRNAs targeting *MITF* were introduced to A375 cells by lentiviral transduction. Cells were seeded at the same density in 6-well plates and cultured in the absence or presence of vemurafenib (for 3 weeks) at the indicated concentrations. The cells were fixed, stained and photographed. All experiments shown except the ones that involve clinical samples were performed independently at least twice.

An acquired vulnerability of drug resistant melanoma with therapeutic potential

4

Liqin Wang[1*], Rodrigo Leite de Oliveira[1*], Sanne Huijberts[2], Evert Bosdriesz[1], Nora Pencheva[1], Diede Brunen[1], Astrid Bosma[1], Ji-Ying Song[3], John Zevenhoven[3], Tijtske Los- de Vries[1], Hugo Horlings[1, 3],Bastiaan Nuijen[4], Jos H. Beijnen[4], Jan H.M. Schellens[2] and Rene Bernards[1#]

* Co-first author
# Correspondence

1 Division of Molecular Carcinogenesis, Oncode Institute, Cancer Genomics Centre Netherlands. The Netherlands Cancer Institute, Plesmanlaan 121, 1066 CX Amsterdam, The Netherlands.
2 Division of Clinical Pharmacology, Oncode Institute, The Netherlands Cancer Institute, 1066 CX Amsterdam, The Netherlands
3 Division of Molecular Genetics, The Netherlands Cancer Institute, Amsterdam, The Netherlands.
4 Department of Pharmacy and Pharmacology, The Netherlands Cancer Institute, Amsterdam, The Netherlands

Cell (2018)

Abstract

BRAF(V600E) mutant melanomas treated with inhibitors of the BRAF and MEK kinases almost invariably develop resistance, which is frequently caused by reactivation of the Mitogen Activated Protein Kinase (MAPK) pathway. To identify novel treatment options for such patients, we searched for acquired vulnerabilities of MAPK inhibitor-resistant melanomas. We find that resistance to BRAF+MEK inhibitors is associated with increased levels of reactive oxygen species (ROS). Subsequent treatment with the histone deacetylase inhibitor vorinostat suppresses *SLC7A11*, leading to a lethal increase in the already elevated levels of ROS in drug-resistant cells. This causes selective apoptotic death of only the drug resistant tumor cells. Consistently, treatment of BRAF inhibitor resistant melanoma with vorinostat in mice results in a dramatic tumor regression. In a study in patients with advanced BRAF+MEK inhibitor resistant melanoma, we find that vorinostat can selectively ablate drug-resistant tumor cells, providing clinical proof of concept for the novel therapy identified here.

Introduction

Approximately half of melanoma skin cancers carry activating mutations in the *BRAF* oncogene, leading to activation of the Mitogen Activated Protein Kinase (MAPK) pathway. Inhibition of the BRAF oncoprotein with targeted drugs provides substantial benefit to patients, albeit that most patients ultimately relapse with resistant disease (Sosman et al., 2012). Dual inhibition of both BRAF and the downstream MEK kinases leads to more sustained clinical benefit, but resistance is still mostly inevitable (Robert et al., 2014). Resistance to MAPK pathway inhibitors in melanoma is frequently caused by reactivation of signaling through this pathway in the presence of drug (Van Allen et al., 2014; Wagle et al., 2014). Multiple mechanisms of MAPK reactivation have been described, including upregulation of Receptor Tyrosine Kinases (RTKs), mutations in *KRAS* and *NRAS*, splice site mutations in BRAF, amplification of *BRAF* and mutation of *MEK* kinases (reviewed by (Manzano et al., 2016)). Drug withdrawal in such drug-resistant patients often does not lead to an immediate disease flare up, but rather to a transient pause in tumor growth, known as the "drug holiday effect" (Seghers et al., 2012). This effect can be explained, at least in part, by hyper-activation of the MAPK pathway signaling following drug withdrawal, leading to a cellular state that has hallmarks of oncogene-induced senescence (Sun et al., 2014). Downregulation of this hyper-active MAPK signaling marks the end of the drug holiday, resulting in re-initiation of tumor growth and regained drug sensitivity upon rechallenge with BRAF inhibitor (Seghers et al., 2012).

Besides targeted therapies, development of immune checkpoint inhibitors has dramatically improved outcomes for patients with melanoma. Such therapies often provide more lasting responses, making checkpoint blockade therapy the first therapy choice in most cancer centers today in most cancer centers (Schadendorf et al., 2015). If checkpoint blockade therapy fails, patients that have a *BRAF* mutant tumor are most often offered treatment consisting of dual blockade of the BRAF and MEK kinases.

The transient proliferation arrest of BRAF inhibitor-resistant melanomas following drug withdrawal points towards an acquired vulnerability of drug-resistant cells that was not present in the parental drug-sensitive cells (Sun et al., 2014). That drug resistance of cancer cells comes at a fitness cost that in turn can cause sensitivity to other drugs was already identified over 50 years ago and is referred to as "collateral sensitivity" (Hutchison, 1963). This phenomenon is widespread in biology, as also bacteria that develop resistance to antibiotics can acquire collateral sensitivity to other antibiotics (Imamovic and Sommer, 2013). Previous studies have pointed towards alterations in mitochondrial oxidative metabolism when signaling through the MAPK pathway is modulated (Baenke et al., 2016; Corazao-Rozas et al., 2013; Haq et al., 2013; Hernandez-Davies et al., 2015; Vazquez et al., 2013). We report here a collateral sensitivity of BRAF-inhibitor resistant melanoma that takes advantage of increased levels of reactive oxygen species (ROS) in drug-resistant cells. We find that increased ROS levels cause an acquired vulnerability to histone deacetylase inhibitors. We demonstrate the potential utility of this sequential therapy in a proof of concept clinical study.

Results

A vulnerability of MAPKi-resistant melanoma

To explore new therapeutic strategies for melanomas having acquired resistance to inhibitors of the MAPK pathway, we generated drug-resistant derivatives of *BRAF* mutant A375 human melanoma cells by long-term culture in the presence of the BRAF inhibitor vemurafenib (A375R, Resistant cells) or a combination of the BRAF inhibitor dabrafenib and the MEK inhibitor trametinib (A375DR, Double Resistant cells). In a short-term proliferation assay A375R and A375DR cells proliferated in the presence of vemurafenib and the combination of dabrafenib plus trametinib, respectively, whereas parental A375 cells were sensitive to MAPK inhibition (Figure 1A). In the absence of MAPK inhibitors (MAPKi), A375R and A375DR cells displayed a slight proliferation impairment, modeling the drug holiday effect seen in the clinic (Seghers et al., 2012). Quantification of cell viability at the end of the proliferation assay confirmed the sustained viability of the MAPKi-resistant A375R and A375DR derivatives in the presence of the drugs (Figure 1B). Further characterization of these derivatives revealed that A375R cells have gained Platelet Derived Growth Factor Receptor B (PDGFRB) expression (Figure 1C), while A375DR cells acquired a secondary $NRAS^{Q61H}$ mutation (Figure 1D). Equivalent findings were observed in Mel888 cells, another BRAFV600E mutated human melanoma model. After a similar long-term culture protocol in MAPKi, we isolated a variant resistant to vemurafenib (Mel888R; Figures S1A, C) and a line resistant to the combination of dabrafenib plus trametinib (Mel888DR; Figures S1B, C). Mel888R cells express a splice variant of BRAF (Figure S1D), whereas Mel888DR harbor a secondary $KRAS^{G12C}$ mutation (Figure S1E). These four resistance mutations commonly found in melanoma patients that develop resistance to drugs that target BRAF and/or MEK kinases converge on the hyper-activation of the MAPK pathway. These data also underscore that, although generated in vitro, our drug-resistant melanoma cell line derivatives faithfully recapitulate clinical drug resistance.

One of the features of increased RAS signaling is the abundant production of reactive oxygen species (ROS), which serve as signaling molecules in multiple cellular pathways (Chio and Tuveson, 2017; Lee et al., 1999; Reczek and Chandel, 2017; Ruefli et al., 2001). To test whether this is also the case in melanoma, we measured ROS levels using fluorescent flow cytometry. Indeed, basal levels of ROS were 2-fold higher in single drug resistant cells (A375R and Mel888R) as compared to parental cells and increased even further in double drug resistant cells (A375DR and Mel888DR; Figures 1E, S1F). We hypothesized that this increase in ROS levels may represent an acquired vulnerability in the sense that a further increase in ROS levels could become detrimental to the drug-resistant cells. To test this, we exposed parental and drug-resistant melanoma cells to paraquat, an established ROS inducer. Indeed, we found that paraquat treatment inhibited the proliferation of single resistant A375R cells and double resistant A375DR cells in a colony formation assay, while it induced only a slight proliferation impairment in the parental cells (Figures 1F, G; S1G, H). The sensitivity to paraquat in resistant melanoma cells was proportional to the higher basal ROS levels (Figures 1E, S1F) and correlated with an increase of DNA damage and apoptosis, as evidenced by the presence of γ-H2AX and cleaved PARP, respectively (Figures 1I, S1J). The notion that increased sensitivity of MAPKi-resistant cells to paraquat is mediated by increased ROS levels is supported by the observation that treatment with the ROS scavenger N-acetyl-cysteine (NAC) negated the sensitivity of BRAFi-resistant cells to paraquat (Figures 1H, S1I) and reduced DNA damage and apoptosis (Figures 1I, S1J). In addition, we confirmed that the ROS levels induced by paraquat were reduced by NAC in our panel of melanoma cells (Figures 1J, S1K). These findings indicate that regardless of the type of mutation responsible for acquired MAPKi-resistance in melanomas, ROS induction is a common vulnerability that can be targeted with ROS inducers.

MAPKi-resistant melanoma cells are sensitive to vorinostat

To take this concept closer to a potential clinical use, we searched for approved drugs that also induce ROS. We selected histone deacetylase inhibitor (HDACi) vorinostat, because vorinostat has a safe pharmacological profile in the clinic and HDACi are known to induce ROS (Petruccelli et al., 2011; Ruefli et al., 2001; Ungerstedt et al., 2005; Wolf et al., 2014). To test whether vorinostat also induces ROS in melanoma, we treated our two cell models with vorinostat for 72 hours and measured intracellular ROS. Indeed, vorinostat induced ROS levels in parental and resistant cells, which could be prevented by co-treatment with NAC (Figure 2A; Figure S2A). In long-term proliferation assays, vorinostat treatment inhibited the growth of drug resistant cells, but the combination of vorinostat and NAC rescued this effect in both melanoma models (Figures 2B, S2B). Again, the vorinostat effect was far more pronounced in MAPKi-resistant melanoma cells, as it only caused a mild proliferation impairment in parental cells. This is also confirmed in a short-term Incucyte assay (Figures 2C, S2C). The differential effect of vorinostat is most likely explained by the much higher ROS levels induced in MAPKi-resistant melanoma cells as compared to the ROS levels induced by vorinostat in parental cells (Figures 2A, S2A). Similar to paraquat treatment, vorinostat induced DNA damage and apoptosis in BRAFi-resistant, but not in parental A375 cells, which was rescued by NAC treatment (Figure 2D). In Mel888 cells, vorinostat treatment also induced apoptosis in MAPKi-resistant cells (Mel888R and Mel888DR) but not in the parental line (Figure S2D). Essentially the same results were obtained with a second ROS scavenger glutathione ethyl ester (GEE) as GEE also reduced ROS levels induced by vorinostat and rescued the proliferation defect induced by vorinostat in MAPK inhibitor resistant cells (Figures 2E, F, S2E, F). These observations suggest that a certain ROS level is required to inflict sufficient DNA damage and to activate cell death pathways, which is only achieved by vorinostat in drug-resistant, but not in parental melanoma cells. We also tested the vorinostat sensitivity in *NRAS* mutant melanoma cells, since this gene is the second most commonly mutated in melanoma patients. We generated *NRAS* mutant SK-MEL-147 melanoma cells resistant to MEK inhibitor by long-term culture in trametinib-containing medium. Vorinostat treatment of parental SK-MEL-147 cells and resistant derivatives (SK-MEL-147R) induced an increase in intracellular ROS levels that could be abrogated with co-treatment with NAC (Figure S2G). Accordingly, in a colony formation assay SK-MEL-147R cells showed increased sensitivity to vorinostat as compared to the parental line. This sensitivity was reversed by the concomitant treatment with NAC (Figure S2H).

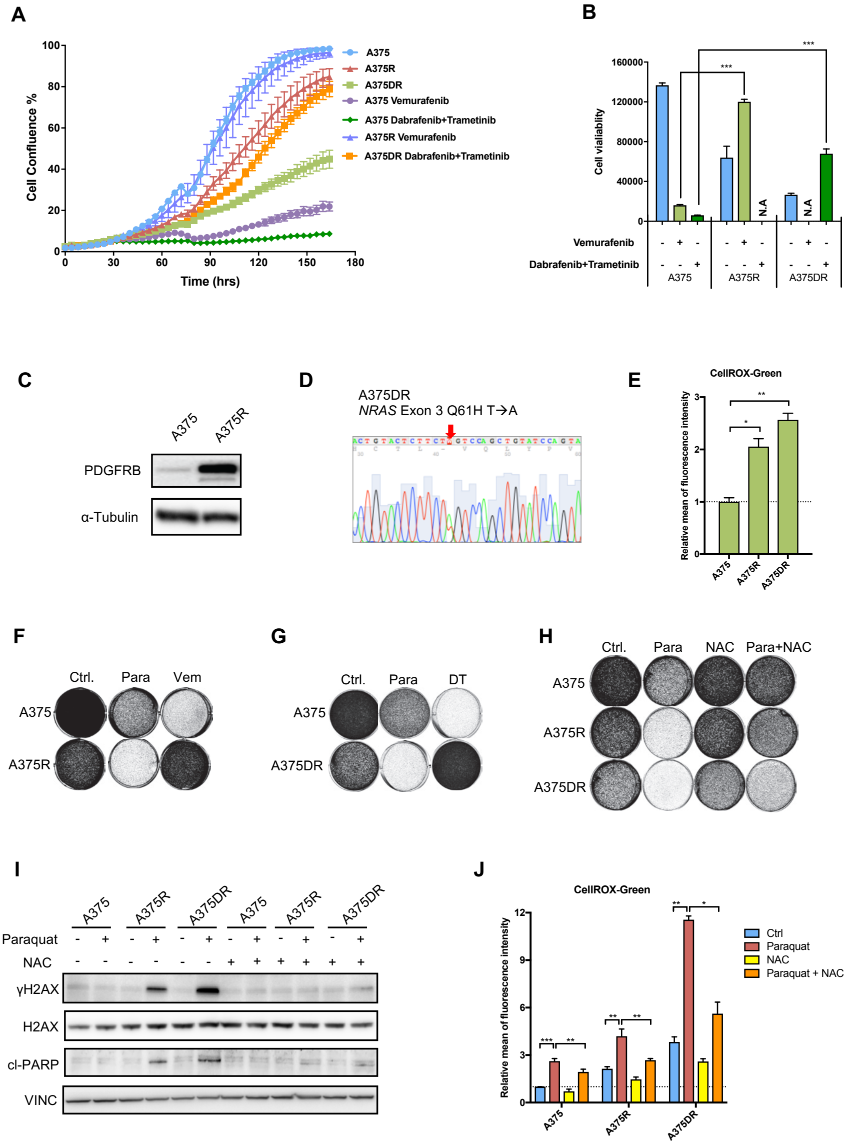

Figure 1. ROS levels and ROS sensitivity of melanoma cells.

(A). Incucyte proliferation assays of parental (A375), BRAFi-resistant (A375R) and BRAFi/MEKidouble resistant (A375DR) melanoma cells in the presence or absence of 2 µM vemurafenib or combination of 0.5 µM dabrafenib and 10 nM trametinib. (B) Quantification of cell viability assay of parental and drug-resistant cells cultured in the presence or absence of MAPK inhibitors shown in panel A at the end of the assay. Cell viability was quantified with CellTiter-Blue®. (C) Western blot analysis of PDGFRB expression in A375 cells and A375R cells. (D) Sanger sequencing analysis of *NRAS* gene in A375DR cells showing gain of *NRAS*^{Q61H} mutation. (E) ROS levels of A375R, A375DR and parental A375 cells measured after 72 hours of culturing without drugs. ROS levels were measured using CellROX-Green flow cytometry assay. Relative ROS levels are plotted. (F, G) Long-term colony formation assays of A375R (panel F), A375DR (panel G) compared to parental A375 cells treated with paraquat and/or MAPK inhibitors (Vem:vemurafenib; DT: dabrafenib+trametinib). Cells were seeded 50,000 cells per well in 6-well plates and treated with 20 µM paraquat, 2 µM vemurafenib or combination of 10 nM trametinib and 0.5 µM dabrafenib for 10 days. Afterwards, the cells were fixed, stained and photographed. (H) Long-term colony formation assays of parental and MAPKi-resistant A375 cells treated with paraquat and/or NAC. Cells were seeded 50,000 cells per well in 6-well plates and treated with 20 µM paraquat and/or 2.5 mM N-acetyl-L-cysteine (NAC) for 10 days. Afterwards, the cells were fixed, stained and photographed. (I) Protein lysates were harvested from the MAPKiresistant (R and DR cells) and parental A375 cells treated with 25 µM paraquat and/or 2.5 mM NAC for 72 hours. Western blot analysis of γH2AX as a DNA damage marker and cleaved-PARP (cl-PARP) as an apoptosis marker, vinculin (VINC) served as the loading control. (J) Parental and MAPKi-resistant A375 cells were treated with 20µM paraquat and/or 2.5 mM NAC for 72 hours. ROS levels were measured using CellROX-Green flow cytometry assay. Error bars in this figure represent as mean ± standard deviations from biological triplicates (*P≤0.05, ** P≤0.01, *** P≤0.001, student's t-test).

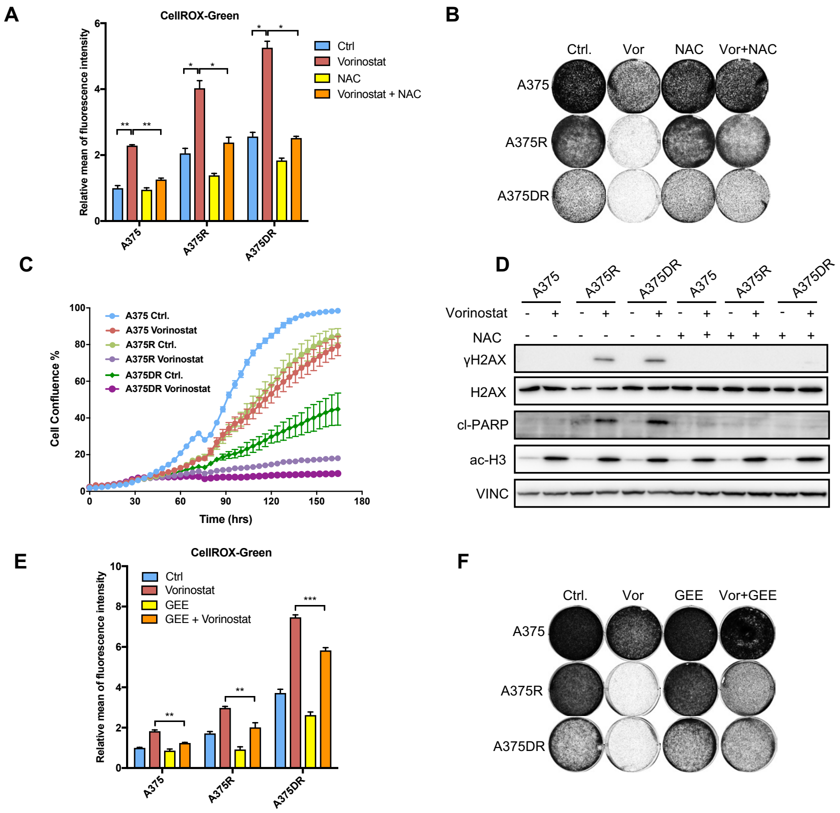

Figure 2. HDACi is detrimental to MAPKi-resistant melanoma cells.
(A) Parental and MAPKi-resistant A375 cells were treated with 2 µM vorinostat and/or 2.5 mM NAC for 72 hours. ROS levels were measured using CellROX-Green flow cytometry assay. Relative ROS levels are indicated. (B) Long-term colony formation assays of parental and MAPKi-resistant A375 cells treated with vorinostat and/or NAC. Cells were seeded 50,000 cells per well in 6-well plates and treated with 1 µM vorinostat and/or 2.5 mM NAC for 8 days. Afterwards, the cells were fixed, stained and photographed. (C) Incucyte proliferation assay of parental and MAPKi-resistant A375 cells were seeded 400 cells per well in a 384-well plate and cultured in the presence or absence of 1 µM vorinostat. (D) Protein lysates were harvested from the MAPKi-resistant and parental A375 cells treated with 1 µM vorinostat and/or 2.5 mM NAC for 72 hours and Western blot analysis performed for gamma-H2AX (γH2AX) as a DNA damage marker and cleaved-PARP (cl-PARP) as an apoptosis marker. Ac-H3 as indicator for levels of acetylated histone H3. Vinculin (VINC) served as the loading control. (E) Parental and MAPKi-resistant A375 cells were treated with 2 µM vorinostat and/or 2.5 mM reduced glutathione ethyl ester (GEE) for 72 hours. ROS levels were measured using CellROX-Green flow cytometry assay. Relative ROS levels are indicated. (F) Long-term colony formation assays of parental and MAPKi-resistant A375 cells treated with vorinostat and/or GEE. Cells were seeded 50,000 cells per well in 6-well plates and treated with 1 µM vorinostat and/or 2.5 mM GEE for 8 days. Afterwards, the cells were fixed, stained and photographed. Error bars in this figure represent as mean ± standard deviations from biological triplicates (*$P \leq 0.05$, ** $P \leq 0.01$, *** $P \leq 0.001$, student's t-test).

MAPK inhibition is antagonized by HDACi

It has been shown in short-term assays that combined HDAC and MAPK inhibition can prevent some forms of MAPK inhibitor resistance in melanoma (Johannessen et al., 2013). It has also been shown, however, that increased ROS levels lead to activation of the MAPK pathway (Son et al., 2011). This would suggest that vorinostat, by virtue of its increase in ROS levels, could activate MAPK signaling and thereby counteract the effects of MAPK inhibitors. Indeed, also in melanoma, vorinostat activated MAPK signaling in A375, A375R and A375DR cells, as evidenced by an increase in phosphorylated MEK (pMEK) and p-P90RSK (Figure 3A, B). While MAPK inhibitors were able to reduce levels of pMEK and p-P90RSK in all three cells, combined treatment with MAPKi and vorinostat resulted in significant residual MAPK signaling (Figure 3A, B). Consistent with this, treatment of A375 or Mel888 cells with a combination of HDACi and MAPKi resulted in continued proliferation (Figure 3C, S3C). Conversely, while A375DR and A375R are hyper-sensitive to three different HDAC inhibitors, the combination of MAPKi and HDACi resulted in a poor response (Figure 3C, D). This finding is most readily explained by the reduced MAPK signaling caused by the MAPKi, resulting in lower ROS levels and hence a lesser effect of ROS increase by HDACi. Indeed, treatment of A375 and A375 DR cells with MAPK inhibitors reduced ROS levels and suppressed in the increase in ROS caused by vorinostat (Figures 3E, F). Essentially the same results were obtained in short-term proliferation assays (Figures 3G-L), in additional *BRAF*^{V600E} mutant melanomas (Figures S3C-G), as well as in the NRAS mutant melanoma models (Figure S3H).

To further study the antagonism of ROS and MAPK inhibition, we performed long-term colony formation on A375 cells treated with the BRAFi vemurafenib and/or the ROS inducer paraquat. Figure 3M and S3I show that the ROS inducers paraquat and DMNQ inhibit the proliferation of the cells in a dose dependent manner, but this was counteracted by vemurafenib. Moreover, paraquat and tert-butylhydroperoxide (tBHP, another ROS inducer) both caused an increase in RAS-GTP loading in A375 cells and prevented vemurafenib from effectively inhibiting MEK activity (Figures 3N-O). These results indicate that indeed ROS can positively regulate MAPK signaling, as previously shown by others (Son et al., 2011). Consistently, vorinostat can increase RAS-GTP loading in A375, but this induction can be abrogated by co-treatment with the ROS scavenger NAC (Figure 3P). Taken together, these data indicate antagonistic effects of HDACi and MAPKi and emphasize the need to administer MAPK and HDAC inhibitors in a therapeutic setting sequentially rather than simultaneously, a notion that is further tested below.

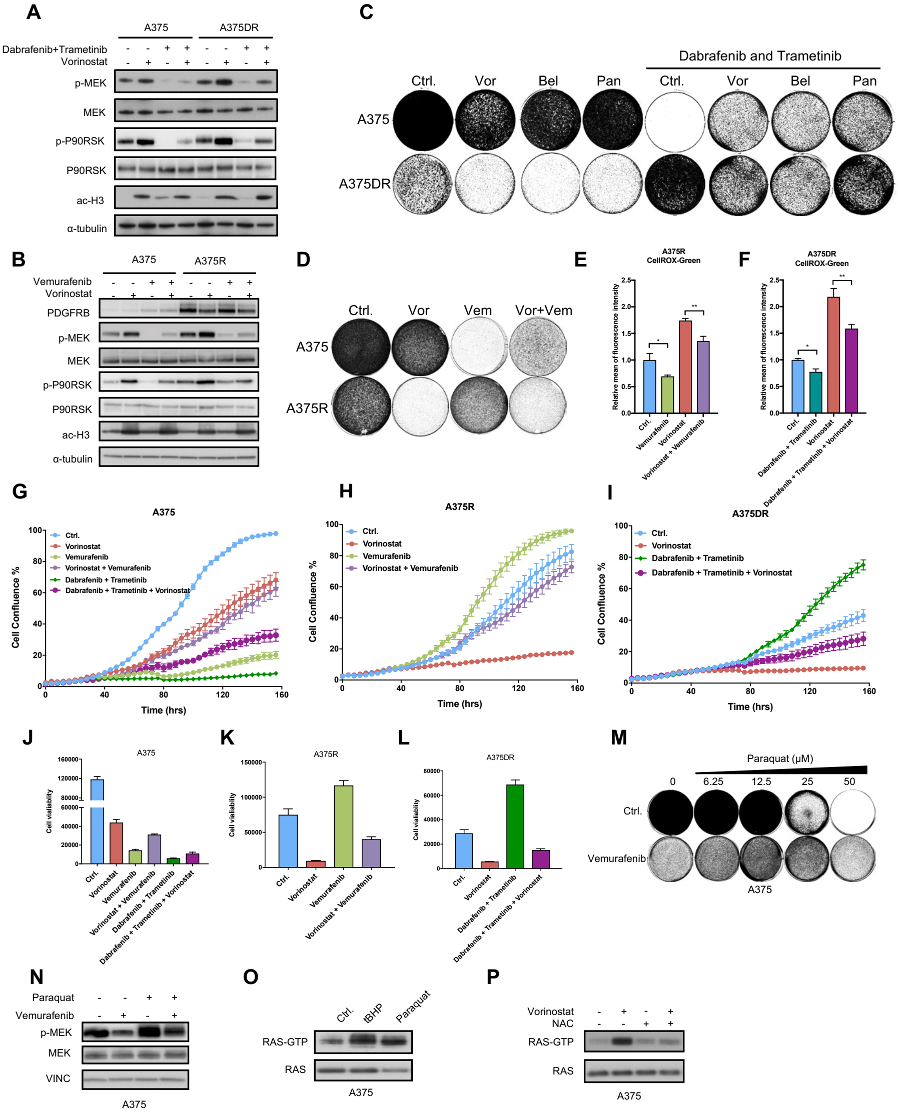

Figure 3. MAPK inhibition is antagonistic with HDAC inhibition.
(A) BRAFi/MEKi-resistant A375DR and the parental A375 cells were treated with 2 μM vorinostat and/or the combination of 0.125 μM dabrafenib and 5 nM trametinib. Protein lysates were harvested after 72 hours. Western blot analysis was carried out for p-MEK and p-P90RSK as indicators of activation of MAPK pathway, ac-H3 as indicator for levels of acetylated histone H3 and α-tubulin as a loading control. (B) A375R and the parental cells were treated with 2 μM vorinostat and/or 0.5 μM vemurafenib for 72 hours after which protein lysates were harvested. Western blot analysis was performed for p-MEK and p-P90RSK as activation of MAPK pathway, ac-H3 indicated levels of acetylated histone H3, PDGFRB, α-tubulin served as the loading control. (C) A375DR and parental cells were seeded 50,000 cells per well in 6-well plates and treated with 1 μM vorinostat (Vor), 0.5 μM belinostat (Bel), 5 nM panobinostat (Pan) and/or combination of 5 nM trametinib and 0.125 μM dabrafenib. (D) A375R and parental cells were seeded 50,000 cells per well in 6-well plates and treated with 1 μM vorinostat and/or 1 μM vemurafenib. After 10 days culturing, the cells were fixed, stained and photographed. (E-F) Relative ROS level meaurements of A375R treated with 2 μM vorinostat and/or 2 μM vemurafenib (E), A375DR cells with 2 μM vorinostst and/or the combination of 0.125 μM dabrafenib and 5 nM trametinib (F). (G-I) Incucyte proliferation assay of A375 cells (G), A375R cells (H) and A375DR (I) cells seeded at 400 cells per well in a 384-well plate cultured in the presence or absence of 1 μM vorinostat, 1 μM vemurafenib and/or combination of 62.5 nM dabrafenib and 5 nM trametinib. (J-L) At the end of the Incucyte assay, the cell viability of A375 cells (J), A375R cells (K) and A375DR cells (L) cells were quantified. Cell viability was measured with CellTiter-Blue®. (M) Long-term colony formation assays of A375 cells treated with 0.25 μM vemurafenib and indicated concentrations of paraquat for 10 days. (N) A375 cells were treated with 50 μM paraquat and/or 0.25 μM vemurafenib and protein lysates were harvested after 48 hours. Western blot analysis was performed for p-MEK and total MEK. Vinculin (VINC) served as the loading control. (O) RAS-GTP loading measurement by western blot in A375 cells treated for 30 minutes with 125 mM tert-Butyl hydroperoxide (tBHP) or 48 hours of 50 μM paraquat treatments. (P) RAS-GTP loading measurement by western blot in A375 cells treated with 2 μM vorinostat and/or 5mM NAC for 72 hours. Error bars in this figure represent as mean ± standard deviations from biological triplicates (*P≤0.05, ** P≤0.01, *** P≤0.001, student's t-test).

HDACi confers a disadvantage to MAPKi resistant melanoma

We have shown previously that acquisition of resistance to vemurafenib leads to a transient proliferation arrest upon drug withdrawal, phenocopying the transient arrest in tumor growth upon drug withdrawal seen in the clinic, known as the drug holiday effect (Seghers et al., 2012; Sun et al., 2014). Biochemically, vemurafenib withdrawal in drug-resistant cells resulted in hyperactivation of the MAPK pathway and indeed such cells have hallmarks of "oncogene-induced senescence" (Sun et al., 2014). Our present data indicate that treatment of MAPKi resistant melanoma with HDACi results in active cell death, suggesting that this treatment is more effective in MAPKi-resistant melanoma than in drug sensitive cells. We tested this prediction in a competition assay using a mixed population of parental and two MAPKi-resistant derivatives (R and DR) of A375 cells and Mel888 cells. Drug sensitive and resistant cells were labeled with Green or Red fluorescent proteins through transduction with lentiviral vectors encoding GFP and RFP. The two cell populations were mixed in a 1:9 or 1:8 ratio of drug resistant cells over drug sensitive cells and cultured with either no drug (drug holiday effect), MAPKi or HDACi, as schematically outlined in Figure 4A. Relative abundance of the two populations was followed over 17 days using quantification by flow cytometry. Figure 4B shows that MAPK inhibition efficiently depleted GFP+ parental cells and enriched RFP+ MAPKi-resistant cells. In contrast, RFP+ MAPKi-resistant cells were depleted by vorinostat treatment, while GFP+ parental cells were enriched. The drug holiday arm followed the same trend as the vorinostat arm, however the changes were moderate and initiated at a later time point (Figure 4B, C, S4A, B). These results support the notion that a switch from MAPKi to HDACi can specifically deplete the drug-resistant cells in a heterogeneous melanoma population that harbors both drug sensitive and drug resistant cells. Moreover, the competition experiment indicates that a switch to HDACi upon development of resistance to MAPKi is more effective in eliminating drug resistant cells than a drug holiday.

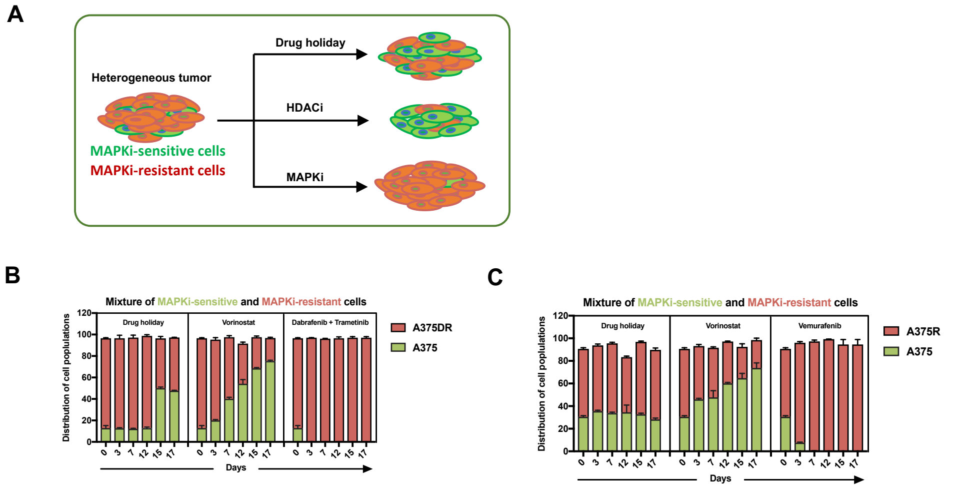

Figure 4. HDACi is detrimental to MAPKi-resistant melanoma.
(A) Schematic of the in vitro competition assay to study the effect of HDAC inhibition in a heterogeneous tumor containing both MAPKi-resistant and MAPKi-sensitive cells. MAPKi-resistant cells were labeled with red fluorescent protein (RFP) through stable infection with a lentiviral vector pLKO-H2B-RFP. MAPKi-sensitive cells were labeled with green fluorescent protein (GFP) by infection with lentiviral vector pLKO-H2B-GFP. After mixing the MAPKi-resistant and sensitive cell populations, the cells were followed after different treatments. MAPK inhibition served as a control. MAPKi treatment resulted in enrichment of RFP+ cells. (B) MAPKi-resistant A375DR cells (RFP+) or A375R cells (C) were mixed in 9 to 1 ratio with MAPKi-sensitive parental A375 cells (GFP+) and then 2,000,000 cells were seeded cells into 10-cm dishes and followed after different treatments. At each time point, the distribution of the cell populations was determined using flow cytometry. The ratio of two cell population were indicated at the starting of the experiment (day 0). The distribution changes of the two cell populations were plotted on the Y-axis against the time on the X-axis. Error bars in this figure panel denoted standard deviations of biological triplicates. Error bars in these figure panels denoted standard deviations of biological triplicates.

HDACi induce ROS through suppression of SLC7A11

To systematically interrogate the molecular pathways governing ROS induction upon HDACi treatment, we performed transcriptome profiling by next-generation RNA sequencing (RNAseq) of A375 parental and MAPKi-resistant derivatives (A375R and A375DR) treated with and without vorinostat. This analysis identified a set of 12 genes commonly downregulated in the three cell lines upon HDACi treatment (Table S1). We focused our attention on SLC7A11, as it encodes the cystineglutamate antiporter xCT. This transporter is responsible for the cellular intake of cystine, the precursor of the major antioxidant glutathione (GSH) (Bannai and Tateishi, 1986; Gout et al., 1997). Suppression of this antiporter can therefore lead to reduction of cellular GSH levels and, consequently, increased cellular ROS. It was shown previously that vorinostat suppresses *SLC7A11* expression in malignant gliomas (Wolf et al., 2014). To investigate whether HDACi can induce ROS through *SLC7A11* suppression in *BRAF* or *NRAS* mutant melanomas, we first quantitated changes in *SLC7A11* expression upon treatment of parental and resistant melanoma cells with HDACi using qRT-PCR. Vorinostat indeed transcriptionally suppresses *SLC7A11* in three melanoma models (Figures 5A, S5A, S5I). Consistent with a role for SLC7A11 in GSH import, vorinostat treatment reduced GSH levels in two melanoma models (Figure 5B, S5B). In addition, genetic silencing of *SLC7A11* using multiple shRNAs significantly increased melanoma ROS levels (Figures 5C, D). It is important to note that ROS induction correlates with the gene knockdown efficiency of the shRNAs used. These shRNAs also suppressed proliferation in our melanoma models, in particular the double-resistant cells (Figures 5E, S5D). Next, we used the most efficient shRNA (shSLC7A11-4) to study the effect of SLC7A11 reduction on ROS induction. We observed that *SLC7A11* suppression correlated with increased ROS levels both in the parental cells and also in the MAPKi-resistant derivatives (Figures 5F, G, S5C, E). This result suggests that the HDACi-mediated ROS induction is (at least in part) due to the reduction of *SLC7A11* expression in melanomas, leading to reduced GSH levels in the cancer cells. The ROS scavenger trolox acts on the lipid peroxidation process only and does not affect ROS levels in A375R and A375DR cells and does not rescue the toxicity of vorinostat in these cells (Valko et al., 2007) (Figure S5M, N). Glutathione in contrast acts more broadly on oxygen radicals and therefore is more efficient in rescuing increased ROS in melanoma (see also Figure 2E, S2E). To further support the notion that *SLC7A11* suppression is responsible for ROS modulation by HDACi, we overexpressed *SLC7A11* using a lentiviral vector leading to a 25- to 30-fold increase in *SLC7A11* mRNA levels (Figure 5I). Our data predict that *SLC7A11* overexpression should rescue the HDACi-mediated ROS induction and consequently also the anti-proliferation effect of vorinostat. The short-term Incucyte proliferation assay (Figures 5J, K) and long-term colony formation assay (Figures 5L, S5G) indicate that the HDACi-mediated antiproliferation effect is reduced by *SLC7A11* overexpression. Quantification of the short-term proliferation assays are shown in Figure S5O. Moreover, HDACi-mediated ROS induction was abrogated by *SLC7A11* overexpression (Figures 5M, S5H). This same mechanism was confirmed in additional *NRAS* mutant melanoma (SK-MEL-147) models (Figures S5I-L).

In vivo study of sequential drug treatment

Next, we tested the effectiveness of sequential treatment of melanoma with BRAFi, followed by a switch to HDACi upon progression on BRAFi *in vivo*. We injected immunodeficient nude

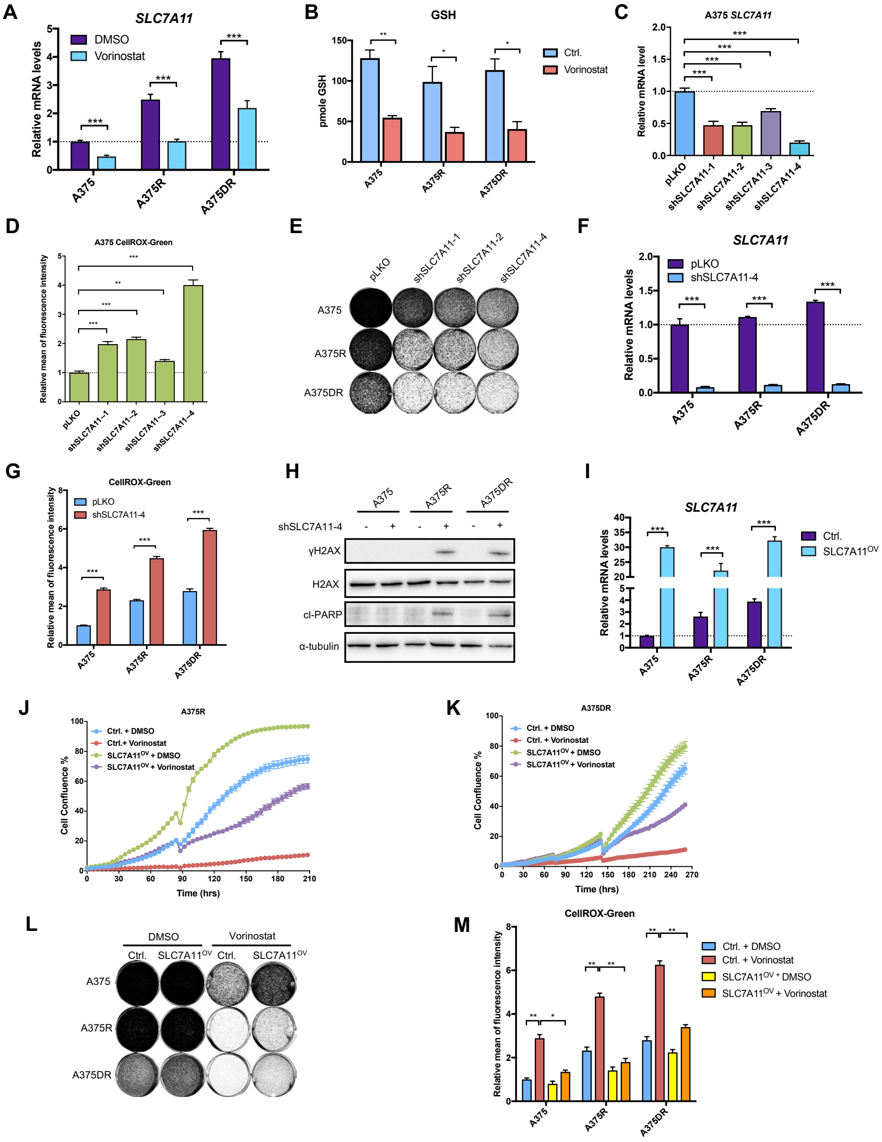

Figure 5. HDACi suppresses SLC7A11 resulting in ROS induction.
(A) mRNA expression analysis of *SLC7A11* by qRT-PCR in parental and MAPKi-resistant A375 cells treated with 2 μM vorinostat for 48 hours. (B) Parental and MAPKi-resistant A375 cells were treated with 2 μM vorinostat for 72 hours. Total intracellular glutathione (GSH) levels were measured using colorimetric based glutathione detection assay. (C) Four independent shRNAs targeting SLC7A11 were individually introduced in A375 cells by lentiviral transduction. pLKO empty vector served as the control. Shown is the level of *SLC7A11* knockdown by each shRNAs was measured by qRT-PCR. (D) Relative ROS induction upon *SLC7A11* knockdown as measured by flow cytometry. (E) Long-term colony formation of parental and MAPKi-resistant A375 cells upon *SLC7A11* knockdown. The cells were seeded 50,000 cells per well in 6-well plate and cultured 10 days. Afterwards, the cells were fixed, stained and photographed. (F) The levels of *SLC7A11* knockdown in parental and MAPKi-resistant A375 cells were measured by qRT-PCR. (G) Relative ROS levels in parental and MAPKi-resistant A375 cells upon *SLC7A11* knockdown were measured by CellROX-Green flow cytometry assay. (H) Protein

lysates were harvested from the MAPKi-resistant and parental A375 cells with/without *SLC7A11* knockdown. Western blot analysis performed for gamma-H2AX (γH2AX) as a DNA damage marker and cleaved-PARP (cl-PARP) as an apoptosis marker, α-tubulin as a loading control. (I) *SLC7A11* was expressed in parental and MAPKi-resistant A375 cells by lentiviral transduction. pLX304 empty vector was used as the control (Ctrl). The level of *SLC7A11* overexpression in parental and MAPKi-resistant cells was measured by qRT-PCR of *SLC7A11* mRNA. (J-K) Incucyte proliferation assays indicating the responsiveness to 1μM vorinostat treatment in A375R (J) and A375DR (K) cells with and without *SLC7A11* overexpression. (L) Long-term colony formation of *SLC7A11* overexpressing parental and MAPKi-resistant A375 cells in the treatment of vorinostat. The cells were seeded 50,000 cells per well in 6-well plate and cultured 10 days with or without 1μM vorinostat. Afterwards, the cells were fixed, stained and photographed. (M) *SLC7A11* overexpressing parental and MAPKi-resistant A375 cells were treated with 2 μM vorinostat for 72 hours. Afterwards, ROS levels were measured using CellROX-Green flow cytometry assay. Error bars in this figure represent as mean ± standard deviations from biological triplicates (*P≤0.05, ** P≤0.01, *** P≤0.001, student's t-test).

mice with A375 cells and after tumors reached 500 mm3, animals were fed a control chow, chow supplemented with PLX4720 (an analogue of vemurafenib) or with vorinostat through daily intraperitoneal injection. Figure 6A shows that in the absence of drug or in the presence of vorinostat, A375 cells formed progressively growing tumors. In the presence of PLX4720 tumors regressed initially, but drug-resistant tumors started to emerge approximately 40-50 days after the start of PLX4720 treatment. To address which mechanisms of PLX4720 resistance operated *in vivo*, we re-established four drug-resistant A375 tumors in cell culture (*ex vivo* A1-A4: Exv. A1-A4). Figure 6G shows that each of these four tumorderived cell lines was highly resistant to vemurafenib, but responded very strongly to vorinostat, belinostat and panobinostat. All four cell lines maintained elevated levels of p-MEK in the presence of vemurafenib (Figure 6C), which is explained by an amplification of BRAF in the case of Exv. A4 cells and a gain of an *NRAS*^{Q61K} mutation in the case of Exv. A3 cells (Figures 6D, E). The other two drugresistant tumor lines exhibited increased expression of bona fide TGFβ target genes, suggestive of the possibility of activated TGFβ signaling in these *ex vivo* clones (Figure 6F), which has also been linked to resistance to vemurafenib (Huang et al., 2012). These data indicate that a range of different mechanisms can operate *in vivo* to confer resistance to BRAF inhibition and that, like in actual patients, in most cases drug resistance results from re-activation of MAPK signaling. Most importantly, these data also indicate that melanoma cells with reactivated MAPK signaling are very responsive to HDACi, irrespective of how MAPK signaling was reactivated.

To test directly in an animal model whether BRAFi-resistant melanomas are responsive to HDACi, we allowed the PLX4720-treated tumors in our mouse cohort to acquire drug resistance (after tumors reached a volume of approximately 400 mm3 in the presence of drug), which took on average 110 days (Figure 6A). After this, mice were randomized into four treatment cohorts: no drug, vorinostat only, PLX4720 only or the combination of vorinostat and PLX4720. Figure 6B shows the response of the PLX4720-resistant tumors to these four treatment regimens. Continuous PLX4720 treatment resulted in the most rapid tumor growth, consistent with the notion that these cells are fully drug-resistant. PLX4720

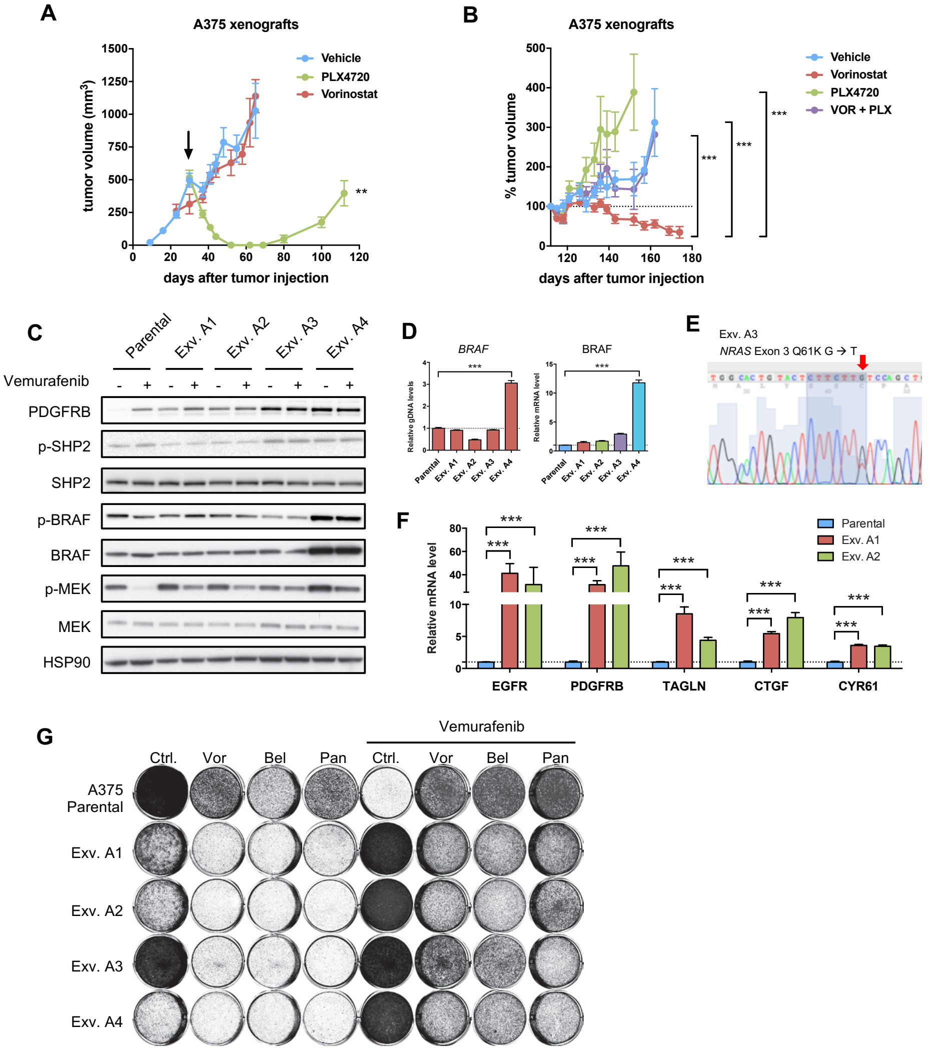

Figure 6. In vivo responses of BRAF-mutant melanoma to HDAC inhibitors.
(A) Tumor growth of A375 parental cells in the flanks of Balb/c nude mice subcutaneously injected with 1*10^6 A375 cells and, when tumors reached approximately 500 mm^3 (black arrow), assigned to either control chow (n=8), PLX4720-supplemented chow (40 mg/kg/day, n=30), or vorinostat (100 mg/kg/day, intraperitoneal injection, n=5). (B) On day 112 post-injection, PLX4720-treated mice were assigned to either control chow (n=7), continuous PLX4720-supplemented chow (40 mg/kg/day, n=6), vorinostat (100 mg/kg/day, intraperitoneal injection, n=11), or combination PLX4720-supplemented chow (40 mg/kg/day) and vorinostat (100 mg/kg/day, intraperitoneal injection, n=6). (C) Four BRAFi-resistant ex vivo clones (Exv. A1, Exv. A2, Exv. A3 and Exv. A4) were isolated from four different A375 tumors receiving continued PLX4720 treatment from the cohort shown in panel B. The protein levels of phosphorylated PDGFRB, p-SHP2, SHP2, p-MEK, MEK and HSP90 were measured by Western blotting and A375 parental cell line treated with 2 µM vemurafenib for 24 hours. HSP90 served as the loading control. (D) BRAF levels in the four BRAFi-resistant *ex vivo* clones and parental A375 line determined by qRT-PCR on genomic DNA (left panel) and mRNA (right panel). (E) Sanger sequencing analysis of *NRAS* exon 3 in A375 BRAFi-resistant Exv.

3 clone. (F) Fold changes in mean expression levels, measured by qRT-PCR, of TGFβ target genes *EGFR, PDGFRB, TAGLN, CTGF* and *CYR61* in A375 BRAFi-resistant Exv. 1 and Exv. 2, and A375 parental line. (G) A375 parental and BRAFi-resistant *ex vivo* clones treated with a panel of HDACi (1 µM vorinostat, 0.5 µM belinostat and 6 nM panobinostat) in single treatment or in combination with 1 µM vemurafenib in a long-term colony formation assay. Error bars in this figure represent as mean ± standard deviations from biological triplicates (*P≤0.05, ** P≤0.01, *** P≤0.001, student's t-test).

withdrawal resulted in a pausing of tumor growth followed by slow growth, analogous to the drug holiday effect seen in drug-resistant patients. A slow-growth phenotype was also seen for tumors treated with a combination of vorinostat and PLX4720, consistent with the notion that these two drugs are antagonistic. Most strikingly, a decline in tumor volume was seen when PLX4720-resistant tumors were switched to vorinostat alone, in agreement with the strong cytotoxic effects of HDACi on BRAFi resistant melanoma cell lines seen *in vitro*.

Clinical validation of sequential drug treatment

To investigate the MAPKi-HDACi sequential treatment efficacy in patients, we initiated a clinical study (NCT02836548) to evaluate the effects of vorinostat treatment in *BRAF*^{V600E} mutated advanced melanoma patients that had progressed on dabrafenib+trametinib therapy. We synthesized vorinostat under GMP conditions in our own pharmacy (see methods). Since the in vitro studies demonstrated that HDACi and MAPKi act antagonistically, we used a one-week MAPKi drug washout in patients before vorinostat administration. After this, patients received vorinostat in a safe single daily oral dose of 360 mg, slightly lower than the 400 mg dose approved for use in cutaneous T cell lymphoma. Tumor measurements were performed every 8 weeks and tumor tissue was collected for exploratory analyses (Figure 7A). Pharmacokinetics of the drug in patients (Table S3) showed very good concordance with literature data (Iwamoto et al., 2013). Currently, six patients have been treated and an additional 15 patients will be enrolled in this ongoing study. A more detailed report of this trial will be published else where. Relevant to the potential therapeutic application reported above, we present here molecular analyses from three patients (see Table S2 for patient details) from whom we were able to obtain pre-, during- and post vorinostat treatment biopsies. Figures 7B-D show radiological volume measurements of multiple metastatic lesions for these three patients. The curves stop at progression, which is the end of treatment of vorinostat. The time points of biopsies are marked with a red triangle on the curve of the lesion from which the biopsy was taken. The red dotted vertical line marks the start of vorinostat therapy. We used the biopsy transcriptome (RNAseq) data to assess *SLC7A11* levels in these pre-, during- and post-vorinostat treated tumor biopsies to ask whether HDACi also suppress this gene in patients. Consistent with our *in vitro* data, we observed that vorinostat repressed *SLC7A11* expression in the patient lesions (Figure 7I). We were particularly interested in whether vorinostat therapy could eradicate tumor cells that had gained resistance to BRAF+MEK inhibitor therapy. To assess this, we isolated DNA from these biopsies and searched for changes in the prevalence of drug resistance mutations in the tumors during vorinostat treatment. Intriguingly, patient A harbored the known MAPKi resistance mutation *KRAS*^{G12C} before vorinostat treatment at an allele frequency of 44%, but this mutation was reduced to 0% after 3 weeks of vorinostat treatment (Figure 7E). Similarly, the analysis of biopsies from patient B who acquired the *NRAS*^{Q61H} mutation at 10% allele frequency during the MAPKi treatment, was reduced to 0% after vorinostat therapy (Figure 7F). Patient C developed an NRAS amplification as judged by the increased read count for the *NRAS* gene and mRNA expression as judged by RNAseq (Figures G, H), but its level of amplification and expression was reduced upon vorinostat treatment (Figures 7G, H). These findings are in line with our in vitro and mouse data and demonstrate that BRAF+MEK inhibitor resistant melanoma cells can be preferentially eliminated by treatment with vorinostat. No significant effects of vorinostat were seen on infiltration of immune cells in the metastatic lesions (Figure S6).

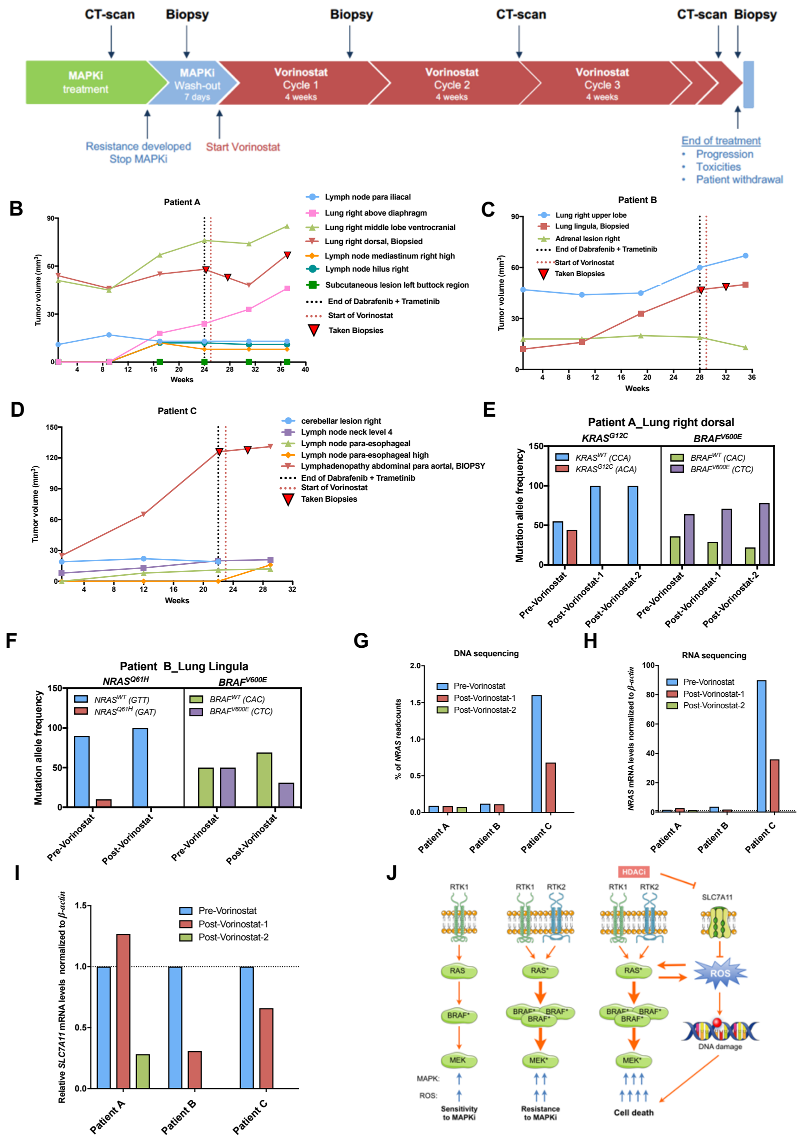

Figure 7. HDACi responsiveness in MAPK inhibitor resistant melanoma patients.
(A) Diagram of the design of clinical trial NCT02836548 proof of concept study of vorinostat treatment in MAPKi-resistant melanoma patients. (B) Tumor responsiveness to vorinostat in MAPKi-resistant melanoma patient A evaluated by CT-scan measurements. The tumor volume of multiple lesions was plotted on the Y-axes against time on the X-axes. (C) as in panel B for patient B. (D) As in panel B for patient C. Biopsies were collected at indicated time points (inverted red triangles) on the curves of the target lesions (solid red lines). (E) Genomic DNA isolated from the biopsied target lesions of patient A was analyzed using the NKI-178 gene panel using targeted NGS, as described (Groenendijk et al., 2016). Representation of the allele frequency of drug-resistance associated *KRAS*^{G12C} mutation in patient A (E) and *NRAS*^{Q61H} in patient B (F) pre- and post-vorinostat treatment. *BRAF*^{V600E} mutation in each panel served as an indication of tumor cell percentage in the biopsy. (G) DNA copy number level of *NRAS* gene, as measured by the percentage of NGS reads for this gene as percentage of total captured reads. (H) Normalized transcript levels of *NRAS* analyzed by RNAseq in the patients' biopsies pre- and post-vorinostat treatment. β-actin served as a housekeeping gene for normalization. (I) Fold change in expression levels of *SLC7A11* in patients' biopsies pre- and post-vorinostat treatment deduced from RNA seq data. (J) Model for the sequential treatment of melanomas. *BRAF*^{V600E} (BRAF*) melanoma cells with normal MAPK signaling and normal ROS levels are sensitive to MAPKi (left). Drug resistance develops through upregulation of RTKs, *RAS* mutations (RAS*), *BRAF* amplification or *MEK* mutations (MEK*), all of which result in enhanced signaling through the MAPK pathway and increased ROS levels (center). Switching therapy from a MAPKi to an HDACi in MAPKi-resistant cells induces ROS through downregulation of *SLC7A11*. The increased ROS also act on RAS to maintain high levels of MAPK signaling. Cellular ROS levels are already increased in MAPKi-resistant tumors and the further increase of ROS by HDACi leads to a massive DNA damage response that has a lethal effect on the cells (right)

Discussion

We identify here a vulnerability of BRAF mutant melanomas that is specifically acquired upon development of resistance to inhibitors of the MAPK pathway. This group of patients represents a major unmet clinical need, as such patients tend to have only few treatment options upon progression on BRAF+MEK inhibitor therapy. When patients progress on first line therapy, subsequent therapies have a tendency to become increasingly less effective. However, theoretically this does not have to be the case. It is a well-established principle that drug resistance comes at a “fitness cost” for the cancer cell that in turn can lead to novel vulnerabilities of the drug resistant cells (Hutchison, 1963). Such acquired vulnerabilities have in the past been searched for through compound screens in pairs of sensitive and chemotherapy resistant cancer cells (Jensen et al., 1997; Rickardson et al., 2006). These efforts have been relatively unproductive from a clinical perspective, most likely because cancer cells have many avenues to become chemotherapy insensitive, making the collateral sensitivities of drug resistant cells equally heterogeneous and unpredictable. This issue is less relevant for *BRAF* mutant melanoma, as resistance to MAPK pathway inhibition more often than not leads to secondary mutations that reactivate the MAPK pathway in the presence of drug. This predictable resistance mechanism may also lead to more foreseeable collateral sensitivities as compared to the chemotherapy resistance models. Indeed, our data show that melanoma cells that have acquired resistance to MAPK inhibitors through different MAPK pathway reactivation mechanisms all become sensitive to HDACi, including PDGFRB overexpression (A375R cells, Figure 1C), *NRAS*^{Q61H} mutation (A375DR cells, Figure 1D), *KRAS*^{G12C} (Mel888DR cells, Figure S1E), *BRAF* splice site mutations (Mel888R cells, Figure 1D) and BRAF amplification (A375 Exv A4, Figures 6C, D). The common vulnerability we identified in these MAPK resistant cells results from the induction of reactive oxygen species (ROS) by hyperactive MAPK pathway signaling. Consequently, further activation of these increased ROS levels by vorinostat leads to significant DNA damage and apoptotic cell death only in the MAPK resistant cells, but not in the drug-sensitive cells that have lower ROS levels. Consistent with this, we see no effect of vorinostat in MAPK inhibitor sensitive melanoma cells.

Vorinostat has proven anticancer activity and was approved in 2006 by the Food and Drug Administration for use in cutaneous T cell lymphoma. HDAC inhibitors have pleiotropic effects on transcription and hence it is difficult to assign the anti-cancer effects of these drugs to one particular gene or pathway. For instance, HDAC inhibitors have been shown to induce CDKN1A (p21cip1) (Richon et al., 2000) and ROS (Ruefli et al., 2001), but effects on DNA damage repair have also been described (Robert and Rassool, 2012). Our data indicate that ROS induction plays a major part in the killing of BRAF inhibitor-resistant melanoma cells, as the ROS scavengers NAC and GEE counteracted the effects of vorinostat. A substantial fraction of the vorinostat effect on ROS induction is caused by suppression of *SLC7A11* by vorinostat, as ectopic *SLC7A11* expression completely rescued ROS induction by vorinostat (Figure 5K, S5G). This gene encodes the importer of cystine, which serves as a precursor to the ROS scavenger glutathione. *SLC7A11* expression did not completely rescue the antiproliferative effect of vorinostat in BRAF inhibitor-resistant melanoma, consistent with the notion discussed above that vorinostat also has ROS-independent effects on cancer cells (Figure 5J, S5F). Together, these data support a model in which the increased ROS level in BRAF-resistant melanoma becomes a liability when ROS levels are increased further by HDACi treatment, leading to DNA damage and apoptotic cell death (Figure 7J).

We find that vorinostat treatment in mouse xenograft tumors that have developed resistance to BRAF inhibitor in vivo leads to tumor regressions. This was not seen when BRAFi-resistant tumor cells were treated with a combination of BRAFi+HDACi, in agreement with our in vitro findings showing that the two drugs are antagonistic. The molecular basis for the notion that BRAFi and HDACi must not be used simultaneously is provided by our finding that increased MAPK signaling resulting from BRAF inhibitor resistance leads to an increase in ROS levels that are increased to toxic levels by subsequent treatment with vorinostat. Conversely, MAPK inhibition with selective drugs diminishes ROS levels. While vorinostat can increase these lower ROS levels in the presence of MAPK inhibitors also, they do not reach toxic concentrations that result in DNA damage and cell death (Figures 3D-F). The finding that BRAF and HDAC inhibitors must be used sequentially was unexpected as a recent publication demonstrated that combination of BRAF and HDAC inhibitors upfront can prevent emergence of resistant melanoma cells in a short-term assay (Johannessen et al., 2013). This difference most likely has its origin in the notion that the effects of epigenetic drugs like vorinostat take considerable time to develop. That lethal ROS levels can be used to kill cancer cells was recently also shown by others using a combination of mTOR and HDAC inhibitors in *NF1*- and *RAS* mutant cancers (Malone et al., 2017). The fundamental difference between this observation and ours is that Malone et al. used simultaneous treatment with two drugs to increase ROS levels to lethal levels, whereas in our melanoma model, it is mandatory to use the drugs sequentially to reach toxic ROS levels. Indeed, most other recent publications that identify combinations of drugs to prevent resistance development use upfront combinations to accomplish this (Hangauer et al., 2017; Sharma et al., 2010). The sequential treatment we identify here has the advantage that it avoids toxicity arising from simultaneous use of drugs. Therefore, sequential drug therapy enables the use of a much larger drug repertoire than simultaneous use. In a pilot study in patients with advanced BRAF mutant melanoma that progressed on BRAF+MEK inhibitor therapy we see that tumor cells harboring a drug-resistance mutation are quickly depleted by vorinostat, consistent with the sensitivity of these cells to vorinostat seen in vitro and in mouse models. In patients, tumors initially stabilize upon switch to vorinostat therapy, but then progression occurs. This is not unexpected, given that parental, MAPK inhibitor sensitive, tumor cells fail to respond to vorinostat. After initial depletion of the drug-resistant clones in the tumor by vorinostat therapy, the BRAF+MEK inhibitor sensitive clones continue to proliferate, leading to progression. To avoid this problem, we plan to adapt the protocol for the ongoing trial NCT02836548 to include monitoring of patients on BRAF+MEK inhibitor therapy for early signs of drug resistance through analysis of cell free tumor DNA in blood (Murtaza et al., 2013). Such mutations are often detectable before radiological progression is evident (Misale et al., 2012). By pulsatile treatment with vorinostat to eradicate emergent drug resistant cells, followed by a switch back to BRAF+MEK inhibition, we expect to get longer progression free survival benefit for patients as compared to an intermittent BRAF inhibitor only regimen (Das Thakur et al., 2013), which in the context of *EGFR* mutant lung cancer does not seem very effective in the clinic (Kaiser, 2017; Yu et al., 2017). Indeed, our in vitro data indicate that switching from MAPK inhibitor therapy to vorinostat is more effective in eradicating drug-resistant cells than a drug holiday (Figures 4, S4). We cannot exclude that drug resistance mechanisms occur in patients that are not associated with re-activation of the MAPK pathway. Using an in vitro genetic screen, it has been shown that vemurafenib resistance can develop without MAPK re-activation (Johannessen et al., 2013). It is not clear how frequent such mechanisms are in patients. If they occur, such drug resistant variants may not respond to vorinostat therapy. We note that all melanoma cells that acquired resistance in vitro or in vivo, including the three patients analyzed here, did upregulate the MAPK pathway to gain resistance and thereby gained susceptibility to HDAC inhibition.

In summary, we have identified a novel sequential drug treatment strategy that exploits an acquired vulnerability of MAPK-inhibitor resistant melanoma cells and show initial patient data to support the potential clinical utility of this approach. More generally, our data highlight that studying how cancer cells acquire resistance to targeted cancer drugs may be fruitful to identify novel vulnerabilities that can be exploited therapeutically.

References

Baenke, F., Chaneton, B., Smith, M., Van Den Broek, N., Hogan, K., Tang, H., Viros, A., Martin, M., Galbraith, L., Girotti, M.R., et al. (2016). Resistance to BRAF inhibitors induces glutamine dependency in melanoma cells. Molecular oncology 10, 73-84.

Bannai, S., and Tateishi, N. (1986). Role of membrane transport in metabolism and function of glutathione in mammals. J Membr Biol 89, 1-8. Chio, I.I.C., and Tuveson, D.A. (2017). ROS in Cancer: The Burning Question. Trends in molecular medicine 23, 411-429.

Corazao-Rozas, P., Guerreschi, P., Jendoubi, M., Andre, F., Jonneaux, A., Scalbert, C., Garcon, G., Malet-Martino, M., Balayssac, S., Rocchi, S., et al. (2013). Mitochondrial oxidative stress is the Achille's heel of melanoma cells resistant to Braf-mutant inhibitor. Oncotarget 4, 1986-1998.

Das Thakur, M., Salangsang, F., Landman, A.S., Sellers, W.R., Pryer, N.K., Levesque, M.P., Dummer, R., McMahon, M., and Stuart, D.D. (2013). Modelling vemurafenib resistance in melanoma reveals a strategy to forestall drug resistance. Nature 494, 251-255. Gout, P.W., Kang, Y.J., Buckley, D.J., Bruchovsky, N., and Buckley, A.R. (1997). Increased cystine uptake capability associated with malignant progression of Nb2 lymphoma cells. Leukemia 11, 1329-1337.

Groenendijk, F.H., de Jong, J., Fransen van de Putte, E.E., Michaut, M., Schlicker, A., Peters, D., Velds, A., Nieuwland, M., van den Heuvel, M.M., Kerkhoven, R.M., et al. (2016). ERBB2 Mutations Characterize a Subgroup of Muscle-invasive Bladder Cancers with Excellent Response to Neoadjuvant Chemotherapy. European urology 69, 384-388.

Hangauer, M.J., Viswanathan, V.S., Ryan, M.J., Bole, D., Eaton, J.K., Matov, A., Galeas, J., Dhruv, H.D., Berens, M.E., Schreiber, S.L., et al. (2017). Drug-tolerant persister cancer cells are vulnerable to GPX4 inhibition. Nature 551, 247-250.

Haq, R., Shoag, J., Andreu-Perez, P., Yokoyama, S., Edelman, H., Rowe, G.C., Frederick, D.T., Hurley, A.D., Nellore, A., Kung, A.L., et al. (2013). Oncogenic BRAF regulates oxidative metabolism via PGC1alpha and MITF. Cancer Cell 23, 302-315.

Hernandez-Davies, J.E., Tran, T.Q., Reid, M.A., Rosales, K.R., Lowman, X.H., Pan, M., Moriceau, G., Yang, Y., Wu, J., Lo, R.S., et al. (2015). Vemurafenib resistance reprograms melanoma cells towards glutamine dependence. J Transl Med 13, 210.

Huang, S., Holzel, M., Knijnenburg, T., Schlicker, A., Roepman, P., McDermott, U., Garnett, M., Grernrum, W., Sun, C., Prahallad, A., et al. (2012). MED12 Controls the Response to Multiple Cancer Drugs through Regulation of TGF-beta Receptor Signaling. Cell 151, 937-950.

Hutchison, D.J. (1963). Cross Resistance and Collateral Sensitivity Studies in Cancer Chemotherapy. In Advances in Cancer Research, A. Haddow, and S. Weinhouse, eds. (Academic Press), pp. 235-350.

Imamovic, L., and Sommer, M.O.A. (2013). Use of Collateral Sensitivity Networks to Design Drug Cycling Protocols That Avoid Resistance Development. Science translational medicine 5, 204ra132- 204ra132.

Iwamoto, M., Friedman, E.J., Sandhu, P., Agrawal, N.G., Rubin, E.H., and Wagner, J.A. (2013). Clinical pharmacology profile of vorinostat, a histone deacetylase inhibitor. Cancer Chemother Pharmacol 72, 493-508.

Jensen, P.B., Holm, B., Sorensen, M., Christensen, I.J., and Sehested, M. (1997). In vitro crossresistance and collateral sensitivity in seven resistant small-cell lung cancer cell lines: preclinical identification of suitable drug partners to taxotere, taxol, topotecan and gemcitabin. British Journal of Cancer 75, 869-877.

Johannessen, C.M., Johnson, L.A., Piccioni, F., Townes, A., Frederick, D.T., Donahue, M.K., Narayan, R., Flaherty, K.T., Wargo, J.A., Root, D.E., et al. (2013). A melanocyte lineage program confers resistance to MAP kinase pathway inhibition. Nature 504, 138-142.

Kaiser, J. (2017). When less is more. Science 355, 1144.

Lee, A.C., Fenster, B.E., Ito, H., Takeda, K., Bae, N.S., Hirai, T., Yu, Z.X., Ferrans, V.J., Howard, B.H., and Finkel, T. (1999). Ras proteins induce senescence by altering the intracellular levels of reactive oxygen species. J Biol Chem 274, 7936-7940.

Malone, C.F., Emerson, C., Ingraham, R., Barbosa, W., Guerra, S., Yoon, H., Liu, L.L., Michor,

F., Haigis, M., Macleod, K.F., et al. (2017). mTOR and HDAC Inhibitors Converge on the TXNIP/Thioredoxin Pathway to Cause Catastrophic Oxidative Stress and Regression of RAS-Driven Tumors. Cancer Discov 7, 1450-1463.
Manzano, J.L., Layos, L., Buges, C., de Los Llanos Gil, M., Vila, L., Martinez-Balibrea, E., and Martinez-Cardus, A. (2016). Resistant mechanisms to BRAF inhibitors in melanoma. Ann Transl Med 4, 237.

Misale, S., Yaeger, R., Hobor, S., Scala, E., Janakiraman, M., Liska, D., Valtorta, E., Schiavo, R., Buscarino, M., Siravegna, G., et al. (2012). Emergence of KRAS mutations and acquired resistance to anti-EGFR therapy in colorectal cancer. Nature 486, 532-536.

Murtaza, M., Dawson, S.J., Tsui, D.W., Gale, D., Forshew, T., Piskorz, A.M., Parkinson, C., Chin, S.F., Kingsbury, Z., Wong, A.S., et al. (2013). Non-invasive analysis of acquired resistance to cancer therapy by sequencing of plasma DNA. Nature 497, 108-112.

Petruccelli, L.A., Dupere-Richer, D., Pettersson, F., Retrouvey, H., Skoulikas, S., and Miller, W.H., Jr. (2011). Vorinostat induces reactive oxygen species and DNA damage in acute myeloid leukemia cells. PLoS One 6, e20987.

Reczek, C.R., and Chandel, N.S. (2017). The Two Faces of Reactive Oxygen Species in Cancer. Annual Review of Cancer Biology 1, 79-98.

Richon, V.M., Sandhoff, T.W., Rifkind, R.A., and Marks, P.A. (2000). Histone deacetylase inhibitor selectively induces p21WAF1 expression and gene-associated histone acetylation. Proc Natl Acad Sci U S A 97, 10014-10019.

Rickardson, L., Fryknäs, M., Haglund, C., Lövborg, H., Nygren, P., Gustafsson, M.G., Isaksson, A., and Larsson, R. (2006). Screening of an annotated compound library for drug activity in a resistant myeloma cell line. Cancer Chemotherapy and Pharmacology 58, 749.

Robert, C., Karaszewska, B., Schachter, J., Rutkowski, P., Mackiewicz, A., Stroiakovski, D., Lichinitser, M., Dummer, R., Grange, F., Mortier, L., et al. (2014). Improved Overall Survival in Melanoma with Combined Dabrafenib and Trametinib. New England Journal of Medicine 372, 30-39.

Robert, C., and Rassool, F.V. (2012). HDAC inhibitors: roles of DNA damage and repair. Adv Cancer Res 116, 87-129.

Ruefli, A.A., Ausserlechner, M.J., Bernhard, D., Sutton, V.R., Tainton, K.M., Kofler, R., Smyth, M.J., and Johnstone, R.W. (2001). The histone deacetylase inhibitor and chemotherapeutic agent suberoylanilide hydroxamic acid (SAHA) induces a cell-death pathway characterized by cleavage of Bid and production of reactive oxygen species. Proceedings of the National Academy of Sciences 98, 10833-10838.

Schadendorf, D., Hodi, F.S., Robert, C., Weber, J.S., Margolin, K., Hamid, O., Patt, D., Chen, T.T., Berman, D.M., and Wolchok, J.D. (2015). Pooled Analysis of Long-Term Survival Data From Phase II and Phase III Trials of Ipilimumab in Unresectable or Metastatic Melanoma. J Clin Oncol 33, 1889-1894.

Seghers, A.C., Wilgenhof, S., Lebbe, C., and Neyns, B. (2012). Successful rechallenge in two patients with BRAF-V600-mutant melanoma who experienced previous progression during treatment with a selective BRAF inhibitor. Melanoma research 22, 466-472.

Sharma, S.V., Lee, D.Y., Li, B., Quinlan, M.P., Takahashi, F., Maheswaran, S., McDermott, U., Azizian, N., Zou, L., Fischbach, M.A., et al. (2010). A chromatin-mediated reversible drug-tolerant state in cancer cell subpopulations. Cell 141, 69-80.

Son, Y., Cheong, Y.K., Kim, N.H., Chung, H.T., Kang, D.G., and Pae, H.O. (2011). Mitogen-Activated Protein Kinases and Reactive Oxygen Species: How Can ROS Activate MAPK Pathways? J Signal Transduct 2011, 792639.

Sosman, J.A., Kim, K.B., Schuchter, L., Gonzalez, R., Pavlick, A.C., Weber, J.S., McArthur, G.A., Hutson, T.E., Moschos, S.J., Flaherty, K.T., et al. (2012). Survival in BRAF V600-mutant advanced melanoma treated with vemurafenib. N Engl J Med 366, 707-714.

Sun, C., Wang, L., Huang, S., Heynen, G.J.J.E., Prahallad, A., Robert, C., Haanen, J., Blank, C., Wesseling, J., Willems, S.M., et al. (2014). Reversible and adaptive resistance to BRAF(V600E) inhibition in melanoma. Nature 508, 118-122.

Ungerstedt, J.S., Sowa, Y., Xu, W.S., Shao, Y., Dokmanovic, M., Perez, G., Ngo, L., Holmgren, A., Jiang, X., and Marks, P.A. (2005). Role of thioredoxin in the response of normal and transformed cells to histone deacetylase inhibitors. Proc Natl Acad Sci U S A 102, 673-678.

Valko, M., Leibfritz, D., Moncol, J., Cronin, M.T., Mazur, M., and Telser, J. (2007). Free radicals and antioxidants in normal physiological functions and human disease. The international journal of biochemistry & cell biology 39, 44-84.

Van Allen, E.M., Wagle, N., Sucker, A., Treacy, D.J., Johannessen, C.M., Goetz, E.M., Place, C.S., Taylor-Weiner, A., Whittaker, S., Kryukov, G.V., et al. (2014). The genetic landscape of clinical resistance to RAF inhibition in metastatic melanoma. Cancer Discov 4, 94-109.

Vazquez, F., Lim, J.H., Chim, H., Bhalla, K., Girnun, G., Pierce, K., Clish, C.B., Granter, S.R., Widlund, H.R., Spiegelman, B.M., et al. (2013). PGC1alpha expression defines a subset of human melanoma tumors with increased mitochondrial capacity and resistance to oxidative stress. Cancer Cell 23, 287-301.

Wagle, N., Van Allen, E.M., Treacy, D.J., Frederick, D.T., Cooper, Z.A., Taylor-Weiner, A., Rosenberg, M., Goetz, E.M., Sullivan, R.J., Farlow, D.N., et al. (2014). MAP kinase pathway alterations in BRAF-mutant melanoma patients with acquired resistance to combined RAF/MEK inhibition. Cancer Discov 4, 61-68.

Wolf, I.M., Fan, Z., Rauh, M., Seufert, S., Hore, N., Buchfelder, M., Savaskan, N.E., and Eyupoglu, I.Y. (2014). Histone deacetylases inhibition by SAHA/Vorinostat normalizes the glioma microenvironment via xCT equilibration. Sci Rep 4, 6226.

Yu, H.A., Sima, C., Feldman, D., Liu, L.L., Vaitheesvaran, B., Cross, J., Rudin, C.M., Kris, M.G., Pao, W., Michor, F., et al. (2017). Phase 1 study of twice weekly pulse dose and daily low-dose erlotinib as initial treatment for patients with EGFR-mutant lung cancers†. Annals of Oncology 28, 278-284.

Materials and methods

METHOD DETAILS

Long-term colony formation assay and IncuCyte cell proliferation assays

Cells were seeded into 6-well plates (50,000 cells per well) or 12-well plates (30,000 cells per well) and cultured both in the absence and presence of drugs as indicated for 10-15 days. At the end of the assay, cells were fixed with 4% of formaldehyde (#1.04002, Millipore) diluted in PBS, stained with 2% of crystal violet (#HT90132 Sigma-Aldrich) diluted in water and photographed. For IncuCyte proliferation assays, cells were seeded in 384-well plate (400 cells per well) and cultured in absence or presence of drugs as indicated. Cell confluence was measured and quantified by the IncuCyte imaging system (Essen Bioscience).

Cell viability measurement

Cell viability was detected using CellTiter-Blue® Cell Viability Assay Kit (G8081, Promega) according to the manufacturer's instructions. The assay measurement was performed using EnVision multi-label plate reader (PerkinElmer).

Protein lysate preparation and immunoblotting

Cells were seeded in DMEM-based medium containing 10% fetal bovine serum (FBS) in the absence or presence of drug for 48 or 72 hours. The drugs were daily refreshed. Afterwards, the cells were washed with PBS and lysed with RIPA buffer supplemented with protease inhibitors (cOmplete, Roche) and phosphatase inhibitor cocktails II and III (Sigma). All lysates were freshly prepared and processed with Novex NuPAGE Gel Electrophoresis Systems (Invitrogen). The detection was performed after 48 or 72 hours drug treatment.

ROS detection

The cells were treated in the absence or presence of drugs for 72 hours, daily refreshed. ROS level in cells was detected using CellROX® Green Flow Cytometry Assay Kit (C10492, Life Technologies) according to the manufacturer's instructions. Drugs remained present during the assay.

Glutathione detection

The cells were treated in the absence or presence of drugs for 72 hours, daily refreshed. Total GSH level in cells was detected using Glutathione detection kit (ADI-900-160, Enzo) according to the manufacturer's instructions.

Competition assay

The MAPKi-resistant cells were stably transfected with pLKO-H2B-RFP. The MAPKisensitive parental cells were stably transfected with pLKO-H2B-GFP. Afterwards, two cell populations were mixed and then seeded 2,000,000 cells into 10-cm dishes for biological replicates and different 6 treatment arms. At each time point, the distribution of the cell populations was determined using flow cytometry (The BD LSRFortessa™ cell analyzer, BD Biosciences). The ratio of two cell populations was indicated. Day 0 is the starting of the assay; this also indicates the ratio of the seeded GFP and RFP cells. The medium containing drugs were refreshed during each time point. During the experiment, when cells reach 80% confluency in the plates, the cells were re-seeded 2,000,000 cells into a new 10-cm dish.

qRT-PCR

Total RNA was extracted from cells using TRIzol reagent from Invitrogen or Quick-RNA™ MiniPrep (# R1055) from Zymo Research. cDNA synthesis was performed using Maxima Universal First Strand cDNA Synthesis Kit (#K1661) from Thermo scientific. qPCR reactions were performed with FastStart Universal SYBR Green Master (Rox) from Roche. The experiments were performed according to the manufacturer's instructions. The sequences of the primers used for qRT–PCR analyses are described in the key resource table. All reactions were run in triplicate. The CT values were calculated using the Standard Curve Method.

Detection of genomic DNA alterations

Genomic DNA was isolated using DNeasy® Blood&Tissue kit (#6950, Qiagen) according to the manufacture's instructions. 40ng gDNA was inputted for 40 cycles of PCR. Next, the PCR products were cleaned with ExoSAP-IT® (#78200, Affymetrix) and capillary sequenced using the BigDye terminator V3.1 sequencing Kit (Applied Biosystems). The sequences of the primers used to detect the genomic alternations in NRAS, KRAS and BRAF are described in Supplementary Table 1. All the sequencing was verified with Forward and Reverse primers.

Lentiviral transduction

A third-generation lentivirus packaging system consisting of pCMV-VSV-G (addgene#8454), pRSV-Rev (Addgene#12253) and pMDLg/pRRE (Addgene#12251) was used to create virus particles of the modified reporter plasmids. A transient transfection was performed in 293T cells and lentiviral supernatants were produced. Destination cells were infected with lentiviral supernatants, using 8μg/ml Polybrene and low virus titer. After 48h of incubation, the supernatant was replaced by medium containing 10 μg/ml Blasticidin or 2 μg/ml Puromycin. After 48h, selection of viral transduced cell lines was completed. All the lentiviral vectors in the study are described in supplemental experiment procedure.

Relative growth rate calculation

The growth rate of each replicate was calculated as the slope a curve fitted through the linear range of the log-transformed confluence measurements (the first 84 hours for A375R and 76 hours for A375DR) of the Incucyte proliferation experiment. For each cell line, the growth rates were normalized to the mean of the untreated controls. The growth rate of untreated control was considered as a basal line and normalized to 1. The relative growth rates of all growth rates of the drug-treated and genetic manipulated arms were compared with the untreated control arm. Error bars indicate standard deviation of 4 replicates.

Active RAS Pull-Down detection

Melanoma cells were treated in the absence or presence of drugs for 72 hours, daily refreshed. RAS-GTP levels were detected using RAS Assay Reagent (RAF-1 RBD, agarose, Merck Millipore according to the manufacturer's instructions.

Vorinostat synthesis

Vorinostat (N-hydroxy-N'-phenyloctanediamide) has been synthesized with suberic acid as starting material. The method is based on the procedure described by Mai and co-workers (Mai et al., 2001). Suberic acid was treated with acetic anhydride to form its cyclic anhydride. By stirring in tert- butylmethylether rather pure cyclized anhydride is obtained. The second step is the reaction of the cyclized anhydride with aniline. This yields three products: suberic acid, mono-anilide (desired product) and bis-anilide. The mono-anilide is isolated in relatively high purity from the mixture. A final trituration in tert-butylmethylether will give 93-96% pure mono-anilide. Last step is the formation of the hydroxylamide to form vorinostat. After multiple crystalizations the desired purity of 99% is obtained. All conversions, after each step, are followed by1H NMR spectroscopy and liquid chromatography with mass spectrometric (LC-MS) detection. Vorinostat capsules have been manufactured under GMP conditions by mixing vorinostat drug substance with microcrystalline cellulose PH102 followed by semi-automatic filling into red, hard gelatin capsules (size 0). Each capsule contains an amount of 90 mg vorinostat. Vorinostat capsules are packed per 28 capsules in HD-PE containers and labeled according to GMP EU Annex 13. Vorinostat capsules are stable for at least 1 year at room temperature. Quality control of vorinostat capsules encompasses determination of identity, content, purity and uniformity of dosage units, using a validated reversed phase high performance liquid chromatography method with UV detection at 241 nm. Column: Symmetry Shield RP8 150 x 2.1 mm ID and particle size 3.5 µm. Mobile phase: A, 0.5 % acetic acid in water; B, 0.5% acetic acid in acetonitrile (90/10). Flow: 300 µL/min. Temperature: 30 °C.

NKI 178 gene panel exosome next generation DNA sequencing

DNA were isolated from the fresh frozen tumour biopsies. Target enrichment DNA nextgeneration sequencing was performed with a custom SureSelect XT2 bait library (Agilent Technologies) covering a selected panel of 178 genes, consisting of (indirect or direct) clinically relevant genes. The experimental details are described (Groenendijk et al., 2016).

Immunohistochemistry

Immunohistochemistry of the FFPE tumor samples was performed on a BenchMark Ultra (CD3, CD4, CD8, CD20, CD56 and CD68) automated stainer (Ventana Medical Systems).

Briefly, paraffin sections were cut at 3 um, heated at 75°C for 28 minutes and deparaffinized in the instrument with EZ prep solution (Ventana Medical Systems). Heat-induced antigen retrieval was carried out using Cell Conditioning 1 (CC1, Ventana Medical Systems) for 32 minutes at 950C (CD3, CD4, CD8, CD20, CD56 and CD68). CD3 was detected using clone SP7 (1/100 dilution, 32 minutes at 370C, Spring / ITK), CD4 clone SP35 (1/50 dilution, 32 minutes at 370C, Cell Marque), CD8 clone C8/144B (Dako / Agilent) using 1/200 dilution 32 minutes at 370C, CD20 using clone L26 (1/800 dilution, 32 minutes at 370C, Dako / Agilent), CD56 clone MRQ-75 (1/2000 dilution, 32 minutes at 370C, Cell Marque), CD68 clone KP1 (Dako / Agilent) using 1/20000 dilution 32 minutes at 370C. detection for CD markers were isualized using the OptiView DAB Detection Kit (Ventana Medical Systems). Slides were counterstained with Hematoxylin and Bluing Reagent (Ventana Medical Systems).

QUANTIFICATION AND STATISTICAL ANALYSIS

Statistical significance was calculated by Student's t test with two tails. Prism and Microsoft Excel were used to generate graphs and statistical analyses. *p-value <0.05, **p-value <0.01, ***p-value <0.001. For animal experiments, no statistics methods were used to predetermine sample size; we used the generally accepted number of tumors per treatment group.

DATA AND SOFTWARE AVAILABILTY

Raw and processed data from the next generation RNA sequencing of patient biopsies before and after therapy with HDAC inhibitors have been deposited to NCBI Gene Expression Omnibus (GEO) under accession number GSE (Data submitted, accession number pending).

ADDITINONAL RESOURCES

The clinical study described in this manuscript was registered under number NCT02836548 and can be accessed at https://clinicaltrials.gov/show/NCT02836548.

SUPPLEMENTAL TABLES

Table S1. Genes downregulated by vorinostat treatment, Related to Figure 5.
12 genes commonly downregulated in A375, A375R, A375DR cells upon vorinostat treatment.

Table S2. Patient characteristics, Related to Figure 7.
Characteristics of three patients in the clinical study.

Table S3. Pharmacodynamics of vorinostat, Related to Figure 7.
Measurements on vorinostat levels in blood of three patients in the clinical study.

(Table submitted, accession links pending)

STAR methods

KEY RESOURCES TABLE

REAGENT or RESOURCE	SOURCE	IDENTIFIER
Antibodies		
HSP 90 (H-114) Rabbit polyclonal antibody	Santa Cruz Biotechnology	Cat#: sc-7947 RRID: AB_2121235
Vinculin / VINC Mouse monoclonal antibody	Sigma-Aldrich	Cat#: V9131 RRID: AB_477629
α-tubulin (CP06) Mouse monoclonal antibody	Millipore	Cat#: CP06 RRID: AB_2617116
β-actin (C-2) Mouse monoclonal antibody	Santa Cruz Biotechnology	Cat#: sc-8432 RRID: AB_626630
Histone 3 / H3 Rabbit polyclonal antibody	Cell Signaling Technology	Cat#: 9715 RRID: AB_331563
acetyl-Histone 3 / ac-H3 Rabbit polyclonal antibody	Millipore	Cat#: 06-599 RRID: AB_2115283
Phospho-Rb (Ser780) Rabbit polyclonal antibody	Cell Signaling Technology	Cat#: 39033 RRID:AB_330015
Phospho-MEK1/2 (Ser217/221) (41G9) Rabbit monoclonal antibody	Cell Signaling Technology	Cat#: 9154S RRID: AB_2138017
MEK1/2 (L38C12) Mouse monoclonal antibody	Cell Signaling Technology	Cat#: 4694S RRID: AB_10695868
SHP2 (C-18) Rabbit polyclonal antibody	Santa Cruz Biotechnology	Cat#: SC-280 RRID: AB_632401
p-SHP2 Rabbit monoclonal antibody	Abcam	Cat#: ab62322 RRID: AB_945452
Pan-Ras (Ras10) Mouse monoclonal antibody	Thermo Scientific	Cat#: MA1-012X RRID: AB_2536665
PDGFRB (C82A3) Rabbit monoclonal antibody	Cell Signaling Technology	Cat#: 4564 RRID: AB_2236927
p-BRAF (Ser445) Rabbit polyclonal antibody	Cell Signaling Technology	Cat#: #2696 RRID: AB_390721
BRAF (F-7) Mouse monoclonal antibody	Santa Cruz Biotechnology	Cat#: sc-5284 RRID: AB_626760
Cleaved PARP (Asp214) (D64E10) XP Rabbit monoclonal antibody	Cell Signaling Technology	Cat#: #5625 RRID: AB_10699459
phospho-Rsk1 (Thr359/Ser363) Rabbit monoclonal antibody	Millipore	Cat#: 04-419 RRID: AB_11213444
RSK1 (D6D5) Rabbit monoclonal antibody	Cell Signaling Technology	Cat#: 8408S RRID: AB_10828594
γH2AX Mouse monoclonal antibody	Millipore	Cat # 05-636 RRID: AB_309864
CD3 (SP7) for IHC Rabbit monoclonal antibody	Spring Bioscience	Cat # M3071 RRID: 1660770
CD4 (SP35) for IHC Rabbit monoclonal antibody	Cell Marque	Cat # 104R-14, RRID: 1516770
CD8 (C8/144B) for IHC Mouse monoclonal antibody	Dako/Agilent	Cat # M7103 RRID: 2075537

CD20 (L26) for IHC Mouse monoclonal antibody	Dako/Agilent	Cat # N/A RRID: N/A
CD68 (KP1) for IHC Mouse monoclonal antibody	Dako/Agilent	Cat # GA60961-2 RRID: 2661840
Chemicals, Peptides, and Recombinant Proteins		
Vorinostat	Selleck Chemicals	Cat#: S1047
Dabrafenib	Selleck Chemicals	Cat#: S2807
Trametinib	Selleck Chemicals	Cat#: S2673
Vemurafenib	Selleck Chemicals	Cat#: S1267
Entinostat	Selleck Chemicals	Cat#: S1053
Panobinostat	Selleck Chemicals	Cat#: S1030
Belinostat	Selleck Chemicals	Cat#: S1085
Paraquat	Sigma-Aldrich	Cat#: 36541
N-Acetyl-L-cysteine (NAC)	Sigma-Aldrich	Cat#: A0150000
tert-Butyl hydroperoxide	Sigma-Aldrich	Cat#: 416665
Vorinostat (used in *in vivo*)	LC Laboratories	Cat#: V-8477
Vorinostat (used in clinic)	Synthesized by J. Beijnen	N/A
PLX4720 chow	Produced by Research Diets Inc PLX4720 was provided by Plexxikon	N/A
Glutathione reduced ethyl ester (GEE)	Sigma-Aldrich	Cat#: G1404
6-Hydroxy-2,5,7,8-tetramethylchromane-2-carboxylic acid (Trolox)	Sigma-Aldrich	238813-1G
Critical Commercial Assays		
RAF-1 RBD Agarose	Merck Millipore	Cat#: 14-278
FastStart Universal SYBR Green Master (Rox)	Roche	Cat#: 04913850001
Quick-RNA™ MiniPrep	Zymo Research	Cat#: R1055
CellTiter-Blue® Cell Viability Assay	Promega	Cat#: G8081
Maxima First Strand cDNA Synthesis Kit for RT-qPCR	Thermo Fisher	Cat#: K1641
Glutathione detection kit	Enzo	Cat#: ADI-900-160
CellROX® Green Flow Cytometry Assay Kit	Life Technologies	Cat#: C10492
Deposited Data		
NKI 178-gene panel exosome DNA sequencing from tumor biopsies	NKI-AVL, The Genomics Core Facility	N/A
Experimental Models: Cell Lines		
A375, SK-MEL-2, SK-MEL-147	ATCC	NA
Colo741	R. Marais (Manchester, UK)	NA
Mel888	D. Peeper (NKI, Amsterdam, The Netherlands)	NA
A375 ex vivo BRAFi-resistant clones	This paper	NA

Plasmids and Recombinant DNA		
pLKO 0.1 (TRC)	Sigma-Aldrich TRC shRNA collection	NA
pLKO-shSLC7A11 shRNAs	Sigma-Aldrich TRC shRNA collection	NA
pLKO-H2A-GFP	K. Lint (NKI, Amsterdam, The Netherlands)	
pLKO-H2A-RFP	K. Lint (NKI, Amsterdam, The Netherlands)	
pLX304-empty	Addgene	Cat#: #25890
pLX304-SLC7A11	SSCB Broad ORF lentiviral expression collection	NA
Sequence-Based Reagents		
shRNA target sequences		
shSLC7A11#1 CCGGCCTGTCACTATTTGGAGCTTTCTCGAGAAAGCTCCAAATAGTGACAGGTTTTTG	Sigma-Aldrich TRC shRNA collection	TRCN0000043123
shSLC7A11#2 CCGGGCTGATTTATCTTCGATACAACTCGAGTTGTATCGAAGATAAATCAGCTTTTTG	Sigma-Aldrich TRC shRNA collection	TRCN0000043127
shSLC7A11#3 CCGGCCTGCGTATTATCTCTTTATTCTCGAGAATAAAGAGATAATACGCAGGTTTTTG	Sigma-Aldrich TRC shRNA collection	TRCN0000288865
shSLC7A11#4 GTACCGGCCCTCTATTCGGACCCATTTACTCGAGTAAATGGGTCCGAATAGAGGGTTTTTG	Sigma-Aldrich TRC shRNA collection	TRCN0000380471
Primers of Genomic DNA mutation detection		
gGAPDH Forward: 5’-CCACCCAGAAGACTGTGGAT-3’	Invitrogen	NA
gGAPDH Reverse: 5’-TTCAGCTCAGGGATGACCTT-3’	Invitrogen	NA
gNRAS exon3 Forward: 5’-TGGCAAATACACAGAGGAAGC-3’	Invitrogen	NA
gNRAS exon3 Reverse: 5’-CACACCCCCAGGATTCTTAC-3’	Invitrogen	NA
gKRAS exon2 Forward: 5’-AGAATGGTCCTGCACCAGTAA-3’	Invitrogen	NA
gKRAS exon2 Reverse: 5’-TTAACCTTATGTGTGACATGTTCTAA-3’	Invitrogen	NA
gBRAF Forward: 5’- CAAGTCACCACAAAAACCTATCGT-3’	Invitrogen	NA
gBRAF Reverse: 5’- AACTGACTCACCACTGTCCTCTGTT-3’	Invitrogen	NA
Gene expression qPCR primer sequences	Invitrogen	NA
GAPDH Forward: 5’-AAGGTGAAGGTCGGAGTCAA-3’	Invitrogen	NA
GAPDH Reverse: 5’-AATGAAGGGGTCATTGATGG-3’	Invitrogen	NA
PDGFRB Forward: 5’- CAGGAGAGACAGCAACAGCA-3’	Invitrogen	NA
PDGFRB Reverse: 5’- TGTCCAGAGCCTGGAACTGT-3’	Invitrogen	NA
EGFR Forward: 5’-TCCTCTGGAGGCTGAGAAAA-3’	Invitrogen	NA
EGFR Reverse: 5’-GGGCTCTGGAGGAAAAGAAA-3’	Invitrogen	NA
TAGLN Forward: 5’-GTCCGAACCCAGACACAAGT-3’	Invitrogen	NA
TAGLN Reverse: 5’- CTCATGCCATAGGAAGGACC-3’	Invitrogen	NA
CYR61 Reverse: 5’- GCTGGAATGCAACTTCGG-3’	Invitrogen	NA

CYR61 Forward: 5'-CCCGTTTTGGTAGATTCTGG-3'	Invitrogen	NA
CTGF Reverse: 5'-TACCAATGACAACGCCTCCT-3'	Invitrogen	NA
CTGF Reverse: 5'- TGGAGATTTTGGGAGTACGG-3'	Invitrogen	NA
BRAF Forward: 5'-GTGGATTATGCTCCCCACC-3'	Invitrogen	NA
BRAF Reverse: 5'-CTGCCATTCCGGAGGAG-3'	Invitrogen	NA
SLC7A11 Forward: 5'-AGCACATAGCCAATGGTGAC-3'	Invitrogen	NA
SLC7A11 Reverse: 5'- GCTGGCTGGTTTTACCTCAA-3'	Invitrogen	NA
Software and Algorithms		
Prism version 7.0	GraphPad Software	NA
FlowJo version 7.6.5	FlowJo, LLC	NA
qPrimerDepot	https://primerdepot.nci.nih.gov/	NA
IncuCyte ZOOM® system	ESSEN Bioscience	NA
4 Peaks version 1.7.2	Nucleobytes	NA
IGV verison 2.3.61 (88)	Broad Institute	NA

Supplemental Data

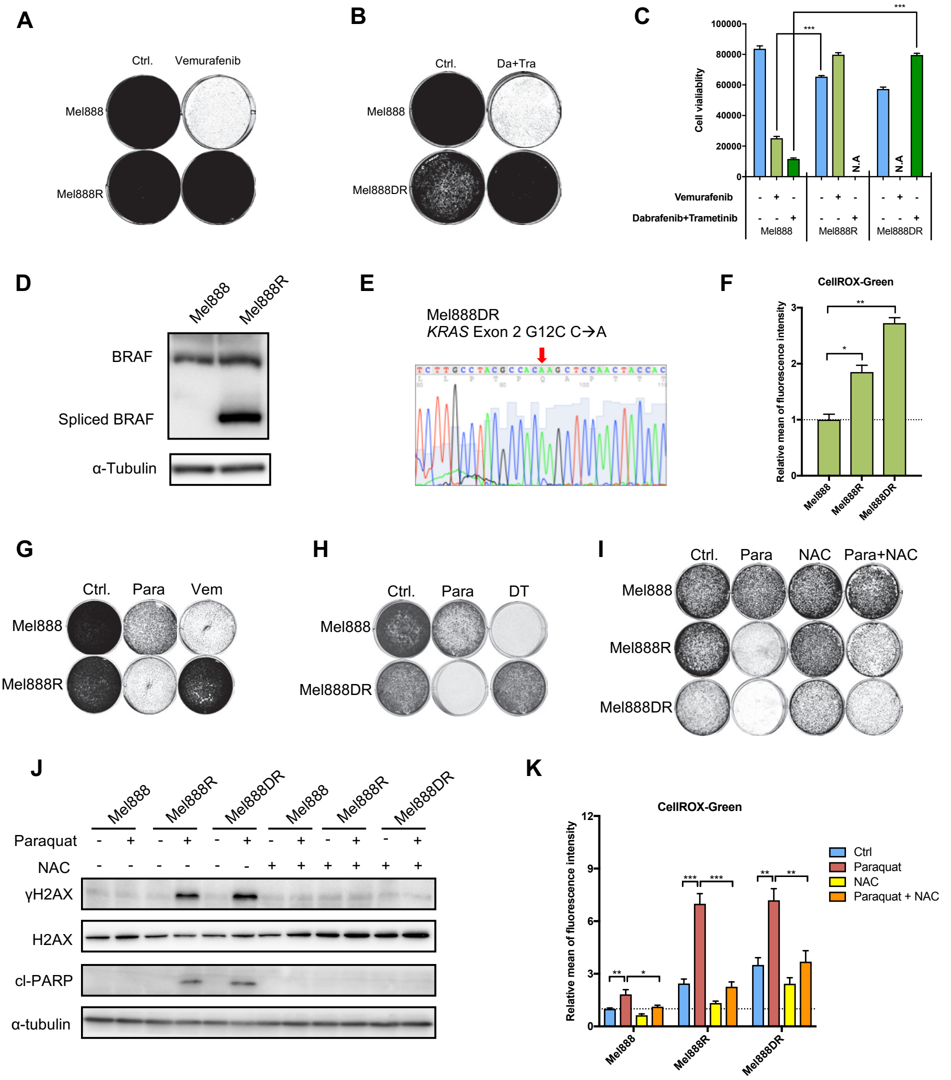

Figure S1. ROS levels and ROS sensitivity of additional melanoma cells, Related to Figure 1.
(A) Long-term colony formation assay of parental (Mel888) and BRAFi-resistant (Mel888R) melanoma cells were seeded 50,000 cells per well in a 6-well plate and cultured in the presence or absence of 2 µM vemurafenib for 10 days. (B) Long-term colony formation assay of parental (Mel888) and BRAFi/MEKi double drug resistant (Mel888DR) melanoma cells were seeded 50,000 cells per well in a 6-well plate and cultured in the presence or absence of 0.5 µM dabrafenib and 10 nM trametinib. (C) Cell viability assay of parental and drug-resistant cells were seeded 3,000 cells per well in a 96-well plate and cultured in the presence or absence of MAPK inhibitors for 96 hours, and then measured with CellTiter-Blue®. (D) Protein Western blot analysis for BRAF indicating that Mel888R cells harbor a 61 kDa BRAF variant. (E) Sanger sequencing of the KRAS gene in Mel888DR cells showing a *KRAS*^{G12C} mutation. (F) ROS levels of Mel888R, Mel888DR and their parental cells were measured after 72 hours culturing without drugs. ROS levels were measured using CellROX Green

flow cytometry assay. Relative ROS inductions are plotted. (G, H) Long-term colony formation assay of Mel888R (panel G), Mel888DR (panel H) and their parental cells in the treatment of paraquat and/or MAPK inhibitors. Cells were seeded 50,000 cells per well in 6-well plates and treated with 20 µM paraquat, 2 µM vemurafenib or combination of 10nM trametinib and 0.5 µM dabrafenib for 10 days. Afterwards, the cells were fixed, stained and photographed. (I) Long-term colony formation assays of parental and MAPKi-resistant Mel888 cells in the treatment of paraquat and/or NAC. Cells were seeded 50,000 cells per well in 6-well plates and treated with 20 µM paraquat and/or 2.5 mM N-acetylcysteine (NAC) for 10 days. Afterwards, the cells were fixed, stained and photographed. (J) Protein lysates were harvest from the MAPKi-resistant (R and DR) and parental Mel888 cells treated with 25 µM paraquat and/or 2.5mM NAC for 72 hours. Western blot analysis showing γH2AX as a DNA damage marker and cleaved-PARP (cl-PARP) as an apoptosis marker; α-tubulin served as the loading control. (K) Parental and MAPKi-resistant Mel888 cells were treated with 20µM paraquat and/or 2.5 mM NAC for 72 hours. ROS levels were measured using CellROXGreen flow cytometry assay. Relative ROS inductions are plotted. Error bars in this figure represent as mean ± standard deviations from biological triplicates (*P≤0.05, ** P≤0.01, *** P≤0.001, student's t-test).

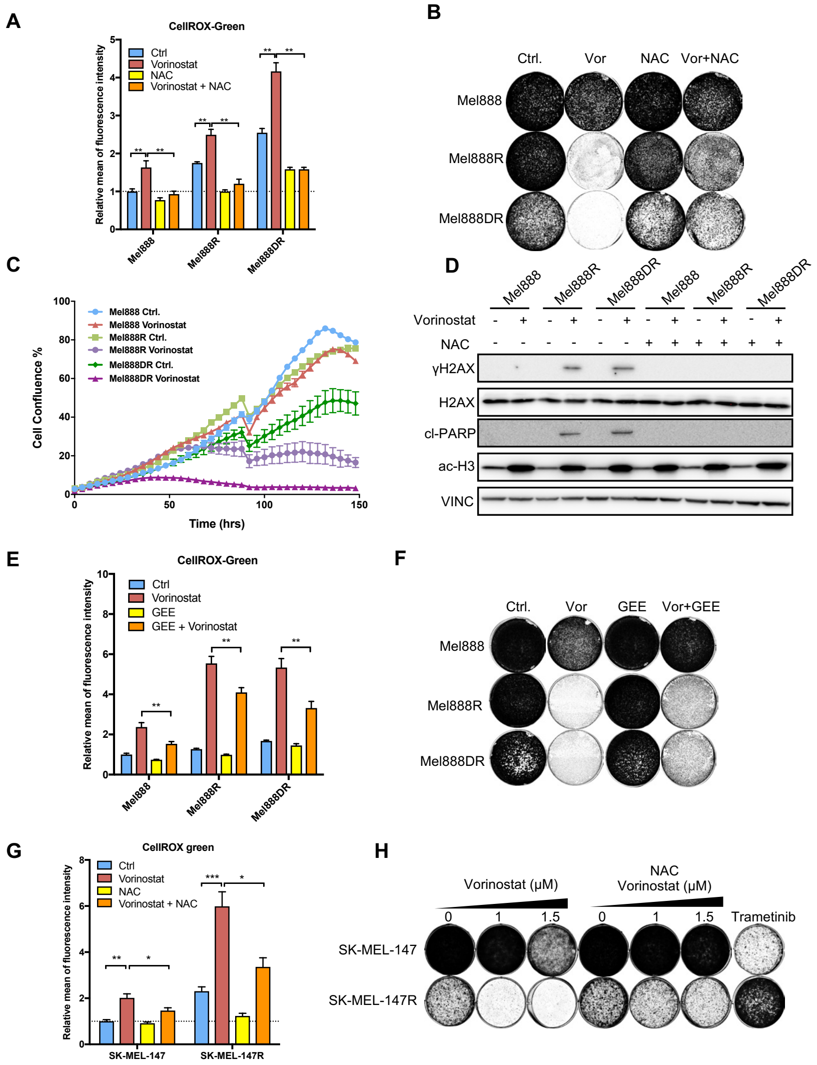

Figure S2. HDACi is detrimental to MAPKi-resistant BRAF and NRAS mutant melanoma cells, related to Figure 2.

(A) Parental and MAPKi-resistant Mel888 cells were treated with 2 μM vorinostat and/or 2.5 mM NAC for 72 hours. ROS levels were measured using CellROX-Green flow cytometry assay. Relative ROS inductions are plotted. (B) Long-term colony formation assays of parental and MAPKi-resistant Mel888 cells treated with vorinostat and/or NAC. Cells were seeded 50,000 cells per well in 6-well plates and treated with 1 μM vorinostat and/or 2.5 mM NAC for 8 days. Afterwards, the cells were fixed, stained and photographed. (C) Incucyte proliferation assay of parental and MAPKi-resistant Mel888 cells, seeded 2,000 cells per well in a 96-well plate and cultured in the presence or absence of 1 μM vorinostat. (D) Protein lysates were harvest from the MAPKi-resistant and parental Mel888 cells treated with 1 μM vorinostat and/or 2.5 mM NAC for 72 hours. Western blot analysis shows γH2AX as a DNA damage marker and cleaved-PARP (cl-PARP) as an apoptosis marker; α-tubulin served as the loading control. (E) Parental and MAPKi-resistant Mel888 cells were treated with 2 μM vorinostat and/or 2.5 mM reduced glutathione ethyl ester (GEE) for 72 hours. ROS levels were measured using CellROX-Green flow cytometry assay. Relative ROS levels are indicated. (F) Longterm colony formation assays of parental and MAPKi-resistant Mel888 cells treated with vorinostat and/or GEE. Cells were seeded 50,000 cells per well in 6-well plates and treated with 1 μM vorinostat and/or 2.5 mM GEE for 8 days. Afterwards, the cells were fixed, stained and photographed. (G) NRAS mutant melanoma cells SK-MEL-147 and its MEKi-resistant variant SK-MEL-147R cells were treated with 2 μM vorinostat and/or 2.5 mM NAC for 72 hours. ROS levels were measured using CellROX-Green flow cytometry assay. Relative ROS inductions are plotted. (H) Long-term colony formation assays of parental and MEKi-resistant SK-MEL-147 cells treated with vorinostat and/or NAC. Cells were seeded 50,000 cells per well in 6-well plates and treated with 1 μM or 1.5 μM vorinostat, 2.5 mM NAC and/or 100 nM trametinib for 8 days. Afterwards, the cells were fixed, stained and photographed. Error bars in this figure represent as mean ± standard deviations from biological triplicates (*P≤0.05, ** P≤0.01, *** P≤0.001, student's t-test).

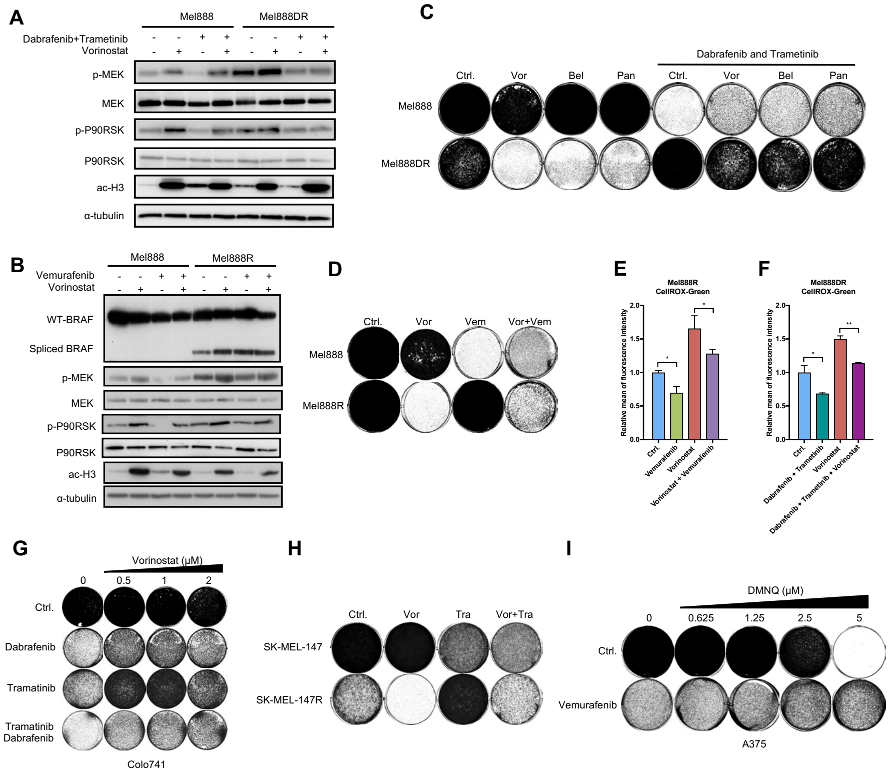

Figure S3. MAPK inhibition is antagonistic with HDAC inhibition in additional BRAF and NRAS mutant melanomas, related to Figure 3.

(A) Mel888DR and parental Mel888 cells were treated with 2 µM vorinostat and/or the combination of 0.125 µM dabrafenib and 5 nM trametinib. Protein lysates were harvested after 72 hours. Western blot analysis was performed for p-MEK and p-P90RSK as indicators of activation of MAPK pathway, ac-H3 indicated levels of acetylated histone H3; α-tubulin served as the loading control. (B) Mel888R and the parental cells were treated with 2 µM vorinostat and/or 0.5 µM vemurafenib for 72 hours. Protein lysates were harvested after 72 hours. Western blot analysis was performed for p-MEK and p-P90RSK as activation of MAPK pathway, ac-H3 indicated levels of acetylated histone H3, Alternative splice variant 61kDa BRAF as the BRAFi-resistance mechanism; α-tubulin served as the loading control. (C, D) Long-term colony formation assays of parental and MAPKi-resistant Mel888 cells treated with vorinostat and/or MAPKi. (C) Mel888DR and parental cells were seeded 50,000 cells per well in 6-well plates and treated with 1 µM vorinostat (Vor), 0.5 µM belinostat (Bel), 5 nM panobinostat (Pan) and/or combination of 5 nM trametinib and 0.125 µM dabrafenib. (D) Mel888R and parental cells were seeded 50,000 cells per well in 6-well plates and treated with 1 µM vorinostat and/or 1 µM vemurafenib. After 10 days culturing, the cells were fixed, stained and photographed. (E-F) Relative ROS level measurements of Mel888R treated with 2 µM vorinostat and/or 2 µM vemurafenib (E), Mel888DR cells with 2 µM vorinostst and/or the combination of 0.125 µM dabrafenib and 5 nM trametinib (F). (G) Long-term colony formation assays of BRAF mutant melanoma cells (Colo741). The cells were seeded 50,000 cells per well in 6-well plates and treated with vorinostat, 5 nM trametinib, 0.125 µM dabrafenib and/or the combinations for 10 days. Afterwards the cells were fixed, stained and photographed. (H) Long-term colony formation assays of parental and MEKi-resistant SK-MEL-147 cells treated with vorinostat and/or MAPKi. The cells were seeded 50,000 cells per well in 6-well plates and treated with 1 µM vorinostat and/or 50nM trametinib. (I) Long-term colony formation assays of A375 cells treated with 0.25 µM vemurafenib and indicated concentrations of 2,3-dimethoxy-1,4-napthoquinone (DMNQ) for 10 days. Error bars in this figure represent as mean ± standard deviations from biological triplicates (*P≤0.05, ** P≤0.01, *** P≤0.001, student's t-test).

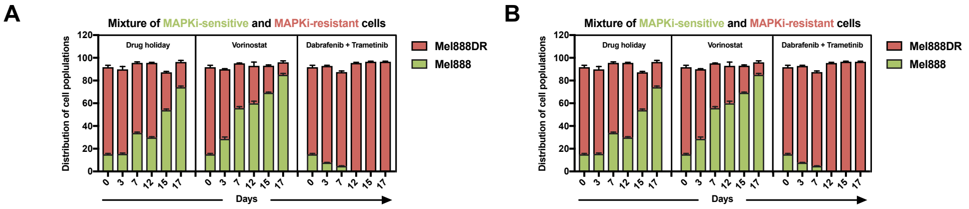

Figure S4. HDACi is detrimental to MAPKi-resistant Mel888 melanoma, related to Figure 4.

(A-B) MAPKi-resistant cells (RFP+) and their MAPKi-sensitive parental cells (GFP+) were mixed in a 9 to 1 ratio. 2,000,000 cells were seeded in a 10-cm dish and subjected to different treatments. At each time point, the distribution of the cell population was determined using flow cytometry. The ratio of two cell populations at the starting of the experiment (day 0) is indicated. The distribution changes of mixed two cell populations are plotted on the Y-axes against the time on the X-axes. Error bars in this figure panel denoted standard deviations of biological triplicates. Panel (A) presents the mixture of Mel888DR and Mel888. Panel (B) presented mixture of Mel888R and Mel888. Error bars in this figure denoted standard deviations of biological triplicates.

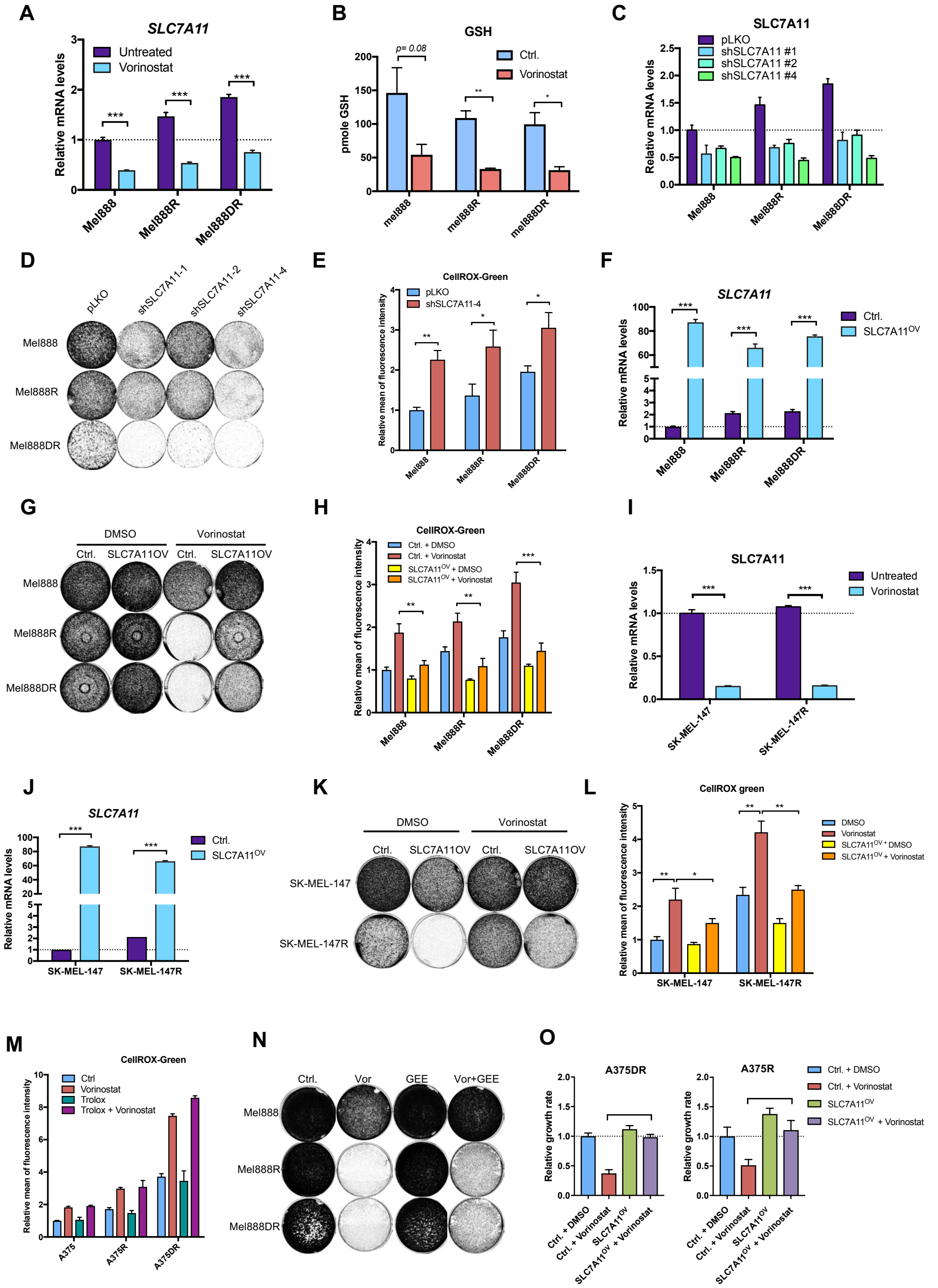

Figure S5. HDACi suppresses SLC7A11 resulting in ROS induction in additional BRAF and NRAS mutant melanoma, related to Figure 5.

(A) mRNA expression analysis of *SLC7A11* measured by qRT-PCR in parental and MAPKi-resistant Mel888 cells treated with 2 µM vorinostat for 48 hours. (B) Parental and MAPKi-resistant Mel888 cells were treated with 2 µM vorinostat for 72 hours. Total intracellular glutathione (GSH) levels were measured using colorimetric based glutathione detection assay. (C-E) Three independent shRNAs targeting *SLC7A11* were individually introduced in parental and MAPKi-resistant Mel888 cells by lentiviral transduction. pLKO empty vector served as the control. (C) The level of *SLC7A11* knockdown by each shRNAs was measured by qRT-PCR. (D) Long-term colony formation of parental and MAPKi-resistant Mel888 cells upon SLC7A11 knockdown. The cells were seeded 50,000 cells per well in 6-well plate and cultured 10 days. Afterwards, the cells were fixed, stained and photographed. (E) Relative ROS levels in parental and MAPKi-resistant A375 cells upon *SLC7A11* knockdown were measured by CellROX-Green flow cytometry assay. (F-H) *SLC7A11* was expressed in parental and MAPKi-resistant Mel888 cells by lentiviral transduction. pLX304 empty vector was used as the control (Ctrl.). (F) The levels of *SLC7A11* overexpression in parental and MAPKiresistant Mel888 cells was measured by qRT-PCR of *SLC7A11* mRNA levels. (G) Long-term colony formation of *SLC7A11* overexpressing parental and MAPKi-resistant Mel888 cells treated with vorinostat. The cells were seeded 50,000 cells per well in 6-well plate and cultured 10 days with or without 1µM vorinostat. Afterwards, the cells were fixed, stained and photographed. (H) *SLC7A11* overexpressing parental and MAPKi-resistant Mel888 cells were treated with 2 µM vorinostat for 72 hours. Afterwards, ROS levels were measured using CellROX-Green flow cytometry assay. Relative ROS inductions was plotted. (I) mRNA expression analysis of *SLC7A11* by qRT-PCR in parental and MEKi-resistant SK-MEL-147 cells treated with 2 µM vorinostat for 48 hours. (J-L) *SLC7A11* cDNA was expressed in parental and MEKi-resistant SK-MEL-147 cells by lentiviral transduction. pLX304 empty vector was used as the control (Ctrl.). (J) The levels of *SLC7A11* overexpression in parental and MEKi-resistant SK-MEL-147 cells were measured by examining the *SLC7A11* mRNA levels by qRT-PCR. (K) Long-term colony formation of *SLC7A11* overexpressed parental and MEKi-resistant SK-MEL-147 cells treated with vorinostat. The cells were seeded 50,000 cells per well in 6-well plate and cultured 10 days with or without 1µM vorinostat. Afterwards, the cells were fixed, stained and photographed. (L) *SLC7A11* overexpressing parental and MEKi-resistant SK-MEL-147 cells were treated with 2 µM vorinostat for 72 hours. Afterwards, ROS levels were measured using CellROXGreen flow cytometry assay. Relative ROS inductions are plotted. (M) Parental and MAPKi-resistant A375 cells were treated with 2 µM vorinostat and/or 0.25 mM 6-hydroxy-2,5,7,8- tetramethylchroman-2-Carboxylic Acid (Trolox) for 72 hours. ROS levels were measured using CellROX-Green flow cytometry assay. Relative ROS levels are indicated. (N) Long-term colony formation assays of parental and MAPKi-resistant A375 cells treated with vorinostat and/or Trolox. Cells were seeded 50,000 cells per well in 6-well plates and treated with 1 µM vorinostat and/or 0.25 mM Trolox for 8 days. (O) The relative growth rate of the responsiveness to 1 µM vorinostat treatment in MAPKi-resistant A375 cells with and without *SLC7A11* overexpression. The growth rates were calculated based on the slope a curve fitted through the linear range of the log-transformed confluence measurements from Incucyte date of figure 5 J-K. For each cell line, the growth rates were normalized to the mean of the untreated controls. The growth rate of untreated control was considered as a basal line and normalized to 1. The relative growth rates of all growth rates of the drug-treated and genetic manipulated arms were compared with the untreated control arm. Error bars in this figure represent as mean ± standard deviations from biological triplicates (*P≤0.05, ** P≤0.01, *** P≤0.001, student's t-test).

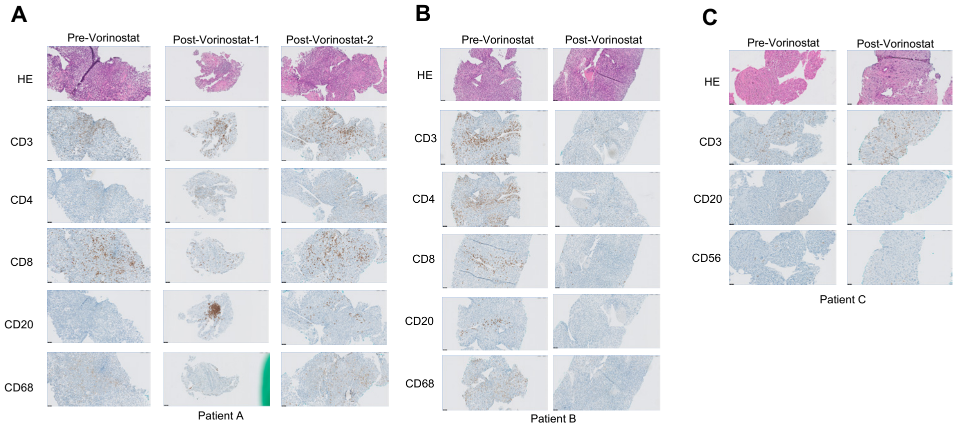
A
Pre-Vorinostat
Post-Vorinostat-1
Post-Vorinostat-2
HE
CD3
CD4
CD8
CD20
CD68
Patient A
B
Pre-Vorinostat
Post-Vorinostat
HE
CD3
CD4
CD8
CD20
CD68
Patient B
C
Pre-Vorinostat
Post-Vorinostat
HE
CD3
CD20
CD56
Patient C

Figure S6. Immune cells staining on the biopsies from vorinostat treated MAPKi-resistant melanoma patients, related to Figure 7.
(A-C) Immunohistochemical staining of immune cells in melanoma tissue section from MAPKiresistant melanoma patients (A-C) pre- and post-treated with vorinostat as indicated. CD3 served as a pan-T cell marker. CD4 served as a T helper cell marker. CD8 served as killer T cells. CD20 served as a B cell marker. CD68 served as a macrophage marker. The black bar in the lower left corner represents 50 µm.

High throughput functional genetic and compound screens identify targets for senescence induction in cancer

5

Liqin Wang[1], Rodrigo Leite de Oliveira[1], Cun Wang[1], João M. Fernandes Neto[1], Sara Mainardi[1], Bastiaan Evers[1], Cor Lieftink[1], Ben Morris[1], Fleur Jochems[1], Lisa Willemsen[1], Roderick L. Beijersbergen[1] and René Bernards[1#]

1 Division of Molecular Carcinogenesis, Cancer Genomics Centre Netherlands.
The Netherlands Cancer Institute, Plesmanlaan 121, 1066 CX Amsterdam, The Netherlands.

5

Cell Report (2017)

Abstract

Senescence is a proliferation arrest that can result from a variety of stresses. Cancer cells can also undergo senescence, but the stresses that provoke cancer cells to undergo senescence are largely unknown. We use here both functional genetic- and compound screens in cancer cells harboring a reporter that is activated during senescence to find targets to induce senescence. We show that suppression of the SWI/SNF component SMARCB1 induces senescence in melanoma through super-activation of the MAP kinase pathway. From the compound screen, we identified multiple aurora kinase inhibitors as potent inducers of senescence in *RAS* mutant lung cancer. Senescent melanoma and lung cancer cells acquire sensitivity to the BCL2 family inhibitor ABT263. We propose a one-two punch approach for the treatment of cancer in which a first drug is used to induce senescence in cancer cells and the second drug is used to kill senescent cancer cells.

Introduction

Senescence was originally identified through the limited ability of primary fibroblasts in culture to undergo cell division. After the replicative potential of primary cells is exhausted due to telomere shortening, they enter into a stable state of growth arrest termed replicative or cellular senescence (Hayflick, 1965). Senescent cells remain viable, but their cellular state is quite distinct and characterized by absence of proliferation markers, expression of tumor suppressor genes, senescence associated β-galactosidase (SA-β-gal) activity and the presence of nuclear foci, referred to as senescence-associated heterochromatin foci (SAHFs) (Munoz-Espin and Serrano, 2014). Senescent cells also secrete a variety of inflammatory cytokines and chemokines, collectively referred to as the Senescence-Associated Secretory Phenotype (SASP), which may help in their clearance from the body (Coppe et al., 2008; Kuilman et al., 2008). With respect to cancer, senescence is generally considered to be a fail-safe mechanism against oncogenic transformation, as expression of an oncogenic RAS gene in primary cells leads to the rapid induction of a post-replicative state referred to as oncogene-induced senescence (OIS) (Serrano et al., 1997). This fail-safe mechanism actually operates in humans to prevent cancer, as melanocytic nevi (moles) often carry an activated BRAF(V600E) oncogene, but stain for many of the senescence markers, indicative of a stable and lasting state of oncogene-induced senescence in these cells (Michaloglou et al., 2005). Importantly, even some advanced cancer cells can be induced to enter a state of senescence, not only as a result of chemotherapy treatment, but also by excessive oncogenic signaling (Ewald et al., 2010; Sun et al., 2014).

The complex mixture of cytokines, chemokines, growth factors, proteases and metabolites (collectively called the SASP) produced by senescent cells represents a potentially double-edged sword with respect to tumor control (Coppe et al., 2010; Coppe et al., 2008). On the one hand, the SASP can inhibit growth of a cancer by triggering an immunological response against the tumor through recruitment of phagocytic cells and lymphocytes from the adaptive immune system (Eggert et al., 2016). On the other hand, the SASP can also be potentially deleterious. When senescent cells remain present in a tumor, they can contribute to a chronic inflammatory response, which can result in acceleration of age-associated conditions (Baker et al., 2016) and cancer metastases (Angelini et al., 2013). An in vivo study showed that elimination of chemotherapy-induced senescent cells reduced several side-effects of treatment, including heart toxicity, bone marrow suppression, loss of strength and physical activity and cancer recurrence and metastasis (Demaria et al., 2017). These latter data indicate that elimination of the senescent cancer cells can be beneficial, while the former data suggest that the SASP may help in immune clearance of cancer cells. The debate whether senescent cancer cells should be eliminated is still ongoing and might ultimately depend on the specific nature of the SASP, as not all senescent cells secrete the same cytokines and chemokines (Hoare et al., 2016).

Senescent cells are quite distinct in terms of gene expression (Fridman and Tainsky, 2008), chromatin structure (Narita et al., 2003) and metabolism (Jiang et al., 2013; Wiley and Campisi, 2016), suggesting that they might be sensitive to certain drugs that do not kill their proliferating counterparts. Indeed, ABT263, a specific inhibitor of the anti-apoptotic proteins BCL-2, BCL-W and BCL-XL, has been shown to selectively kill senescent cells in vivo in a mouse model to delay several age-associated hematopoietic disorders (Chang et al., 2016; Zhu et al., 2016). This begs the question whether such so called senolytic agents can also be used in a "one-two punch" consecutive therapy approach for cancer in which a first drug is used to induce senescence selectively in cancer cells and a subsequent senolytic therapy serves to eradicate the senescent cancer cells.

Here, we begin to investigate the feasibility of this one-two punch cancer treatment model by performing functional genomic and compound screens to find ways to induce senescence in cancer cells. We show that CRISPR/Cas9 based genetic screens and high throughput compound screens in cancer cells can be used to identify targets for senescence-inducing therapies. We show that such senescent cancer cells are subsequently sensitive to senolytic agents.

Results

A reporter-based CRISPR screen for senescence-inducing genes

Kang et al. recently demonstrated that human primary fibroblasts strongly upregulate the expression of microRNA 146a (*miR146a*) during the process of senescence, irrespective of how senescence was induced. They also demonstrated that a reporter construct in which the promoter of miR146a was linked to Enhanced Green Fluorescent Protein (eGFP) was activated during induction of senescence (Kang et al., 2015). We asked whether this miR146a-eGFP reporter was also suited to detect induction of senescence in human cancer cells. We inserted the reporter gene in A375 melanoma cells and induced senescence through treatment with chemotherapy or induction of high levels of Reactive Oxygen Species (ROS). Figure 1A, E show that both treatment of the miR146a-eGFP reporter-containing cells with doxorubicin or the ROS inducer paraquat resulted in a significant upregulation of the eGFP signal, which was associated with the induction of a senescent cell morphology and senescence associated β-galactosidase (SA-β-gal) activity (Figure 1B, C, F, G), loss of phosphorylated retinoblastoma protein (p-RB) and the induction of the tumor suppressor protein CDKN1A (also known as p21cip1, Figure 1D, H).

We used these miR146a-eGFP A375 cells for a loss of function genetic screen using a library of 5130 CRISPR vectors targeting 446 enzymes involved in chromatin remodeling and modulation of epigenetic marks (the "epigenome" CRISPR library, (Table S1), as outlined schematically in Figure 1I, J. The rationale for the screen is that cells should become eGFP-positive upon the knockout of a gene that induces senescence. After 8 days of culturing, cells were harvested and subjected to Fluorescence Activated Cell Sorting (FACS) into eGFP- and eGFP+ fractions. Cells without epigenome library served as a control. After this, gRNA sequences from eGFP- and eGFP+ cells were recovered by PCR and quantified through deep sequencing as described (Figure 1I) (Evers et al., 2016). A list of significantly enriched gRNAs is provided in Table S1. This list was used for the robust rank algorithm as part of

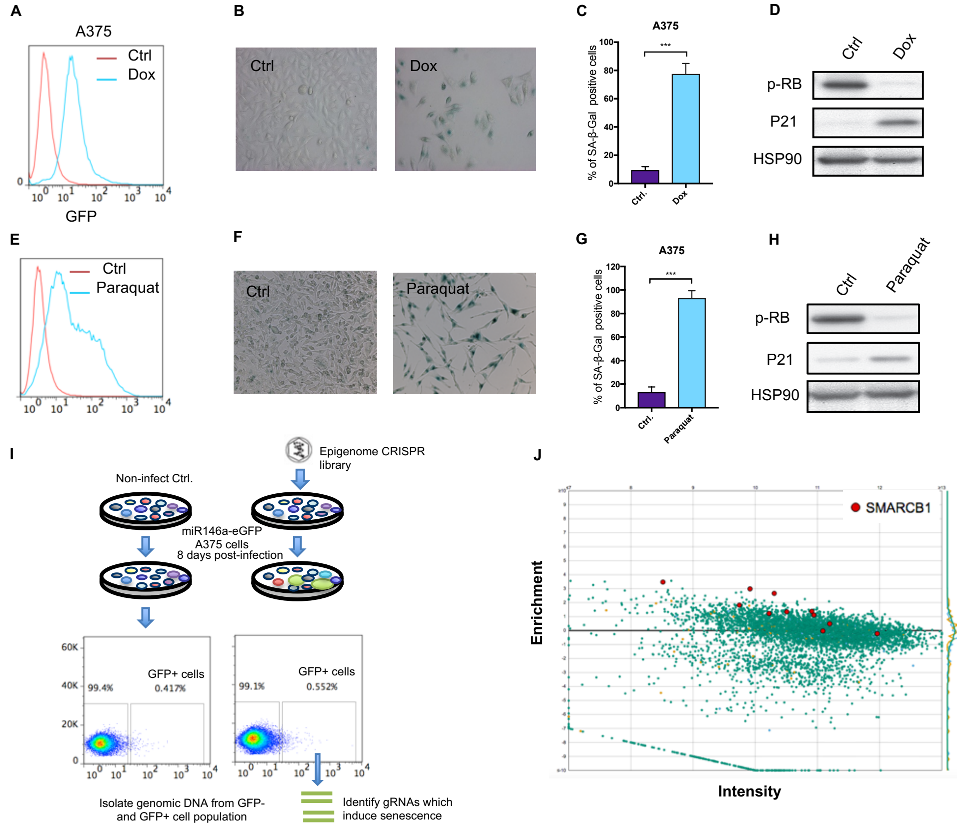

Figure 1. The miR-146a-EGFP Reporter Detects Senescence in Melanoma.

(A–D) A375 cells expressing the miR-146-EGFP reporter were treated with 100 ng/mL doxorubicin (DOX) for 120 hr. (A) EGFP fluorescence was measured by flow cytometry. Doxorubicin treatment also induced classic senescence markers: (B) senescence-associated b-galactosidase activity (data were represented as mean ± SD) and (D) loss of phosphorylated-RB and induction of CDKN1A (p21cip1). (C) Quantification of data shown in (B). (E–H) A375 cells expressing the miR-146-EGFP reporter were treated with 100 mM paraquat (a ROS inducer) for 120 hr. (E) EGFP fluorescence was measured by flow cytometry. Doxorubicin treatment also induced classic senescence markers. (F) Senescence-associated b-galactosidase activity. Data are represented as mean ± SD. (G) Quantification of data shown in (F). (H) Loss of p-RB and induction of CDKN1A (p21cip1). (I) Schematic outline of the FACS-assisted CRISPR screen. Polyclonal human "epigenome" CRISPR library virus was generated to infect senescence reporter embedded A375-miR146-EGFP cells. These cells were then cultured and collected after 8 days. The collected cells were sorted by fluorescence-activated cell sorter (FACS) into EGFP and EGFP+ fractions. The cells without epigenome library viral infection served as a negative control. Subsequently, gRNA inserts from EGFP and EGFP+ cell fractions were recovered by PCR and quantified by deep-sequencing. (J) Representation of the relative abundance of gRNA barcode sequences from the CRISPR screen described in (I). The y axis shows relative abundance (log2 value) of gRNA in EGFP+ cell fraction versus EGFP cell fraction, and the x axis shows the average number of sequence reads for each gRNA. Positions of the gRNAs targeting SMARCB1 are indicated in red.

the MAGeCK software, identifying SMARCB1, a component of the SWI/SNF chromatin remodeler complex as top candidate from the screen.

SMARCB1 knockout induces senescence

Since loss of function mutations in *SMARCB1* are seen in a range of tumors, including rhabdoid tumors, brain tumors, soft tissue sarcoma, kidney cancer and Wilms tumor (Hodges et al., 2016), we focused on this gene for further validation. Figure 2A, B shows that infection of both A375 and Mel888 melanoma cells with two independent gRNAs targeting *SMARCB1* resulted in a dramatic inhibition of proliferation, associated with reduced p-RB and increase in p21cip1 and p27kip1, both known to be associated with the senescent phenotype. Cells harboring the *SMARCB1* gRNAs also had clear signs of senescence as judged by cell morphology and SA-β-gal staining (Figure 2B, C, D). Transcriptome analysis of cells infected with gRNAs targeting *SMARCB1* revealed that a senescence-associated signature was significantly enriched in these cells (Figure 2G, Table S2). To investigate whether *SMARCB1* depletion may also result in cell death, we incubated *SMARCB1* knock-out cells with caspase-3/7-green fluorescent apoptosis assay reagent, which couples the activated caspase-3/7 recognition motif to a DNA intercalating dye. This enables the quantification of apoptosis. The result shows that *SMARCB1* depletion can slightly induce apoptosis in A375 and Mel888 melanoma cells (Figure 2 E, F). Similar results were seen in two additional melanoma cell lines: Mel526 and Mel624 (Figure. S1A-E), Note that shortly after infection with *SMARCB1* gRNA protein levels were significantly repressed, whereas after 30 days of culturing, the *SMARCB1* knockout cells were counter-selected, consistent with an anti-proliferative effect of SMARCB1 loss (Figure S1F-H). This is consistent with the notion that a reduction in SMARCB1 levels is associated with a non-proliferative phenotype. Moreover, in miR146a-eGFP A375 cells infected with *SMARCB1* gRNA, stronger eGFP positivity was correlated with a stronger anti-proliferative effect and a more pronounced senescence phenotype (Figure 2H, I). Similar results were obtained when we used shRNAs targeting *SMARCB1* instead of gRNAs: three distinct shRNAs against *SMARCB1* suppressed *SMARCB1* (Figure 2L), induced miR146a-eGFP in two melanoma cell line models (Figure 2K), resulted in suppressed proliferation (Figure 2J) and were associated with a senescent (SA-β-gal positive) morphology (Figure 2 M, N).

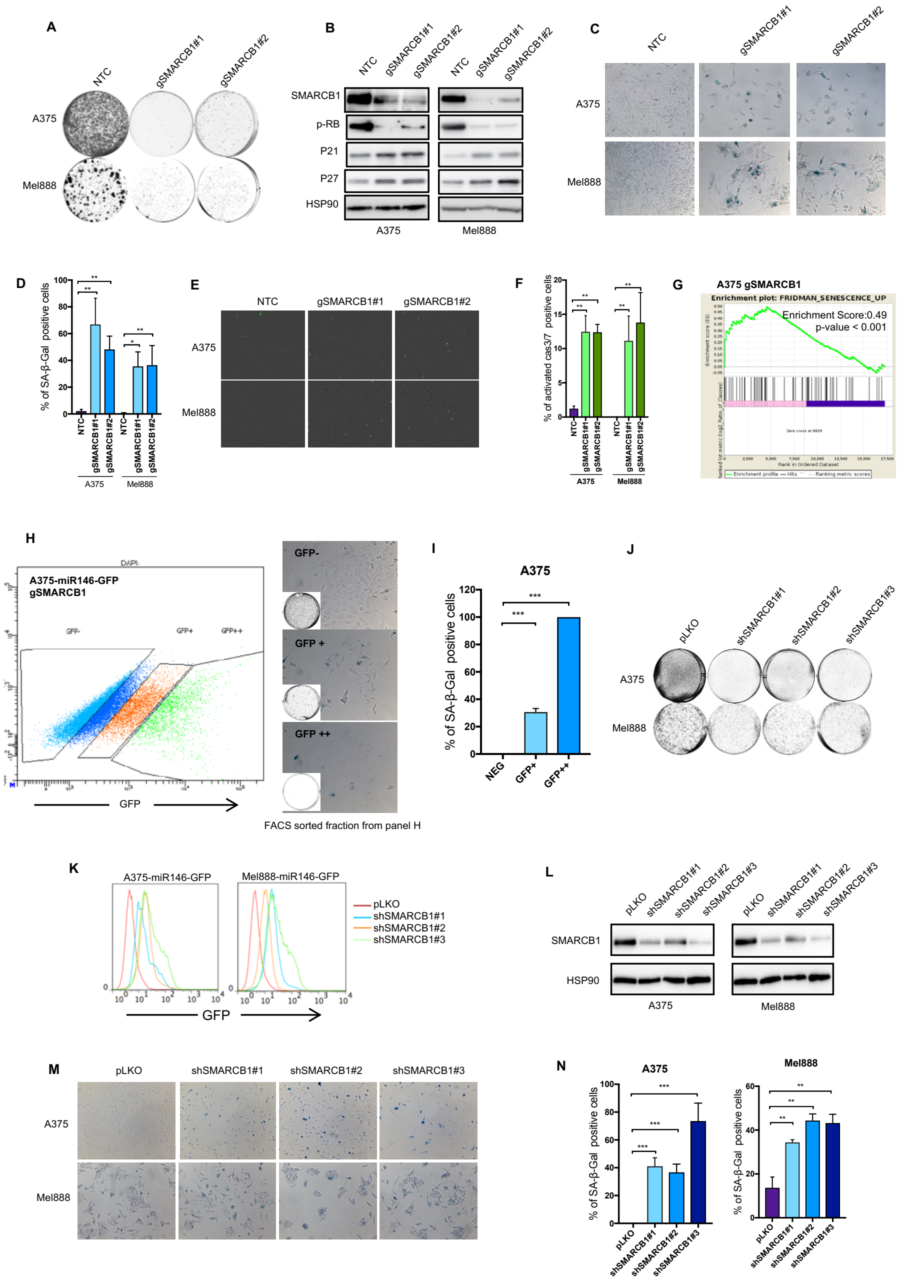

Figure 2: SMARCB1 depletion induces senescence in melanoma cells.
(A,B,C,D) A375 and Mel888 cells expressing the miR146a-eGFP reporter were infected with two independent *SMARCB1* gRNAs-CAS9 (gSMARCB1) virus and cultured for 10 days. (A) Depletion of *SMARCB1* reduced cell proliferation and upregulated classic senescence markers: (B) Loss of p-RB, induction of CDKN1A (p21cip1), CDKN1B (27kip1) and (C,D) increased senescence-associated β-galactosidase activity (quantification shown in panel D, data were represented as Mean ± SD). Non-targeted gRNA vector (NTC) served as a control. (E,F) A375 and Mel888 infected with two

independent *SMARCB1* gRNAs-CAS9 (gSMARCB1) virus and cultured for 5 days. Afterwards, the cells were seeded in 96 well plate and incubated with caspase-3/7 green apoptosis assay reagent next day. Images were taken by Incucyte after 4 days. Green fluorescent staining indicated caspase-3/7 dependent apoptosis (quantification shown in panel F, data were represented as Mean ± SD). (G) A375 cells were infected with gRNAs gSMARCB1 virus and cultured for 8 days, RNA sequencing was performed on these cells, and followed by GSEA analysis of a A375 gSMARCB1 infected cells versus an A375 infected with non-targeting control for the 'FRIDMAN_SENESCENCE_UP' geneset (see methods). The Enrichment Score was 0.49 with a p-value of < 0.001. (H,I) A375 cells expressing the miR146a-eGFP reporter were infected with gRNAs pooled gSMARCB1 virus and cultured for 8 days, (H) subsequently FACS sorted into GFP-, GFP+ and GFP++ cell fraction. The sorted cells were seeded 20K in a 6-well plate, cultured for additional 7 days, followed by senescence β-galactosidase staining; quantification shown in panel I. Data were represented as Mean ± SD. (J,K,L,M,N) A375 and Mel888 cells expressing the miR146a-eGFP reporter were infected with three independent shRNAs targeting *SMARCB1* (shSMARCB1). Empty vector pLKO served as a control. (K) shRNAs activated miR146-eGFP senescence reporter, (J) reduced cell proliferation, (L) suppressed *SMARCB1* expression, (M,N), induced senescence-associated β-galactosidase activity; Quantification shown in panel N. Data were represented as Mean ± SD.

SMARCB1 activates EGFR through reduced SOX10 expression

To gain insight into how *SMARCB1* knockout induces senescence, we performed transcriptome analysis using RNAseq. We observed that *SOX10* was downregulated upon *SMARCB1* depletion (Table S2). We have shown previously that SOX10 suppression can cause resistance to BRAF inhibitors in BRAF mutant melanoma through upregulation of EGFR through activation of JUN (Sun et al., 2014). Indeed, western blot analyses of cells infected with *SMARCB1* gRNAs shown reduced SOX10 protein, which was again associated with an increase in *JUN* and *EGFR* mRNA and protein levels (Figure 3A, B). Upregulation of EGFR was also associated with increased signaling through the MAP kinase pathway, as evidenced by the increase in p-MEK and p-p90RSK, resulting in hypo-phosphorylation of RB and P27kip1 induction (Figure 3A). These data suggested that *SMARCB1* knockout could trigger a state that has hallmarks of oncogene-induced senescence, reminiscent of what is seen by ectopic EGFR expression in melanoma (Sun et al., 2014). Indeed, like EGFR expression, *SMARCB1* knockout or shRNA mediated suppression caused resistance to vemurafenib in A375 cells (Figure 3F, G). To ask whether SOX10 suppression is causal in the induction of senescence, we ectopically expressed *SOX10* in *SMARCB1* knockout cells. Figure 3C shows that *SOX10* expression rescues the anti-proliferative effect of *SMARCB1* knockout. Biochemically, *SOX10* expression downregulates EGFR expression in the presence of low levels of SMARCB1 and causes reversal of the induction of p27kip1, restoration of RB phosphorylation (Figure 3D), and reduction of SA-β-gal activity (Figure 3E). Conversely, knockdown of *SOX10* by shRNA vector activated the miR146a-eGFP vector, consistent with a state of oncogene-induced senescence (Figure S2A, B).

The specific inhibitor of the anti-apoptotic proteins BCL-2, BCL-W and BCL-XL, ABT263 (navitoclax), selectively kills senescent cells, but no data are published on senescent cancer cells (Chang et al., 2016; Zhu et al., 2016). We therefore tested whether senescence induced by SMARCB1 downregulation in melanoma cells made them vulnerable to ABT263. Figure

3H-J show that ABT263 had little effect on parental A375 cells, but effectively ablated cells harboring a gRNA targeting *SMARCB1*. Figure 3K, L show that ABT263 can massively induce apoptosis in melanoma cells made senescent through *SMARCB1* depletion. Similar results were obtained in Mel624 cells (Figure S2C, D). Together, these data demonstrate the feasibility of killing cancer cells with a sequential therapy in which a vulnerability is acquired by a first drug, that is targeted by a second drug.

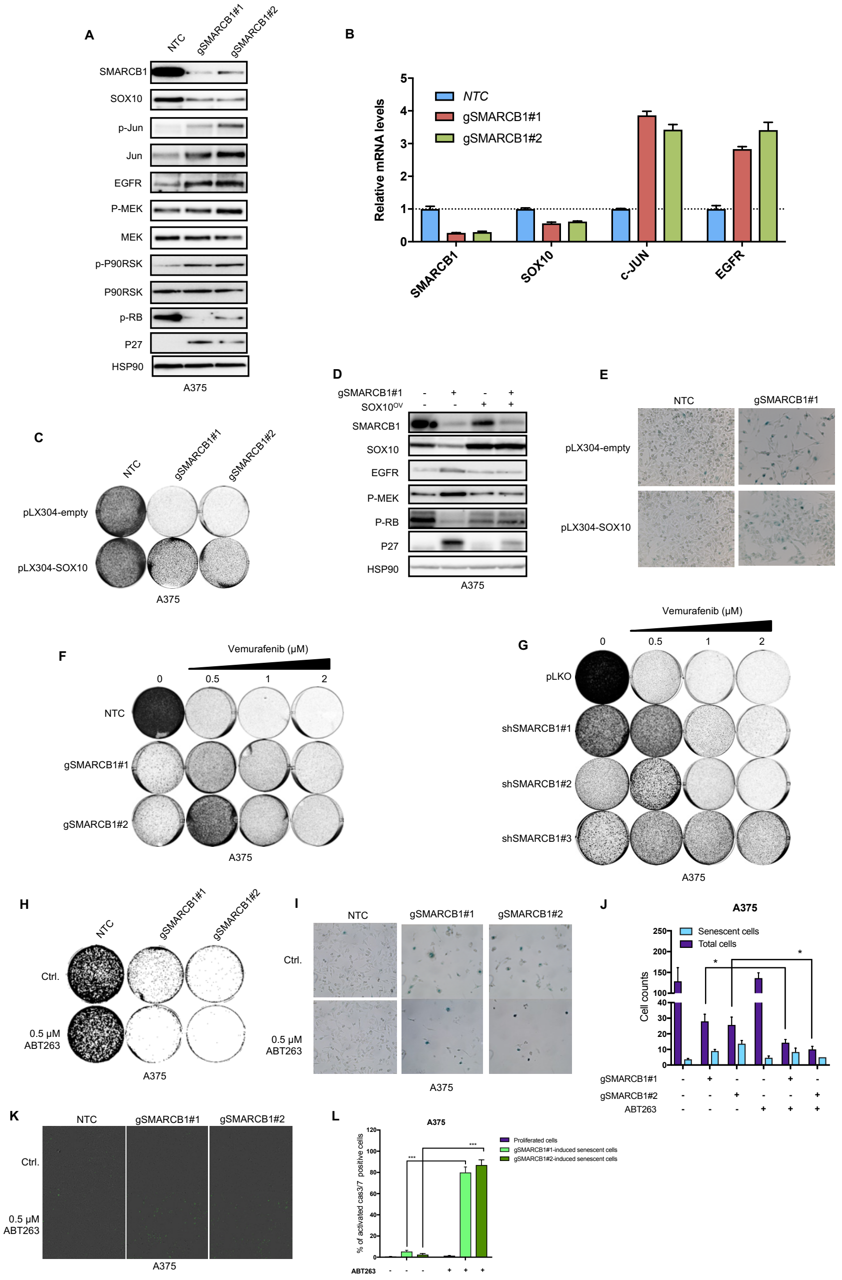

Figure 3: SMARCB1 depletion induces oncogene-induced senescence through down-regulation of SOX10

(A,B). A375 cells expressing the miR146a-eGFP reporter were infected with two independent gSMARCB1 and cultured for 10 days. (A) Western blot analysis shows that depletion of SMARCB1 results in a reduction of SOX10, induction of JUN, phosphorylated-JUN (p-JUN), EGFR and hyper-activated MAP kinase signaling as judged by phosphorylated-MEK (p-MEK), phosphorylated-P90RSK (p-P90RSK), phosphorylated-RB (p-RB) and P27kip. HSP90 served as a loading control. (B) Real-time PCR showing relative mRNA level of *SOX10*, *JUN* and *EGFR* upon *SMARCB1* depletion. Data were represented as Mean ± SD. (C,D,E) A375 cells were infected with SOX10 overexpressing lentiviral vector and selected with blasticidin. Subsequently, cells were infected with gRNAs-CAS9 targeting *SMARCB1* and selected with puromycin. (C) Colony formation assay demonstrating that depletion of *SMARCB1* reduced cell proliferation, but this can be rescued by overexpressing *SOX10*. (D) Protein level of SMARCB1, SOX10, EGFR, p-MEK, p-RB, p27 were measured by western blot. HSP90 served as a loading control. (E) *SOX10* overexpressing partially reduced the SA-β-gal activity that was induced by *SMARCB1* depletion. (F) Depletion of *SMARCB1* using gRNAs-CAS9 confers a proliferation disadvantage in the absence of the BRAF-inhibitor vemurafenib, but induces vemurafenib resistance in A375 cells. After 5 days post-infection of gSMARCB1-CAS9, the cells were seeded 50K per well in 6 well plates and cultured for 12 days in the presence or absence of vemurafenib. (G) A375 cells were infected with shRNAs targeting *SMARCB1*, seeded 50K per well in 6 well plates and cultured in the presence or absence of vemurafenib for 10 days. (H,I,J) A375 cells were infected with SMARCB1 gRNAs-CAS9 virus. 4 days post-infection, the cells were seeded into 6-well plate and treated with 0.5 µM ABT263 for 120 hours. (H) Colony formation assay showed that ABT263 selectively depleted cells, which were infected with SMARCB1 gRNAs-CAS9. (I,J) Cells with increased senescence-associated β-galactosidase activity are vulnerable to ABT263. The quantification of remaining cells and senescent cells shown in panel J. Data were represented as Mean ± SD. (K,L) A375 infected with two independent SMARCB1 gRNAs-CAS9 (gSMARCB1) virus and cultured for 8 days. Afterwards, the cells were seeded in 96 well plate, treated with 0.5µM ABT263 and incubated with caspase-3/7 green apoptosis assay reagent. Images were taken by incucyte after 72hrs. Green fluorescent staining indicated caspase-3/7 dependent apoptosis. The quantification shown in panel L. Data were represented as Mean ± SD.

Compound screens for senescence induction

To screen for compounds that induce senescence in RAS mutant lung cancer, we reconfigured the miR146a-eGFP vector to express the secreted Gaussia luciferase (Gluc) under control of the miR146a promoter. *KRAS* mutant A549 lung cancer cells were stably transfected with the miR146a-Gluc reporter and then seeded into 384 well plates. After 24 hours, cells were incubated with 0.2, 1 and 5 µM of 941 unique compounds from 4 independent libraries, including inhibitors of G-protein-coupled receptors, a library targeting kinases, an epigenetic modifying enzyme library and an NCI approved oncology drug set. After 7 days, senescence induction was assessed by the luminescence signal, quantified with an Envision plate reader, while the cell viability was determined by a cell titer blue assay (Figure 4A). The chemotherapeutic agent etoposide was included in the screen as a positive control. Figure S3 A-E shows that etoposide indeed efficiently induces senescence in both A549 and H358 lung cancer cells.

Figure 4B shows the normalized values of cell titer blue (ctb) and Gaussia luciferase (luc) per compound. There are two major categories of hits in the screen: those with high luciferase in the presence of high cell titer blue and relatively high luciferase with low cell titer blue.

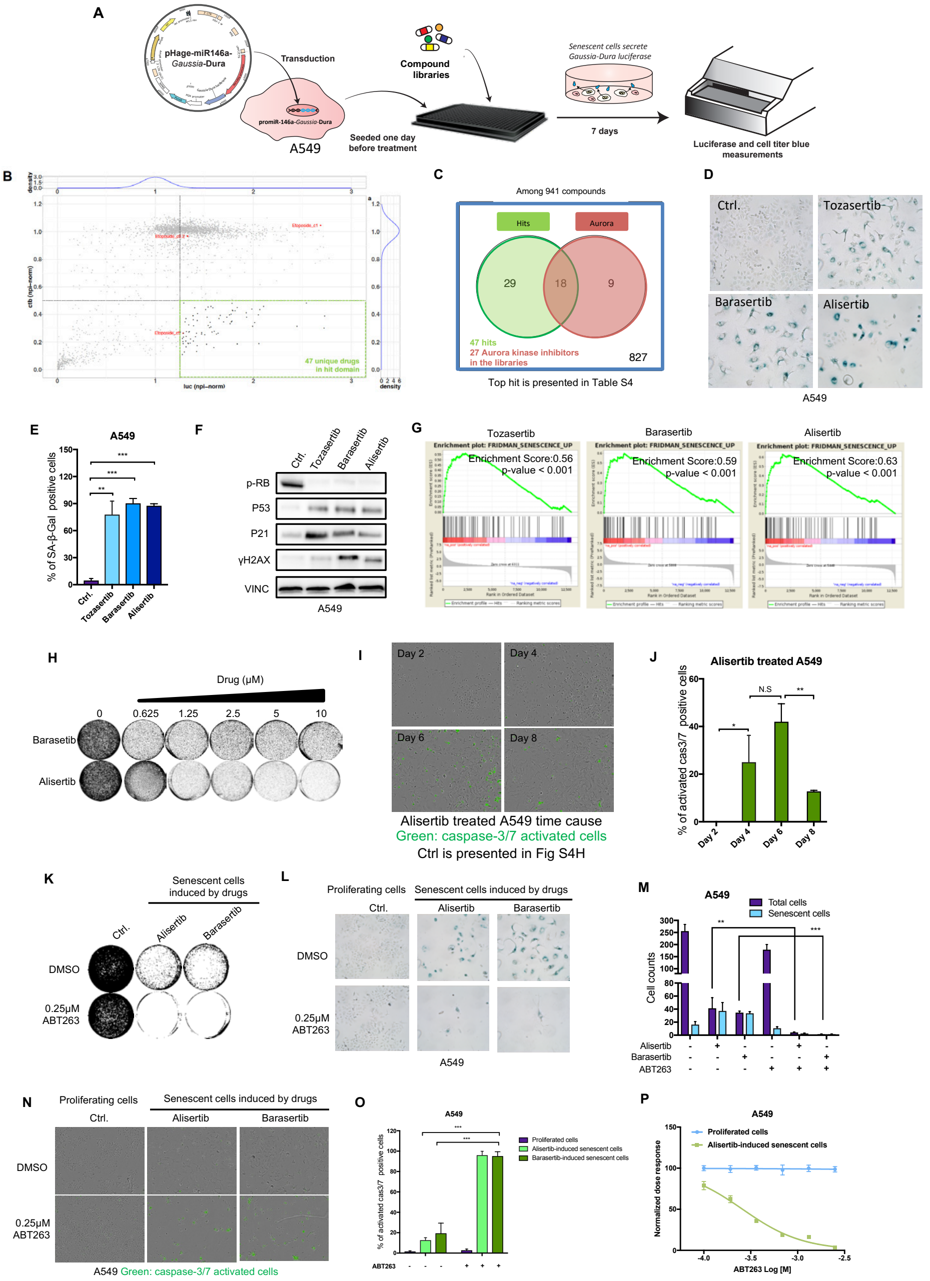

Figure 4. A compound screen identifies aurora kinase inhibitors as inducers of senescence.
(A) Schematic outline of compound screen. The miR146-GFP reporter was modified to express Gaussia luciferase. The reporter was introduced into a *KRAS* mutant lung cancer line A549 through lentiviral infection. The infected cells were seeded into 384-well plates. After 24hrs, the compound library containing 941 unique pharmacologically active compounds was added into the plates. Three concentrations were used: 0.2 μM, 1 μM and 5 μM in 3 biological replicates. After 7 days, the Gaussia luminescence signal was measured with 5μg/ml coelenterazine and cell viability signal was

measured with 25 times diluted CellTiter-Blue® with Envision Multilabel Plate Reader. (B) Results from the compound screen. The NPI normalized (npi-norm) values for cell titer blue signal (ctb) and luminescent signal (luc) were plotted for each compound. The hits were defined based on the selection criteria that: (1) the value for the Luciferase readout should be ≥ 1.25 and corresponds with a p-value of 0.032. (2) the value of the CellTiterBlue readout should be ≤ 0.5 and corresponds with a p-value of 4.1e-14. The p-values were calculated based on the null-distributions formed by the negative control (DMSO). Etoposide served as a positive control. The top hits were presented in the hit domain. (C) Among 941 unique compounds in the combined drug library, there were 27 unique aurora kinase inhibitors. 47 compounds were considered as hits. Among these 47 drug hits were 18 independent aurora kinase inhibitors. (D,E,F,G,H) A549 cells were treated with 0.2µM tozasertib, 1µM alisertib or 1µM barasertib for 7 days. (D,E) Treatment with three independent aurora kinase inhibitors induced senescence-associated β-galactosidase activity (quantification shown in panel E, data were represented as Mean ± SD). (F) Aurora kinase inhibitor treatment also induced classic senescence markers: Loss of phosphorylated-RB, upregulation of P53 and CDKN1A (p21cip1). Induction of γH2AX was also observed. VINC served as a loading control. (G) RNA sequencing was performed on these cells, and followed by GSEA analysis of tozasertib, barasertib or alisertib treated cells versus untreated control for the 'FRIDMAN_SENESCENCE_UP' geneset. (H) Aurora kinase inhibitors treatment also reduced proliferation in A549. (I,J) A549 cells were seeded in 96 well plate, treated with 0.5µM alisertib and incubated with caspase-3/7 green apoptosis assay reagent. Images were taken by incucyte at different time points. Green fluorescent staining indicated caspase-3/7 dependent apoptosis. Quantification shown in panel J. (K,L,M) The aurora kinase inhibitors-induced senescent A549 cells were seeded into 6 well plate and treated with ABT263. Parental A549 were used as a control. (K) Colony formation assay demonstrated that aurora inhibitors-induced senescent cells were selectively sensitive to ABT263 compared to proliferating cells. (L) Alisertib pre-treated cells stained strong positively with senescence-associated β-galactosidase activity, and these cells can be significantly depleted with ABT263 within 96 hours. The quantification of remaining cells and senescent cells is shown in panel M. Data were represented as Mean ± SD. (N,O) The aurora kinase inhibitors-induced senescent A549 cells were seeded into 96 well plate, treated with ABT263 and incubated with caspase-3/7 green apoptosis assay reagent. (N) Images were taken by incucyte at 48hrs. Green fluorescent staining indicated for caspase-3/7 dependent apoptosis. The quantification is shown in panel O. Data were represented as Mean ± SD. (P) The aurora kinase inhibitors-induced senescent A549 cells were seeded into 96 well plate with three biological replications and treated with different dose of ABT263 for 72hrs. Drug dose response was determined based on Cell Titer Blue measurement. Data were represented as Mean ± SD.

This may be explained by a rapid versus a slow onset of a senescence response following compound addition (Figure 4B, Table S3). Among the 47 top outliers are 18 independent aurora kinase inhibitors as strong inducers of the reporter construct (Figure 4C, Table S4). Indeed, treatment of A549 KRAS mutant lung cancer cells with aurora kinase inhibitors induced a marked senescence response, as judged by morphology and SA-β-gal expression (Figure 4D, E), induction of p21cip1 and hypo-phosphorylated RB (Figure 4F), enrichment of senescence-associated gene signature (Figure 4G, Table S2) and reduction of proliferation (Figure 4H). Notably, aurora kinase inhibition initially induced apoptosis. However, apoptosis rate was significantly reduced once the cells started to show the flat senescence-associated morphology (Figure 4I, J, S4H, I). Similar results were obtained in p53 null H358 KRAS mutant lung cancer cells (Figure S4A-F), indicating that aurora kinase inhibitor-induced senescence is p53-independent. Additionally, aurora kinase inhibitor alisertib also induced senescence in several other cancer models, including RAS mutant melanoma (SK-MEL-2), colorectal cancers (HCT116 and SW1463), a pancreatic cancer cell line (Panc1), a triple negative breast cancer (Cal51) and two liver cancer lines (Huh7 and Hep3B) (Figure S4 J, K). Moreover, when aurora kinase inhibitors were used to induce senescence in A549 or H358 lung cancer cells, they became sensitive to the senolytic agent ABT263 (Figure 4K-P, S4G). Similar results were obtained with etoposide (Figure S3F-I). ABT199, which inhibits only BCL2 and not BCL-XL, did not eliminate the senescent A549 cells (Figure S3J, K), indicating a critical role for BCL-like factors in killing senescent cancer cells (Souers et al., 2013). Together, these data indicate that both functional genetic screens and compound screens using miR146a reporter assays can identify targets and compounds that induce senescence in cancer cells.

Discussion

Drug resistance is the biggest obstacle to the effective treatment of cancer. When patients fail first line treatment, they are often offered second and even third line therapies in the hope to provoke a response with a drug that is mechanistically distinct from the first line therapy. In general, such subsequent therapies are less effective than first line therapy. To address these issues, we explore here the induction of senescence as a potential anti-cancer strategy. Although speculative, senescence-inducing therapies may help ameliorate drug resistance in two different ways. First, drug resistance is often the result of the selective outgrowth of a pre-existing sub-population of drug-resistant cells in the tumor. Senescence is known to induce a strong inflammatory response through the secreted SASP and such tumor-infiltrating inflammatory cells may help killing the subset of non-senescent cells through a bystander effect. In this context, it is interesting to note that treatment of BRAF mutant melanoma is almost invariably associated with resistance after 6-8 months, whereas CTLA-4 mediated immune cell activation for the same cancers leads to far longer-lasting effects (Flaherty et al., 2010; Schadendorf et al., 2015). A priori, there is no reason to believe that there are pre-existing variants conferring resistance to BRAF inhibitor treatment (explaining the rapid resistance development), but that mutations that confer resistance to CTLA-4 therapy are not pre-existent in the tumor. A possible explanation for this discrepancy is that immune infiltrates can kill sub-fractions of unresponsive tumor cells through a bystander effect. If correct, such bystander effect may also help prevent resistance to senescence-inducing therapies.

Induction of a senescence-like phenotype has been described as a side effect of a number of cancer drugs (Ewald et al., 2010). The difference with the approach used here is that through high throughput screens we aim to identify the most potent senescence inducing agents. Such strong pro-senescence agents may be more powerful than the therapy-induced senescence described in the literature. It will be important to address in future experiments, which fraction of a cancer cell population must be made senescent to eradicate the tumor completely. This will help elucidate to which extent a bystander effect is helping in clearing subsets of non-senescent cancer cells.

A second way in which senescence inducing cancer therapies could help in fighting drug resistance relates to the fact that second line therapies are often less effective than first line therapy. Senescent cells are very different from their proliferating counterparts in terms of gene expression, chromatin state and metabolism that killing them with selective agents should be feasible (Fridman and Tainsky, 2008; Narita et al., 2003; Wiley and Campisi, 2016). Indeed, a first generation of senolytic agents has been described to kill senescent cells, but such compounds were not tested extensively on senescent cancer cells to date. We show here that ABT263, but not the related ABT199, can kill a range of senescent cancer cells, independent of how senescence was induced. Based on our findings, we propose a "one-two punch" approach to the treatment of cancer. In the first treatment of the cancer, senescence is induced selectively in the cancer, which is exploited in a consecutive therapy that kills senescent cells. The attractive aspect of a sequential treatment strategy is that the second therapy takes advantage of a major vulnerability induced by the first therapy. For this reason, a second therapy could be very effective in this scenario. A further attractive thought, albeit highly speculative at present, is that senolytic agents have been shown to increase lifespan in mice due to the delay of age-related pathologies (Baar et al., 2017; Baker et al., 2016). Thus, a senolytic agent used in the treatment of cancer could contribute to patient rejuvenation, a significant departure from the side effects caused by current cancer therapies. How senescence-inducing and senolytic agents should be administered (sequential, overlapping, concurrent) will require extensive testing in immunocompetent animal models and may also depend on the nature of the SASP produced by the cancer cells.

We show here that large-scale functional genomic screens can be used to identify drug targets that would be useful in achieving a senescent state in cancer cells. There are a number of important questions that must still be addressed. Which are the most effective triggers to induce senescence in cancer cells? Are these senescence triggers similar or distinct in cancers originating from different tissues? Are there commonalities in the senescence triggers in relation to their genotype? Having high throughput screening systems in place to find these senescence triggers, we should be able to address these question in the near future.

References

Angelini, P.D., Zacarias Fluck, M.F., Pedersen, K., Parra-Palau, J.L., Guiu, M., Bernado Morales, C., Vicario, R., Luque-Garcia, A., Navalpotro, N.P., Giralt, J., et al. (2013). Constitutive HER2 signaling promotes breast cancer metastasis through cellular senescence. Cancer Res 73, 450-458.

Baar, M.P., Brandt, R.M.C., Putavet, D.A., Klein, J.D.D., Derks, K.W.J., Bourgeois, B.R.M., Stryeck, S., Rijksen, Y., van Willigenburg, H., Feijtel, D.A., et al. (2017). Targeted Apoptosis of Senescent Cells Restores Tissue Homeostasis in Response to Chemotoxicity and Aging. Cell 169, 132-147.e116.

Baker, D.J., Childs, B.G., Durik, M., Wijers, M.E., Sieben, C.J., Zhong, J., A. Saltness, R., Jeganathan, K.B., Verzosa, G.C., Pezeshki, A., et al. (2016). Naturally occurring p16Ink4a-positive cells shorten healthy lifespan. Nature 530, 184-189.

Chang, J., Wang, Y., Shao, L., Laberge, R.M., Demaria, M., Campisi, J., Janakiraman, K., Sharpless, N.E., Ding, S., Feng, W., et al. (2016). Clearance of senescent cells by ABT263 rejuvenates aged hematopoietic stem cells in mice. Nature medicine 22, 78-83.

Coppe, J.P., Desprez, P.Y., Krtolica, A., and Campisi, J. (2010). The senescence-associated secretory phenotype: the dark side of tumor suppression. Annu Rev Pathol 5, 99-118.

Coppe, J.P., Patil, C.K., Rodier, F., Sun, Y., Munoz, D.P., Goldstein, J., Nelson, P.S., Desprez, P.Y., and Campisi, J. (2008). Senescence-associated secretory phenotypes reveal cell-nonautonomous functions of oncogenic RAS and the p53 tumor suppressor. PLoS Biol 6, 2853-2868.

Demaria, M., O'Leary, M.N., Chang, J., Shao, L., Liu, S., Alimirah, F., Koenig, K., Le, C., Mitin, N., Deal, A.M., et al. (2017). Cellular Senescence Promotes Adverse Effects of Chemotherapy and Cancer Relapse. Cancer Discov 7, 165-176.

Eggert, T., Wolter, K., Ji, J., Ma, C., Yevsa, T., Klotz, S., Medina-Echeverz, J., Longerich, T., Forgues, M., Reisinger, F., et al. (2016). Distinct Functions of Senescence-Associated Immune Responses in Liver Tumor Surveillance and Tumor Progression. Cancer Cell 30, 533-547.

Evers, B., Jastrzebski, K., Heijmans, J.P., Grernrum, W., Beijersbergen, R.L., and Bernards, R. (2016). CRISPR knockout screening outperforms shRNA and CRISPRi in identifying essential genes. Nat Biotechnol 34, 631-633.

Ewald, J.A., Desotelle, J.A., Wilding, G., and Jarrard, D.F. (2010). Therapy-induced senescence in cancer. J Natl Cancer Inst 102, 1536-1546.

Flaherty, K.T., Puzanov, I., Kim, K.B., Ribas, A., McArthur, G.A., Sosman, J.A., O'Dwyer, P.J., Lee, R.J., Grippo, J.F., Nolop, K., et al. (2010). Inhibition of mutated, activated BRAF in metastatic melanoma. N Engl J Med 363, 809-819.

Fridman, A.L., and Tainsky, M.A. (2008). Critical pathways in cellular senescence and immortalization revealed by gene expression profiling. Oncogene 27, 5975-5987.

Hayflick, L. (1965). The limited in vitro lifetime of human diploid cell strains. Exp Cell Res 37, 614-636.

Hoare, M., Ito, Y., Kang, T.-W., Weekes, M.P., Matheson, N.J., Patten, D.A., Shetty, S., Parry, A.J., Menon, S., Salama, R., et al. (2016). NOTCH1 mediates a switch between two distinct secretomes during senescence. Nat Cell Biol 18, 979-992.

Hodges, C., Kirkland, J.G., and Crabtree, G.R. (2016). The Many Roles of BAF (mSWI/SNF) and PBAF Complexes in Cancer. Cold Spring Harb Perspect Med 6.

Jiang, P., Du, W., Mancuso, A., Wellen, K.E., and Yang, X. (2013). Reciprocal regulation of p53 and malic enzymes modulates metabolism and senescence. Nature 493, 689-693.

Kang, C., Xu, Q., Martin, T.D., Li, M.Z., Demaria, M., Aron, L., Lu, T., Yankner, B.A., Campisi, J., and Elledge, S.J. (2015). The DNA damage response induces inflammation and senescence by inhibiting autophagy of GATA4. Science 349, aaa5612.

Kuilman, T., Michaloglou, C., Vredeveld, L.C., Douma, S., van Doorn, R., Desmet, C.J., Aarden, L.A., Mooi, W.J., and Peeper, D.S. (2008). Oncogene-induced senescence relayed by an interleukin-dependent inflammatory network. Cell 133, 1019-1031.

Michaloglou, C., Vredeveld, L.C., Soengas, M.S., Denoyelle, C., Kuilman, T., van der Horst, C.M., Majoor, D.M., Shay, J.W., Mooi, W.J., and Peeper, D.S. (2005). BRAFE600-associated senescence-like cell cycle arrest of human naevi. Nature 436, 720-724.

Munoz-Espin, D., and Serrano, M. (2014). Cellular senescence: from physiology to pathology. Nat Rev Mol Cell Biol 15, 482-496.

Narita, M., Nunez, S., Heard, E., Lin, A.W., Hearn, S.A., Spector, D.L., Hannon, G.J., and Lowe, S.W. (2003). Rb-mediated heterochromatin formation and silencing of E2F target genes during cellular senescence. Cell 113, 703-716.

Schadendorf, D., Hodi, F.S., Robert, C., Weber, J.S., Margolin, K., Hamid, O., Patt, D., Chen, T.T., Berman, D.M., and Wolchok, J.D. (2015). Pooled Analysis of Long-Term Survival Data From Phase II and Phase III Trials of Ipilimumab in Unresectable or Metastatic Melanoma. J Clin Oncol 33, 1889-1894.

Serrano, M., Lin, A.W., McCurrach, M.E., Beach, D., and Lowe, S.W. (1997). Oncogenic ras provokes premature cell senescence associated with accumulation of p53 and p16INK4a. Cell 88, 593-602.

Souers, A.J., Leverson, J.D., Boghaert, E.R., Ackler, S.L., Catron, N.D., Chen, J., Dayton, B.D., Ding, H., Enschede, S.H., Fairbrother, W.J., et al. (2013). ABT-199, a potent and selective BCL-2 inhibitor, achieves antitumor activity while sparing platelets. Nature medicine 19, 202-208.

Sun, C., Wang, L., Huang, S., Heynen, G.J.J.E., Prahallad, A., Robert, C., Haanen, J., Blank, C., Wesseling, J., Willems, S.M., et al. (2014). Reversible and adaptive resistance to BRAF(V600E) inhibition in melanoma. Nature 508, 118-122.

Wiley, C.D., and Campisi, J. (2016). From Ancient Pathways to Aging Cells-Connecting Metabolism and Cellular Senescence. Cell Metab 23, 1013-1021.

Zhu, Y., Tchkonia, T., Fuhrmann-Stroissnigg, H., Dai, H.M., Ling, Y.Y., Stout, M.B., Pirtskhalava, T., Giorgadze, N., Johnson, K.O., Giles, C.B., et al. (2016). Identification of a novel senolytic agent, navitoclax, targeting the Bcl-2 family of anti-apoptotic factors. Aging Cell 15, 428-435.

Materials and methods

METHOD DETAILS

Cell lines

The A375, SK-Mel-2 melanoma cell lines, H358 and A549 lung cancer cell lines, HCT116, SW1463 colon cancer cell lines and Panc1 pancreatic cancer cell line were obtained from ATCC. Mel888, Mel624 and Mel526 cells were gifts from D. Peeper (Amsterdam, The Netherlands). Cal51 breast cancer line was obtained from K. Jastrzebski (NKI, Amsterdam, The Netherlands). Huh7 and Hep3B liver cancer cell lines were obtained from S. Huang (NKI, Amsterdam, The Netherlands). A375, Mel888, Mel624, Mel526, Huh7, Hep3B, SK-Mel-2 were cultured in a DMEM-based medium supplemented with 10% FBS, 1% penicillin/streptomycin and 2 mM L-glutamine. Cal51 were cultured in a DMEM-based medium supplemented with 20% FBS, 1% penicillin/streptomycin and 2 mM L-glutamine. HCT116, SK1463, Panc1, A549 and H358 were cultured in a RPMI-based medium supplemented with 10% FBS, 1% penicillin/streptomycin and 2 mM L-glutamine. All the cell lines have been validated by STR profiling and regularly tested for Mycoplasma spp with PCR-based assay.

FACS-assisted genetic screen with a customized CRISPR epigenetic library

Lentiviral CRISPR V2.1 (LC2.1) encoding gRNAs that target epigenetic genes are listed in Table S1. Lentiviral supernatants of the plasmids were produced as described at http://www.broadinstitute.org/rnai/public/resources/protocols.

A375-miR146-GFP cells were infected with 3 independent biological replicates. Cells were then seeded at 350.000 cells per 15cm dish and the medium was refreshed every 3 days for 8 days. Non-infected A375-miR146-GFP cells were taken as the control. Then, the cells were collected and suspended in D-MEN medium containing 2% FCS. BD FACSAria™ III (BD Bioscience) was used to sort out GFP positive cells. The FACS data was analyzed by FlowJo program version 7.6.5 (Tree Star). The genomic DNA was isolated from GFP- and GFP+ cells using DNasy® Blood and Tissue Kit (#69506 Qiagen). gRNA inserts were recovered from DNA following by the experimental steps of PCR amplification (PCR1 and PCR2) PCR product purification was performed using High Pure PCR Product Purification Kit according to manufactures' instruction (#11732676001, Roche). Screen result analysis details is described in Evers et al. 2016.

PCR, next-generation sequencing and data analysis.

Each sample is divided over PCR reactions containing 500 ng DNA, with a maximum of 20 µg DNA to cover the complexity. Barcoded PCR primers were used for the first PCR reaction. Each PCR reaction consisted of 500 ng DNA, 10 µl GC buffer (5x), 1 µl forward primer (10µM), 1 µl reverse primer (10µM), 1 µl dNTPs (10mM), 1.5 µl DMSO, 0.5 µl polymerase in a total volume of 50 µl. PCR program consisted of initial denaturation at 98°C for 2 min;

16 cycles of 30 s denaturation at 98°C, 30 s of annealing at 60°C, and 30 s elongation at 72°C; with a final extension at 72°C for 5 min. PCR products of each sample were pooled, and 2.5 µl was used for a second PCR reaction, in technical duplicates. Primers in this reaction contained barcodes and an adapter sequence for next-generation sequencing. PCR mixtures and program were the same as for the first PCR. PCR products of the second PCR were purified with a DNA purification kit (28-9034-70; GE Healthcare,). Sample concentrations were measured with BioAnalyzer and were pooled equimolarly. Inserted gRNA sequences were identified by Illumina HiSeq 2500 genome analyzer at the Genomics Core Facility (NKI). The mapped read counts were normalized using DESeq2, and used as input for the alpha Robust Rank Algorithm of MAGeCK software version 0.5.

Drug screen with compound libraries

Using the Multidrop Combi (Thermo Scientific), 200 A549 cells expressing miR-146a-Gaussia-Dura-luciferase were seeded in 60 µl into 384-well plates. After 24h, the combined compound libraries of inhibitor including G-protein-coupled receptors, kinome, epigenetic modifying enzymes and NCI approved oncology drug set were added. This library was stored and handled as recommended by the manufacturer. Compounds from the master plate were diluted in daughter plates containing complete RMPI medium, using the MICROLAB STAR liquid handling workstation (Hamilton). From the daughter plates, 15 µl of the diluted compounds was transferred into 384-well assay plates, in triplicate, with final concentrations of 0.2µM, 1µM and 5µM. After seven days, the protein levels of Gaussia-Dura luciferase were determined by a luciferase assay as described in Degeling et al. (2013). Five minutes before measurement, 10 µl coelenterazine diluted to 5 µg/ml was added. The luminescence signal was measured with the Envision Multilabel Plate Reader (PerkinElmer) at 400-700 nm. After this, a CellTiter-Blue assay was performed (G8081/2; Promega), as recommended by the manufacturer. Both the fluorescent and CTB data were normalized per plate using the normalized percentage inhibition (NPI) method. NPI sets the mean of the positive control value to 0 and mean of the neg. control to 1. Per compound and concentration, the mean was determined over the three replicates for both the CellTiterBlue readout and for the Luciferase readout. A null distribution of the negative controls was created, and the mean value of the biological replicates was tested for significance. Etoposide was considered as a positive control in the screen.

CRISPR eipgenome library generation

For the design of the CRISPR library, 5130 gRNAs were selected targeting 446 genes involved in epigenetic processes. gRNAs were designed such that when possible, 10 gRNAs target each transcript associated with the gene in the first 50% of the ORF. Further selection involved maximizing sequence divergence from potential off-target sites and optimizing the library size by choosing gRNAs that were shared between transcripts targeting the same gene. In addition, 50 gRNAs targeting 10 essential genes and 50 non-targeting gRNAs were added to the design. Oligo's with gRNA sequences flanked by adapters were ordered from CustomArray Inc (Bothell, WA) and cloned as a pool by GIBSON assembly in LentiCRISPRv2.1 (Evers et al., 2016).

qRT-PCR

Total RNA was extracted from cells using TRIzol reagent from Invitrogen or Quick-RNA™ MiniPrep (# R1055) from Zymo Research. cDNA synthesis was performed using Maxima Universal First Strand cDNA Synthesis Kit (#K1661) from Thermo scientific. qPCR reactions were performed with FastStart Universal SYBR Green Master (Rox) from Roche. The experiments were performed according to the manufacturer's instructions. The sequences of the primers used for qRT–PCR analyses are described in STAR Methods. All reactions were run in triplicate. The CT values were calculated using the Standard Curve Method.

CRISPR gRNA generation

Oligonucleotides containing gRNA sequences (STAR method table) flanked by 20-30 nt of overlapping backbone sequence were obtained from ThermoFisher scientific Guide RNA (gRNA) sequences were cloned into LentiCRISPRv2.1 via BsmBI sites, using Gateway cloning strategy.

Lentiviral transduction

A third-generation lentivirus packaging system consisting of pCMV-VSV-G (addgene#8454), pRSV-Rev (Addgene#12253) and pMDLg/pRRE (Addgene#12251) was used to create virus particles of the modified reporter plasmids. A transient transfection was performed in 293T cells and lentiviral supernatants were produced. Destination cells were infected with lentiviral supernatants, using 8μg/ml Polybrene and low virus titer. After 48h of incubation, the supernatant was replaced by medium containing 10 μg/ml BSD or 2 μg/ml Puromycin. After 48h, selection of viral transduced cell lines was completed.

Long-term Cell Proliferation Assays

Cells were seeded into 6-well plates and cultured both in the absence and presence of drugs as indicated. Afterwards the cells were cultured for indicated time (in figure legend). At the end of assay, the cells were fixed with 4% PFA, stained with crystal violet and photographed.

Staining for β-galactosidase activity

β-galactosidase activity in cells was detected using Histochemical Staining Kit (CS0030-1KT) from Sigma-Aldrich. β-galactosidase detection was carried out according to the manufacturer's instructions. SA-beta-gal staining positive cells were quantified based on 3 independent images from different regions of the stainings.

IncuCyte® Caspase-3/7 Greeen apoptosis assay

Cells were seeded in 96 well-plate. After 24 hours, IncuCyte® Caspase-3/7 Green Apoptosis Assay Reagent (#4440) from Essen Bioscience was added with 1000 times dilution to each well. Experiments were performed with 3 independent biological triplicates. The pictures were taken using incucyte. Caspase-3/7 activated cells were quantified based on 3 images generated from independent biological replicates.

Protein lysate preparation and Immunoblots

Cells lysates were collected followed by washing with PBS and lysing with RIPA buffer supplemented with protease inhibitor (cOmplete, Roche) and Phosphatase Inhibitor Cocktails II and III (Sigma). All lysates were freshly prepared and processed with Novex® NuPAGE® Gel Electrophoresis Systems (Invitrogen).

Flow-cytometry

Cells were harvested and suspended in 300 µl medium. GFP positivity was determined with excitation at 486 nm, at the CyAn ADP flow cytometer (DakoCytomation). The mean value of mGFP fluorescent signal was determined with FlowJo version 7.6.5. Graphpad prism version 7.0 was used for data analysis.

STATISTICAL ANALYSIS

Throughout all figures: *p≤0.05, **p≤0.01, and ***p≤0.001 and N.S (Not significant) p>0.05. Statistical t-test analyses were performed using Microsoft Excel or PRISM.

ACCESSION CODES

Raw and processed data from the next generation RNA sequencing to profile senescence gene signature upon SMARCB1-knockout on A375, Etoposide, Tozasertib, Barasertib, Alisertib treated A549 have been deposited to NCBI Gene Expression Omnibus (GEO) under accession number GSE102639.

SUPPLEMENTAL INFORMATION

Supplemental Information includes 4 figures, 4 tables and Supplemental Experimental Procedures and can be found with this article online at http://www.cell.com/action/showMethods?pii=S2211-1247%2817%2931390-6

ACKNOWLEDGEMENTS

We thank Stephen Elledge for the kind gift of the miR-146a-eGFP vector. This work was funded by a grant from the Dutch Cancer Society (KWF) and the Center for Cancer Genomics (CGC). The authors report no conflict of interest.

Supplemental Figures

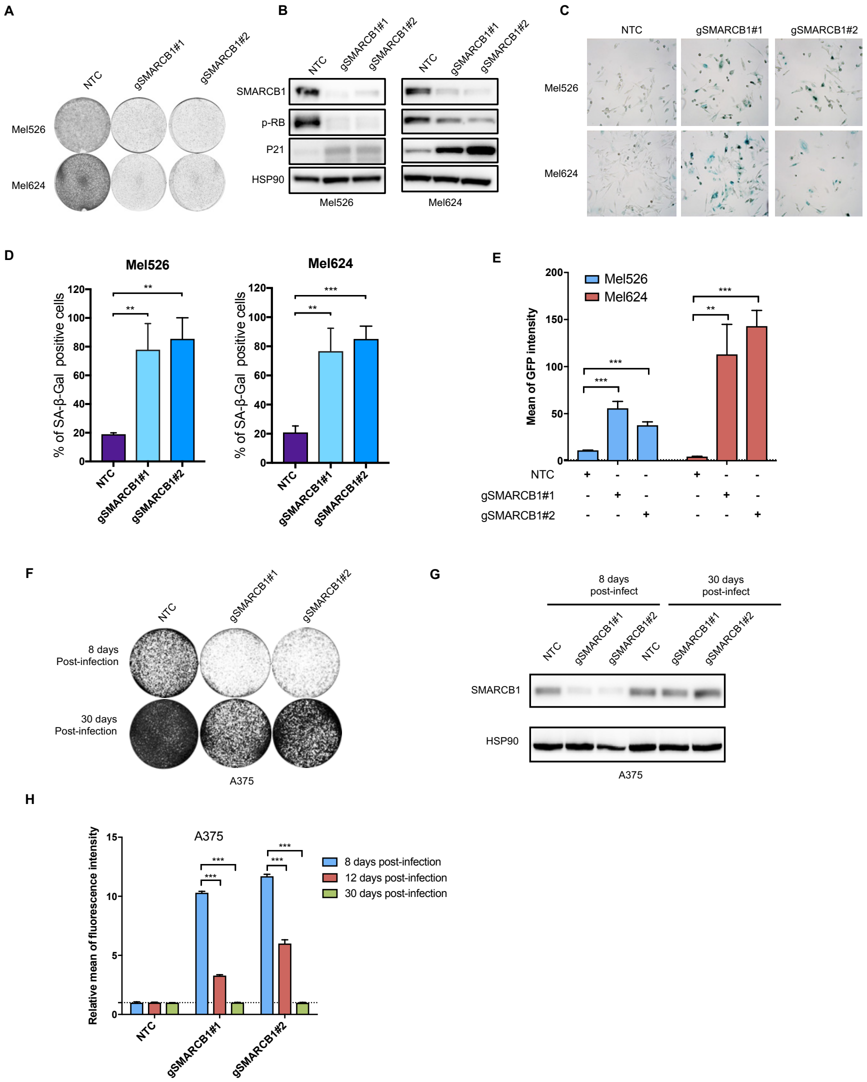

Figure S1: Effects of SMARCB1 depletion on melanoma cells. Related to Figure 2.

(A,B,C,D,E) Mel526 and Mel624 cells expressing the miR146a-eGFP reporter were infected with two independent *SMARCB1* gRNAs-CAS9 (gSMARCB1) viruses and cultured for 10 days. (A) Depletion of *SMARCB1* reduced cell proliferation, upregulated classic senescence markers: (B) Loss of p-RB, induction of CDKN1A (p21cip1), (C) senescence-associated β-galactosidase activity (quantification shown in panel D) and activated miR146-eGFP senescence reporter (E) in Mel526 and Mel624. Non-targeted gRNA vector served as a control. (F,G,H) A375 cells expressing the miR146a-eGFP reporter infected with gRNAs-CAS9 targeting SMARCB1. Non-targeted gRNA vector (NTC) served as a control. (F) The infected cells were cultured, fixed and stained after 8 and 30-day post-infection. (G) The SMARCB1 expression after 8 and 30-day post-infection with gRNAs-CAS9 targeting *SMARCB1* were measured by western blot. HSP90 served as a loading control. (H) Relative GFP fluorescence was examined by flow cytometry at the indicated time point after the viral infection.

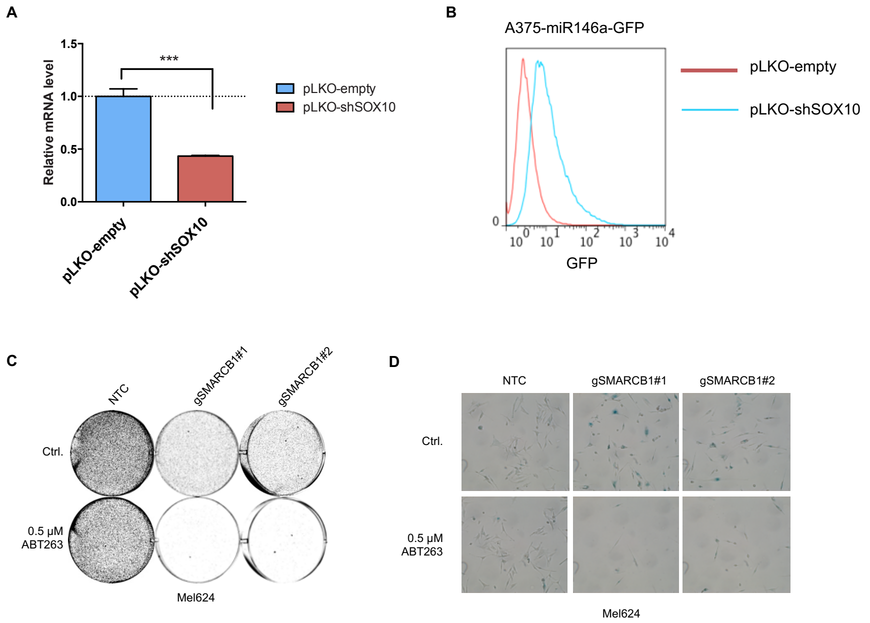

Figure S2. Effects of SOX10 suppression and ABT263 on melanoma cells. Related to Figure 3.
(A) Real-time PCR was used to quantify the relative mRNA levels of *SOX10* upon shSOX10 viral infection in A375. (B) A375 cells expressing the miR146a-GFP reporter and infected with shSOX10 virus showed induction of the GFP signal. (C,D) Mel624 cells were infected with SMARCB1 gRNAs-CAS9 virus. After 8 days post-infection, the cells were seeded into 6-well plate and treated with 0.5 μM ABT263. (C) Colony formation assay showed that ABT263 selectively depleted cells with *SMARCB1* gRNAs-CAS9. (D) Cells with increased senescence-associated β-galactosidase activity are vulnerable to ABT263.

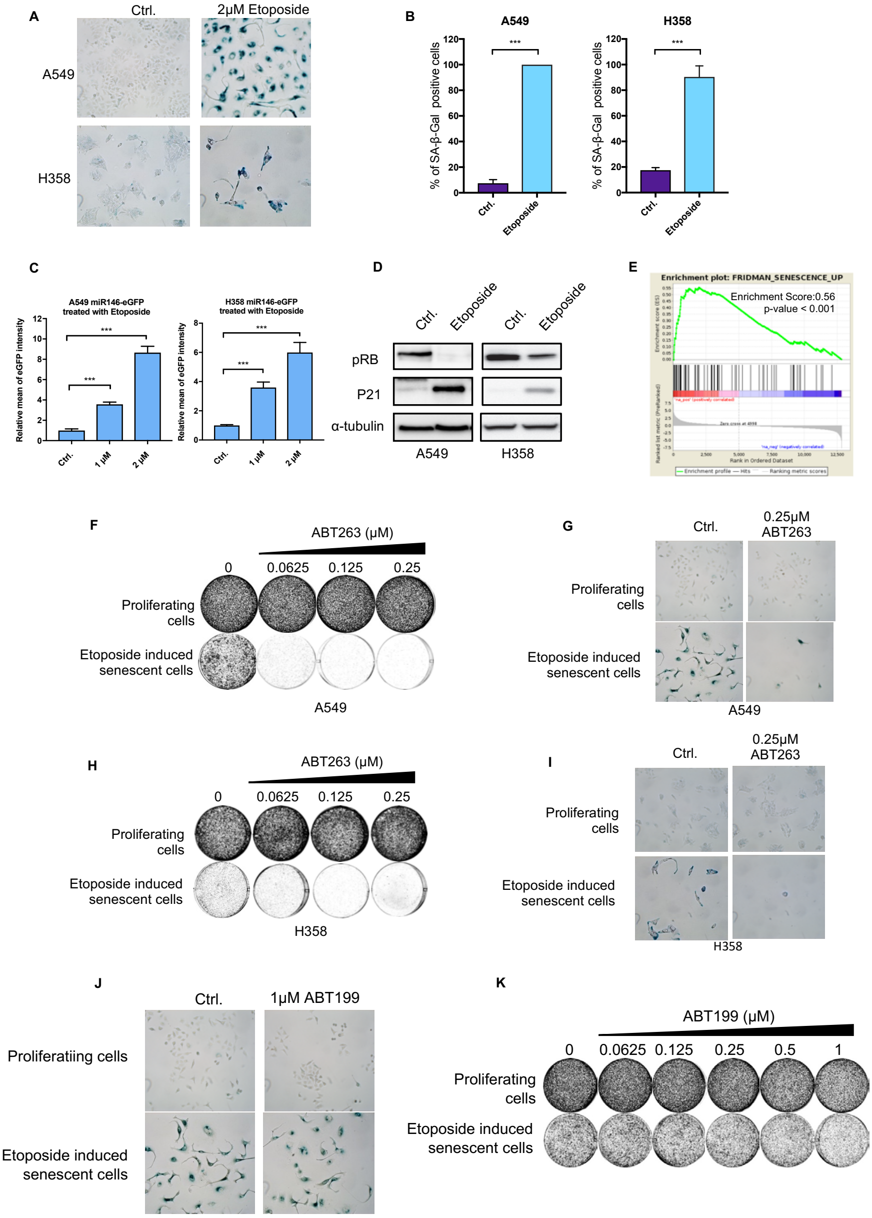

Figure S3. Etoposide can be used as an efficient senescence inducer. Related to Figure 4.

(A,B,C,D) A549 and H358 cells expressing the miR-146-eGFP reporter were treated with 2µM etoposide for 7 days. (A,B) Etoposide treatment induced senescence-associated β-galactosidase activity (quantification shown in panel B), (C) activated reporter and increased GFP fluorescence signal measured by flow cytometry. (D) Etoposide treatment induces classic senescence markers: Loss of phosphorylated-RB and induction of P53 and CDKN1A (p21cip1). (E) RNA sequencing was performed on etoposide treated cells, and followed by GSEA analysis of etoposide treated cells versus untreated control for the 'FRIDMAN_SENESCENCE_UP' geneset. (F, G) The etoposide-induced senescent A549 cells were seeded into 6 well plates and treated with ABT263. Parental A549 were used as a control. (F) Colony formation assay demonstrated that etoposide-induced senescent cells were selectively sensitive to ABT263 compared to proliferating cells. (G) Etoposide pre-treated cells stained strong positively with senescence-associated β-galactosidase activity, and these cells can be significantly depleted with ABT263 within 96 hours. (H, I) The etoposide-induced senescent H358 cells were seeded into 6 well plate and treated with ABT263. Parental H358 were used as a control. (H) Colony formation assay demonstrated that etoposide-induced senescent cells were selectively sensitive to ABT263 compared to proliferating cells. (I) Etoposide pre-treated cells stained strong positively with senescence-associated β-galactosidase activity, and these cells can be significantly depleted with ABT263 in 96 hours. (J, K) The etoposide-induced senescent A549 cells were seeded into 6 well plate and treated with ABT199. Parental A549 were used as a control. (J) Etoposide pre-treated cells were stained for senescence-associated β-galactosidase activity, and these cells were not sensitive to ABT199. (K) Colony formation assay demonstrated that etoposide-induced senescent cells were not responsive to ABT199 compared to proliferated cells.

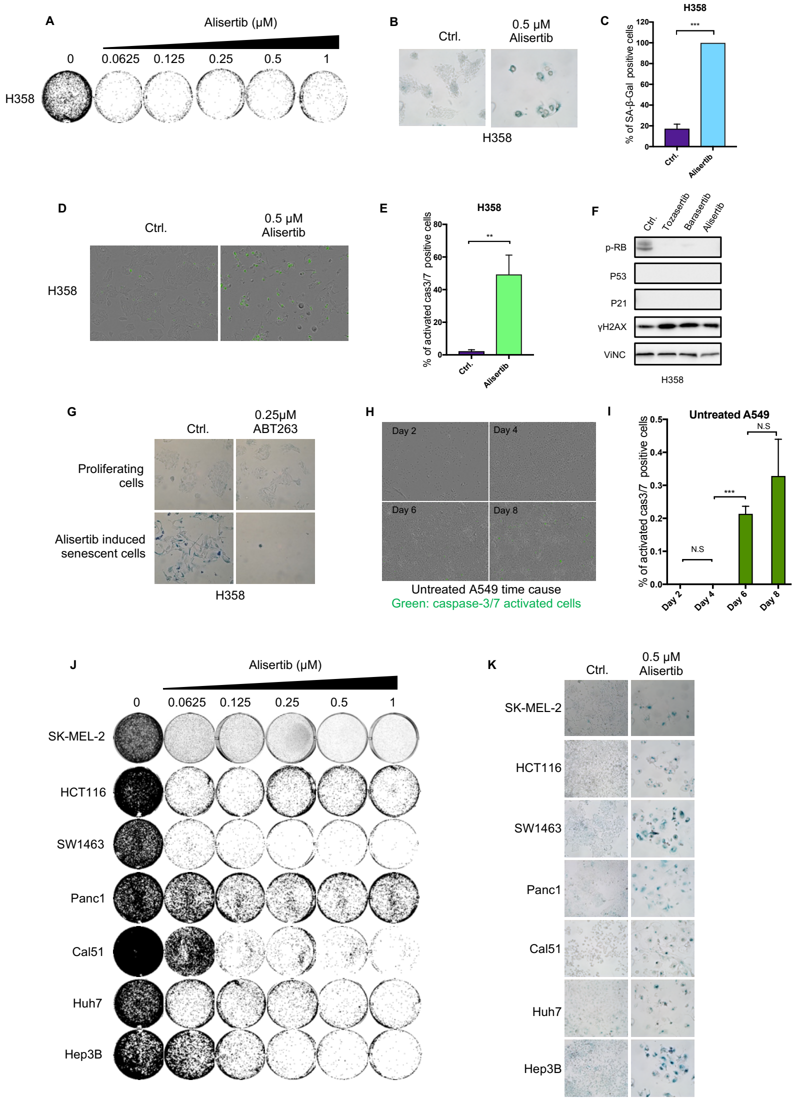

Figure S4. Alisertib induces senescence in additional cancer models. Related to Figure 4.
(A) Colony formation assay using H358 cells in the presence of alisertib demonstrating that treatment of alisertib reduces cell proliferation. (B,C) H358 cells were treated with 0.5μM alisertib for 7 days and stained for senescence-associated β-galactosidase activity (quantification shown in panel C). (D, E) Alisertib treatment also induced apoptosis in H358 at day 6. The quantification is shown in panel E. Data were represented as Mean ± SD. (F) Three independent aurora kinase inhibitors treatments induced classic senescence markers in H358: Loss of phosphorylated-RB, upregulation of P53 and CDKN1A (p21cip1). Induction of γH2AX was also observed. VINC served as a loading control. (G) The Alisertib-induced senescent H358 cells were seeded into 6 well plate and treated with ABT263. Parental H358 were used as a control. Alisertib pre-treated H358 cells were stained for senescence-associated β-galactosidase activity, and these cells can be significantly depleted with ABT263 in 96 hours. (H, I) The control for experiment in Figure 4H, A549 cells were seeded in 96 well plate and incubated with caspase-3/7 green apoptosis assay reagent. Images were taken by Incucyte at different time points. Green fluorescent staining indicated caspase-3/7 dependent apoptosis. The quantification was shown in panel I. Data were represented as Mean ± SD. (J, K) Various cancer models were treated with alisertib for 7 days. (J) Alisertib treatment reduced cell proliferations. (K) 0.5μM of alisertib induced senescence-associated β-galactosidase activity in these cancer cell lines.

General discussion

6

Discoveries during the last decade have identified recurrent “driver" mutations in some types of cancer. The cancer cells that harbor these genetic alterations, often exhibit dependence on the activated oncogenic pathway or protein for its sustained proliferation and survival. The mechanistic rationale of targeted approaches is to destroy the tumor by blocking aberrant cell signaling to which the cancer cell is addicted, but dispensable for healthy tissues. The targeted drugs have been designed to effectively target the oncogenic proteins in the major signaling pathways. These drugs have been a clinical success, and often significantly improve the quality of life of individuals with cancer. Unfortunately, the initial clinical responses to targeted drugs are almost always temporary and increase progression-free survival, but this improvement does not necessarily translate into a meaningful overall survival, as acquired resistance to these drugs almost invariably develops. In the previous chapters of this thesis, I have shown several treatment strategies to overcome drug resistance, such as how we can use rational drug combinations to prevent drug resistance (Chapter 2), how we can take advantage of the new vulnerabilities that have arisen in drug-resistant cancer cells (Chapters 3 and 4), and a new therapeutic strategy, how we can drive cancer cells into senescence, and then eradicate them with a senolytic drug (Chapter 5). These treatment strategies open many opportunities to treat cancer, but there are still several issues that remain to be solved. In this chapter, I discuss these potential issues around these strategies and how to solve them in order to improve these treatment concepts.

In chapter 2 of this thesis, I described how we have applied a functional genetic screen to identify several PI3K-AKT signaling pathway genes that, upon loss, would sensitize *FGFR*-mutant bladder and lung cancer cells to FGFR inhibitors. We have shown that combining FGFR and PI3K inhibitors can synergistically kill a majority of *FGFR*-mutant bladder and lung cancer cell models. However, we also found out that several *FGFR*-mutant bladder and lung cancer models either had limited or no responsiveness to the drug combination. We found that these cell line models also harbored downstream mutations in *AKT1*, which allow the cells ignore the upstream signaling blockades through constitutive activation of downstream signaling and theraby maintain proliferative capacity in the presence of the FGFR and PI3K inhibitors (Wang et al., 2017). As another example, the the BEACON phase 3 trial in *BRAF*-mutant colon cancer the combination of BRAF and EGFR inhibitors is currently being validated. Initial results show a dramatic increase in median progression-free survival in this patient group when the two drugs are combined. However, as with all cancer therapies, resistance developed over time in the majority of patients. To investigate the resistance mechanism in these patients, biopsies have been taken and sequenced, which resulted in the identification of an additional KRAS mutation in some of these patients. These KRAS mutations can further activate the MAPK signaling and thereby limit the efficacy of the drug combination (Oddo et al., 2016; van Geel et al., 2017). Apparently, cancer cells can be creative in developing resistance, even against drug combinations. The robustness of the adaptive abilities of the cancer cells is a “Déjà Vu” experience, as similar escape from combination therapies is seen with chemotherapies.

As we have learned the hard way, cancer can always find one way or another to adapt to the stress imposed by the cancer drugs to survive. If cancer drug-resistance development is unavoidable, why do not take advantage of the drug-resistance of cancer cells? In chapter 4 we study whether melanoma cells that have developed resistance to BRAF and MEK inhibitors acquire novel vulnerabilities that can be exploited therapeutically. We find that elevated ROS levels can serve as a vulnerability of *BRAF*-mutant melanomas that is specifically acquired upon the development of resistance to inhibitors of the MAPK pathway. Consequently, further activation of these increased ROS levels by HDAC inhibitor leads to significant DNA damage and apoptotic cell death only in the MAPKi-resistant cells, but not in the drug-sensitive cells that have lower ROS levels. In our proof-of-concept study in patients with advanced BRAF-mutant melanoma that progressed on MAPK inhibitors therapy, we see that MAPKi-resistant cells in the tumor can be quickly depleted by HDAC inhibitor treatment. In patients, tumors initially stabilize upon switch to HDAC inhibitor, but then progression occurs. This is not unexpected, given that parental, MAPK inhibitor sensitive, tumor cells fail to respond to HDAC inhibition. After initial depletion of the drug-resistant clones in the tumor by HDAC inhibitor, the MAPK inhibitor sensitive cells continue to proliferate, leading to progression.

We have to keep in mind that clonal dynamics in the tumor is not always easily manipulated by treatment interruption. This raises a number of questions: when will be a good time to switch treatment from MAPK inhibitors to HDAC inhibitor? Is there a method to detect mutations that confer drug-resistance? This method must be accurate and allow repeat sampling, in order to guide the timing of alternating between MAPK inhibitors and HDAC inhibitors. Russo and colleagues shown that sequencing of circulating tumor DNA (ctDNA) of a colon cancer patient treated with cetuximab can identify the emergence of a $MEK1^{K57T}$ mutation. In this patient, combined treatment with trametinib and EGFR therapy subsequently led to tumor regression. However, in the ctDNA, the mutant MEK1 levels declined with treatment, but an additional $KRAS^{Q61H}$ mutation emerged and resulted in drug-resistance to the combination treatment (Russo et al., 2016). This study shows the feasibility to monitor through liquid biopsy followed by sequencing of ctDNA the emergence of drug-resistance at an early stage. Thus, ctDNA, may be a good tool to time the switch in therapies to better control the drug-resistant clones in a tumor. In our MAPKi-HDACi alternating treatment, we plan to adapt the the ongoing trial NCT02836548 to include liquid biopsy for the detection of mutations, which cause MAPKi-resistance (such as, *KRAS* mutations). During the HDAC inhibitor treatment, liquid biopsy can be used to monitor the decline of the resistance mutation. Once the resistance mutation has declined significantly, suggesting that MAPKi-resistant cells are depleted in the tumor, the switch back to MAPK inhibition therapy can be made. By pulsatile treatment with HDAC inhibitor to eradicate emergent drug-resistant cells, followed by a switch back to MAPK inhibition, we expect to get longer progression-free survival benefit for patients as compared to an intermittent dosage with BRAF inhibitor or BRAF+MEK inhibitor (Das Thakur et al., 2013), and may possibly improve the outcome of patients compared to the ongoing intermittent dosage trials (NCT01894672, NCT02263898 and NCT02196181) (Luke et al., 2017).

Besides optimization in the monitoring of how the tumors respond to the therapy, we could also consider improving the effectivenenss of the therapy. For example, vorinostat can be combined with other drugs to eliminate the MAPKi-resistant melanoma cells more efficiently. A number of recent studies also discovered that cancer cells that become tolerant to a variety of cancer drugs adopt a mesenchymal cell state, which is associated with higher ROS levels compared to their parental drug-sensitive cells. These resistant cells are highly dependent on the lipid hydro-peroxidase GPX4 to tolerate the high ROS level to survive. This specific dependency could be explored as a selective vulnerability of the drug-resistant cells. Indeed, these drug-resistant cells were shown to be highly vulnerable to a GPX4 inhibitor, which caused a massive ROS induction leading to a non-apoptotic cell death called ferroptosis (Hangauer et al., 2017; Viswanathan et al., 2017). Our study with HDAC inhibitor shares the same concept with these studies. However, the molecular mechanism of HDAC inhibitor is to suppress the expression of *SLC7A11* that leads to less cellular uptake of the precursor of antioxidant glutathione. The GPX4 inhibitor serves to block the activity of GPX4 that reduces the redox efficiency of glutathione from the oxidized state to the reduced state. Since our common goal is to elevate ROS levels to eliminate the drug-resistant cells, we could consider to combining both drugs, as this might potentially achieve a better efficiency to eliminate the drug-resistant cells even at lower doses of both drugs.

Having established that drug-resistant cancer cells do develop novel vulnerabilities, we studied whether such a "one-two" punch treatment strategy could be applied more widely to treat cancer. The reason to choose senescence-inducing therapy as the first punch is because senescent cells no longer divide and thereby represents a first step in tumor control. In addition, senescence is known to induce a strong inflammatory response through the secreted "Senescence Associated Sectretory Phenotype (SASP), which leads to recruitment of a range of tumor-infiltrating inflammatory cells. Such cells may kill senescent cancer cells and help to kill the subset of non-senescent tumor cells through a bystander effect. Among the cells that participate in the clearance of senescent cells are natural killer cells, macrophages, and T cells (Kang et al., 2011; Krizhanovsky et al., 2008; Tchkonia et al., 2013). The cytokines of the SASP that are responsible for these immune responses are incompletely understood but are very likely numerous (Chien et al., 2011). This also represents an opportunity to combine senescence-inducing therapy with immunotherapy, such as immune-checkpoint blockade, T cells-based or NK cells-based immunotherapies. Thus, senescent cells, in part by virtue of the SASP, appear to be programmed to mobilize the immune system to ensure their eventual elimination. However, the effects of senescent cells within the tumor microenvironment are complex and highly dependent on physiological context. Instead of recruiting immune cells to fight tumor cells, senescent cells can contribute to stimulating the infiltration of leukocytes (Freund et al., 2010; Kang et al., 2011), which produce reactive toxic moieties that can cause DNA damage, which in turn can fuel malignant phenotypes and tumor growth. Some studies also suggested that some SASP factors, particularly those secreted by cells that senesce in response to DNA-damaging radiation, chemotherapeutic or other senescence-inducing agents, can not only contribute to side effects, but also protect neighboring tumor cells from being killed by those same chemotherapeutic agents (Demaria et al., 2017; Gilbert and Hemann, 2010; Sun et al., 2012). Due to these reasons, it may be particularly important to consider adjuvant therapies aimed at eliminating senescent cells to preclude negative effects on non-senescent cells. Such therapies could enhance tumor shrinkage by senescence-inducing therapies though preventing the development of senescence-associated side effects. By adding senolytic drugs as the second therapy, perhaps we could also inhibit cancer recurrence by preventing senescent cells from stimulating the proliferation of any residual cancer cells.

As discussed previously, tumor heterogeneity can lead to heterogeneous drug responses. Tumor heterogeneity can also limit the effectiveness of senescence-inducing therapy within atumor. The senolytic drug aims to eradicate the senescent cells. If the first treatment does not induce senescence, the senolytic will not work either. Therefore, there is an unmet need to develop a method to track the accumulation of senescent cells within the tumor in order to assess the efficiency of the senescence-inducing drug and the potential timing for adding the senolytic drug. It has been demonstrated that one of the most widely used markers of senescent cells, senescence-associated beta-galactosidase can be detected with a 18F-labeled tracer (Liu and Mason, 2010; Rempel et al., 2017). This opens a possibility to track senescence induction within the tumors in patients using PET-CT scan, which can be considered as the biomarker to monitor the timing to use the senolytic drugs.

Conclusion

In the past years, we have learned that advanced cancers can always find one way or another to adapt to the stress induced by cancer therapy to survive. We have to realize the issue we are dealing with is not that there are no good drugs to inhibit targets; it is more about how to use these drugs in the optimal way to prevent or overcome drug-resistance. We must rethink how we use existing cancer drugs to optimize therapy responses. Dosing all drugs to maximum tolerated dose and combine drugs haphazardly in the hope to find more effective drug combinations should be reconsidered. We need to identify vulnerabilities of drug-resistant cancer cells and selectively target these acquired vulnerabilities. We can also consider to first trap the cancer cells into a state, such as senescence, that expose novel vulnerabilities that can be targeted. Last, but not least, we need to combine the therapies with sensitive monitoring methods to monitor clonal evolution during therapy to target these vulnerabilities optimally. This strategy appears more appealing than fighting a losing battle against the inevitable development of drug resistance.

Appendix

7

Nederlandse samenvatting
English summary
Publication list
Curriculum Vitae
Acknowledgments

Nederlandse samenvatting

Kanker ontstaat door mutaties in genen die celdeling, migratie en overleving reguleren. Conventionele chemotherapie is gericht tegen processen zoals het aanmaken, vermenigvuldigen en herstellen van DNA en celdeling. Deze processen zijn ook cruciaal voor normale celdeling en daarom hebben deze geneesmiddelen tal van bijwerkingen. In de laatste 10 jaar zijn een aantal mutaties gevonden in kankergenen die het proces van ontspoorde celdeling aandrijven. Kankercellen die deze mutaties hebben zijn vaak afhankelijk geworden van deze mutaties voor hun groei en overleving. De ontwikkeling van een nieuwe klasse van doelgerichte kankermedicijnen maakt het mogelijk om specifiek die ontregelde kanker-veroorzakende genen te blokkeren waar de kankercel van afhankelijk is. Deze geneesmiddelen zijn heel succesvol in de kliniek omdat ze vaak de kwaliteit van het leven van kankerpatiënten aanzienlijk verbeteren. Helaas bieden deze geneesmiddelen vaak maar tijdelijk verlichting voor de patiënten omdat resistentie tegen deze middelen op den duur onvermijdelijk is. In dit proefschrift bestudeer ik hoe resistentie tegen deze geneesmiddelen ontstaat en hoe we de nieuwe gevoeligheden die zijn ontstaan in resistente kankercellen kunnen gebruiken om ze alsnog te doden.

In hoofdstuk 1 wordt een overzicht gegeven van de resistentiemechanismen tegen de verschillende doelgerichte geneesmiddelen. Ik bespreek daar ook mogelijke therapeutische strategieën om resistentie te voorkomen.

In hoofdstuk 2 tonen wij aan waarom blaastumoren en longkankers die een mutatie hebben in een van de FGFR genen een matige reactie vertonen op selectieve FGFR-remmers. Wij laten zien dat remming van de FGF receptoren in deze kankercellen leidt tot een snelle activatie van de EGFR en HER3 receptoren, waardoor de werking van het geneesmiddel teniet wordt gedaan. We laten zien dat gelijktijdige remming van zowel FGFR en PI3K (een eiwit dat werkzaam is in de signaleringsroute van alle bovengenoemde receptoren) een synergistisch effect heeft in het veroorzaken van celdood en remming van groei van FGFR mutant blaastumoren in muizen. Deze vindingen suggereren dat een combinatie van FGFR en PI3K remmers in de kliniek effectief zouden moeten zijn voor de behandeling van deze klasse van tumoren.

In hoofdstuk 3 tonen wij aan dat melanomen met een BRAF-mutatie resistent kunnen worden tegen BRAF-remmers door de EGFR receptor te activeren. In deze studie tonen we ook aan hoe dat proces tot stand komt. Verlies van activiteit van het SOX10 gen leidt tot TGF-bèta signalering, wat resulteert in activatie van de EGFR en PDGFRB-receptoren. En verassende vinding in dit onderzoek was dat de activatie van deze twee receptoren leidt tot een staat die kenmerken vertoont van “oncogen-geïnduceerde senescentie” in afwezigheid van BRAF en MEK-remmers, terwijl deze receptoren een groeivoordeel veroorzaken in de aanwezigheid van deze twee remmers. Deze vinding verklaart naar alle waarschijnlijkheid het "drug holiday" effect: een klinische observatie dat patiënten die stoppen met het slikken van de BRAF en MEK-remmers nadat er resistentie is ontstaan, vaak een tijdelijke onderbreking van de groei van de tumor doormaken. Deze studie toont verder aan dat patiënten die resistent worden tegen BRAF en MEK remmers, en wiens tumor positief wordt voor EGFR en/of PDGFRB baat zouden kunnen hebben van een "drug holiday".

In hoofdstuk 4 beschrijven wij een nieuwe behandelstrategie voor patiënten met een BRAF-mutant melanoom die resistent zijn geworden tegen therapie die bestaat uit een combinatie van BRAF en MEK-remmers. Wij hebben gezocht naar nieuwe gevoeligheden die ontstaan als de kankercellen resistent worden tegen deze geneesmiddelen. Wij vonden dat resistentie tegen deze geneesmiddelen gepaard gaat met een toename in reactieve zuurstof species (ROS) in de kankercellen. Als deze resistente kankercellen vervolgens worden behandeld met het bestaande kankergeneesmiddel vorinostat dan leidt dat tot repressie van het SLC7A11 gen, waardoor de ROS-niveaus in de resistente kankercellen zodanig verder toenemen dat ze niet overleven. In een kleine klinische studie laten we zien in drie patiënten dat deze strategie om met vorinostat selectief de kankercellen die resistent zijn geworden tegen BRAF en MEK-remmers te doden ook daadwerkelijk werkt in patiënten. Onze studie is uniek omdat we niet alleen een nieuwe behandeloptie voor patiënten ontdekken die resistent zijn geworden tegen een geneesmiddel, maar deze aanpak ook direct testen in patiënten.

In hoofdstuk 5 tonen wij aan dat door middel van genetische screens en screens met grote aantallen chemische verbindingen het mogelijk is om middelen te vinden die senescentie veroorzaken in kankercellen. In deze studie tonen we ook aan dat we zulke senescente kankercellen selectief kunnen doden met de BCL2 remmer ABT263. Hiermee hebben we een mogelijke sequentiële strategie ontwikkeld voor de behandeling van kanker. Deze strategie wijkt in belangrijke mate af van andere kankerbehandelingen, waarin geneesmiddelen vaak tegelijkertijd worden gegeven. We noemen deze aanpak van achtereenvolgende behandelingen de "one-two punch" behandeling. Hierbij veroorzaakt het eerste geneesmiddel een belangrijke nieuwe gevoeligheid in de kankercel (senescentie) die vervolgens door het tweede geneesmiddel wordt gebruikt om de senescente kankercellen te doden.

In hoofdstuk 6 bespreken wij het toekomstperspectief en mogelijke verdere verbeteringen die in de eerdere hoofdstukken van dit proefschrift zijn beschreven.

English summary

Malignant cells are the result of mutations in genes controlling cell proliferation, invasion, and survival. Conventional chemotherapeutic drugs were designed to target vital cellular processes, such as DNA repair and replication, cytoskeleton structure, and cell division. These processes are also critical for normal proliferating cells, that as a consequence, such drugs = are associated with unavoidable toxicities. Discoveries during the last decade have identified recurrent "driver" mutations in some types of cancer. The cancer cells that harbor these genetic alterations; often exhibit dependence on an activated oncogenic pathway or protein for its sustained proliferation and survival. The mechanistic rationale of targeted approaches is to destroy the tumor by blocking aberrant cell signaling to which the cancer cell is addicted, but dispensable for healthy tissues. The targeted drugs have been designed to effectively target the oncogenically activated nodes in the major signaling pathways. These drugs have been a clinical success, and often significantly prolong the lives of individuals with cancer. Unfortunately, the initial clinical responses to targeted drugs are almost always temporary and increase progression-free survival, but this improvement does not necessarily translate into a meaningful overall survival, as acquired resistance to these drugs almost invariably develops.

In chapter 1, an overview of the drug-resistance mechanisms to various targeted drugs is described. Afterwards, potential therapeutic strategies to overcome the drug-resistance are discussed.

Chapter 2 we demonstrate why do FGFR mutant bladder and lung cancer only have a modest response to FGFR inhibitors. Inhibition of FGF receptors in these cancer cells causes a rapid feedback activation of EGFR and HER3. co-targeting FGFRs and PI3K (a common downstream signaling node downstream of these RTKs) synergistically induces apoptosis and suppresses tumors growth in FGFR mutant bladder xenograft model. These findings provide a strong rationale for clinical testing of FGFR inhibitors in combination with PI3K inhibitors in cancers harboring genetic activation of FGFR genes.

Chapter 3 we show that BRAF mutant melanoma can upregulate their EGFR to become resistant to BRAF inhibition. The study also provides mechanistic insight how do these melanomas upregulate EGFR. In these melanoma cells, SOX10 loss triggers TGF-beta signaling, which in turn results in the induction of EGFR and PDGFRB. Intriguingly the induction of these receptors in these cells triggers a state of oncogene-induced senescence in the absence of BRAF or MEK inhibitor treatment, while their expression confers a growth advantage in the presence of the inhibitors. This notion potentially explains why some BRAF inhibitor-resistant melanoma patients may regain sensitivity to BRAF inhibition after a "drug holiday". In addition, this study also suggests that induction of RTK expression in drug-resistant tumors canserve as a biomarker to identify those melanoma patients that may benefit from drug-holiday after progression on a BRAF inhibitor therapy.

In chapter 4 we present a novel treatment option for BRAF-mutant melanoma patients,that have progressed upon ‘BRAF and MEK inhibitors. We searched for acquired vulnerabilities of these MAPK inhibitor-resistant melanomas and found that resistance to BRAF+MEK inhibitors is associated with increased levels of reactive oxygen species (ROS). Subsequent treatment with the histone deacetylase inhibitor (HDACi) vorinostat represses SLC7A11 that leads to a lethal increase in the already elevated levels of ROS in drug-resistant cells, thereby causing the selective apoptotic death of only the drug-resistant tumor cells. We validate these findings in a proof of concept study in melanoma patients, which support the clinical utility of Vorinostat in the selective killing of BRAF+MEK inhibitor resistant melanoma cells. Our study is unique in that not only discovers a novel treatment option for drug resistant cells in pre-clinical models, but validates it in patients also.

Chapter 5 We present data to demonstrate that CRISPR-mediated genetic screens and chemical compound screens serve as two types of high-throughput methods to identify senescence inducers in cancer cells. The study also shows that the BCL2-family inhibitor ABT263, providing a potential sequential drug treatment strategy for cancer, can kill senescent cancer cells selectively. This demonstrates a completely novel anti-cancer therapeutic strategy which we have dubbed the “one-two punch” approach, in which a drug is first used to induce a mojor vulnerability in cancer cells (senescence), which is subsequently eploired by the second drug to kill senescent cancer cells.

In Chapter 6, we discuss the future perspectives and possible refinements of the novel therapeutic strategies proposed in the earlier chapters.

Curriculum vitae

Liqin Wang was born on the 10th of August 1985 in HengYang, Hunan, China. In 2008, he received his Bachelor's degree in Life Sciences from HAN University of Applied Sciences in the Netherlands. For his Bachelor thesis, he did an internship in the group of Prof. dr. Menno Prins in PHILIPS High Tech Campus Eindhoven. He worked on the development of lab-on-chip biosensor to detect pathogens in the blood. Afterwards, he worked as a research technician in the laboratory of Dr. Anna Pavlina Haramis in The Netherlands Cancer Institute (NKI). The work focused on genome engineering with zinc-finger nucleases and LKB1-AMPK pathway in metabolism control. In 2011, Liqin started his master's study in Biomedical Sciences at University van Amsterdam. He managed to finish the 2 years Master programme within 9 months. To this end, he completed the Master thesis by studying the differentiation of hematopoietic stem cells in the laboratory of Prof. dr. Jannie Borst in NKI. In 2012, Liqin joined the laboratory of Prof. dr. Rene Bernards at NKI to work as a Ph.D. student. In 2017, he received the Chinese government award for outstanding Ph.D. student abroad. The research described in this thesis was the main focus of his work from November 2012 until February 2018.

Publication list

Wang, L.*, Leite de Oliveira, R.*, Huijberts, S., Bosdriesz, E., Pencheva, N., Brunen, D., Bosma, A., Song, JY., Zevenhoven, J., Los- de Vries, T., Horlings, H., Nuijen, B., Beijnen, JH., Schellens, JHM and Bernards, R. (2018) An acquired vulnerability of drug resistant melanoma with therapeutic potential. ***Cell*** *173,* 1-13

Wang, L., and Bernards, R. (2018) Taking advantage of drug resistance, a new approach in the war on cancer. ***Frontiers of Medicine (in press)***

Wang, C., Jin, H., Gao, D., **Wang, L.**, Evers, B., Xue, Z., Jin, G., Lieftink, C., Beijersbergen, RL., Qin, W., Bernards, R. (2018) A CRISPR screen identifies CDK7 as a therapeutic target in hepatocellular carcinoma. ***Cell Res***. 2018 Mar 5. doi: 10.1038/s41422-018-0020-z.

Wang, L.*, Leite de Oliveira, R., Wang, C., Fernandes Neto, JM., Mainardi, S., Evers, B., Lieftink, C., Morris, B., Jochems, F., Willemsen, L., Beijersbergen, RL., Bernards, R. (2017). High-Throughput Functional Genetic and Compound Screens Identify Targets for Senescence Induction in Cancer. ***Cell Rep*** 21, 773-783.

Wang, L.*, Sustic, T.*, Leite de Oliveira, R.*, Lieftink, C., Halonen, P., van de Ven, M., Beijersbergen, R.L., van den Heuvel, M.M., Bernards, R., and van der Heijden, M.S. (2017). A Functional Genetic Screen Identifies the Phosphoinositide 3-kinase Pathway as a Determinant of Resistance to Fibroblast Growth Factor Receptor Inhibitors in FGFR Mutant Urothelial Cell Carcinoma. ***Eur Urol*** 71, 858-862.

Sun, C.*, **Wang, L.***, Huang, S.*, Heynen, GJ., Prahallad, A., Robert, C., Haanen, J., Blank, C., Wesseling, J., Willems, SM., Zecchin, D., Hobor, S., Bajpe, PK., Lieftink, C., Mateus, C., Vagner, S., Grernrum, W., Hofland, I., Schlicker, A., Wessels, LF., Beijersbergen, RL., Bardelli, A., Di Nicolantonio, F., Eggermont, AM., and Bernards, R. (2014). Reversible and adaptive resistance to BRAF(V600E) inhibition in melanoma. ***Nature*** 508, 118-122.

van der Velden, Y.U., **Wang, L.**, Zevenhoven, J., van Rooijen, E., van Lohuizen, M., Giles, R.H., Clevers, H., and Haramis, A.P. (2011). The serine-threonine kinase LKB1 is essential for survival under energetic stress in zebrafish. ***Proc Natl Acad Sci U S A*** 108, 4358-4363.

van der Velden, Y.U., **Wang, L.**, van Lohuizen, M., and Haramis, A.P. (2012). The Polycomb group protein Ring1b is essential for pectoral fin development. ***Development*** 139, 2210-2220.

Xiao, Y., Zijl, S., **Wang, L.**, de Groot, D.C., van Tol, M.J., Lankester, A.C., and Borst, J. (2015). Identification of the Common Origins of Osteoclasts, Macrophages, and Dendritic Cells in Human Hematopoiesis. ***Stem Cell Reports*** 4, 984-994.

Koets, M., van Ommering, K., **Wang, L.**, Testori, E., Evers, T.H., and Prins, M.W. (2014). Influence of dsDNA fragment length on particle binding in an evanescent field biosensing system. ***Analyst*** 139, 1672-1677.

(* Co-first author)

Acknowledgement

Six years of Ph.D. life is coming to an end. All the times of ups and downs, utter excitement when the hypotheses are proven, as well as fear or depressed when I am in the limbo of producing disappointing results. With this in mind, it is the time to write the most rewarding section of this thesis and then you all who have contributed to an extremely educating and fun time at NKI and to this tiny book.

Firstly, **Rene**, I would like to thank you for your continuous supporting me to complete this journey. I am very grateful for your enormous insightful guidance during my Ph.D. I appreciate that you always encouraged me to tackle the various challenge of different screening strategies. I can still remember exactly the Friday afternoon when you propose the idea to combine FACS with a genetic screen to look for regulators of EGFR in BRAFi-resistant melanoma. It was a flash-idea, but who knew, it eventually turned into a Nature paper. Through these years, I have enjoyed learning a lot from you, not only about the scientific knowledge but also your positive enthusiasm attitude. This positive enthusiasm motivates me to carry on through these 6 years and teach me not give up easily. I respect this a lot and I am very grateful for the opportunity that you gave me to join your lab and led me to this point.

I want to thank my reading committee – **Hans Bos, Boudewijn Burgering, Jan Schellens, Daniel Peeper** and **Thijn Brummelkamp**. Thank you very much for taking your time to evaluate this thesis.

All the works established in this book would not have been manageable without the help from my Portugal brother. Thank you, **Rodrigo**, for your stimulating discussions, helpful suggestions and countless hours of collaborative efforts in the lab. I really appreciate you for being by my side and fight together as a brother in arms when we face the difficult moments of the projects. Without you, more than half of this book will not exist.

Sanne and **Jan**, thank you very much for your enthusiasm in our research and your tremendous efforts to translate our research from bench to bedside. I also like to thank Jos Beijnen very much for taking care of the vorinostat production. Without all your help, we would never complete this story at this stage. And eventually, we made our story into *Cell*. I really appreciate all your efforts very much!

Big thanks also go to my three talented students, **Fleur, Lisa** and **Tijske**, who helped quite much for the works showing in this book. Especially **Fleur**, I am really glad that you have joined B7 as a Ph.D. student. I believe that you will do well during your Ph.D. study. And together, we shall soon rock more nice stories out!

Chong and **Sid**, I would like to thank you to support and guide me with a good start in the lab. For the sleepless nights, we were working together before deadlines, we could push our *Nature* paper out in the second year of this journey.

I also like to thank my "Melania", **Živa**, the mother of grumpiness, the queen of depression, the lady of drama, the guardian of good science, and the goddess of literature. Thank you very much for bringing all the fun to our office, because of you, our office is now the most popular office on the floor. And you truly made office37 more colorful!

Diede, you are one step ahead early to complete the journey. Now, you became a venture capitalist, I wish you all the best for all your investments, and I am very looking forward to seeing that one day soon you shall manage your own VC firm!

Furthermore, I would like to acknowledge all the authors and collaborators. Many of my projects would not be possible without the advice, materials, and help from our collaborations. Thank you, **Evert, Hugo, Cor, Ben, Nora, Joao, Sara, Guus, Aniruld, Astrid, Ji-ying, John, Tonci, Pasi, Prashanth, Ingrid, Andreas, Lodewyk** and **Michiel**.

Next, I would like to acknowledge **Roderick**, the lord of screens. Thank you very much for many of your helpful advice, especially to design the screen in a smart way. I appreciate all the scientific discussions we had, I took them as very valuable lectures. And I am very looking forward to our possible future collaborations. I also like to thank **Bastiaan**, thank you very much for not only you made the CRISPR screen possible in the lab, but also many critical ideas for the studies in this book.

I also thank **Thijn, Maarten, Roderick** and **Lodewyk** for being my Ph.D. progress committee. I am very grateful for all your advice from you and helping me to reach every milestone through this journey.

I also like to thank **Yanling** and **Jannie**, who helped me very much during my master's study, Yme and Anna trained me well during my technician time. With all your guidance, supports and helps, I could have a good preparation to start this adventure in my Ph.D. life.

I have been very enjoyable these years working in this lively and friendly group. Dear Current and Former B7, I thank you very much, **Katrien, Annemieke, Josephine, Jackie, Floris, Antonio, Sake, Stefan, Begona, Valentina, Arnout, Winny, Klaas, Kathy, Jos, Sander, Kristan, Maarten, Gergana, Daniel, Andy,** and **Lore**. And Our mother of B7, **Patty**, thank you very much for your help through all these years!

Thank you, **Wouter** and **Marielle** for keeping the lab up and running. So, we can focus on our work, without worrying about the reagents and lab equipment. And in these past years, all the works relied on the help and services of many NKI facilities. Here, I would like to express my gratitude to **Frank** and **Anita**, **Lenny** and **Lauran, Iris, Onno, Roel, Wim, Marja** and **Ron**, **Marieke** and her **intervention team members**. You guys made NKI a great place.

I also like to thanks some of my chinese friends in NKI: **陈韬, 陈春, 陈玮, 何友吉, 黄馨瑶, 韩瑞琦, 孔祥俊, 林凡, 刘真, 李礼, 庞宝旭, 乔晓航, 宋继莹, 徐国泰, 王耀赓, 王玮, 甘昌培, 王静, 郭小虎, 朱燕韵, 浩杰, 薛贞** 和 **王存.** 能够与大家在同一个研究所工作是一种缘分, 祝大家在科研上越做越好. 也祝我的兄弟**平臻**, 早日毕业, 在今后事业上越走越顺. 在这里, 我想特别感谢我和皓波的月老, **桦哥,** 谢谢你牵起了我们这段姻缘！

At last but not least, I am deeply thankful to my family for their love, support, and sacrifices. Without them, this thesis would never have been written. Especially to my parents, 谢谢**爸爸妈妈**对我的养育之恩和温暖慈爱的关怀. 也感谢**岳父岳母**祝福我和皓波婚姻. 你们身体健康, 安享晚年是我们做儿女最大的心愿.

This last word of acknowledgment, I have saved for my dear wife **皓波 Haobo**, who has been with me all these years and has made them the best years of my life. Every day I am more and more grateful to have you in my life, being with you, every day is the valentine's day 有了你，幸福很简单，很真实。亲爱的，有你的每一天都是情人节.

End of the thesis

22-Feb-2018